

https://dspace.org/

Microstructural characterisation and mechanical properties of laser beam welded dissimilar joint

Ramaphoko, Nkopane Angelina

2022

https://hdl.handle.net/10539/34931

Downloaded from a DSpace repository. https://dspace.org/



Microstructural characterization and mechanical properties of laser beam welded dissimilar joint

Prepared by

Nkopane Angelina Ramaphoko

481333

A dissertation submitted to the School of Chemical and Metallurgical Engineering, Faculty of Engineering and the Built Environment, University of the Witwatersrand, Johannesburg, South Africa in fulfilment of the requirements of the degree of Master of Science.

Johannesburg, 2022

DECLARATION

- I understand that plagiarism is unacceptable.
- I validate that the work presented for evaluation for the degree of MSc (Eng.) Metallurgy and Materials course is my own unassisted work.
- I obeyed the necessary rules in referencing the views and opinions of others.
- I acknowledge that the University of the Witwatersrand might consider taking legal steps against me should it be believed that this submission is not my individual unassisted work or that I did not recognize the origin of the concepts or terms in my dissertation.

Student Name: Nkopane Angelina Ramaphoko

Student number: 481333

Student signature: 

ABSTRACT

The automotive industry has been identified as one of the greatest contributors of greenhouse gases (GHG) which result in global warming. Therefore, there is an urgent need for the industry to adopt innovative means of producing lightweight vehicles while maintaining passenger safety. Decreasing the total body mass of vehicles has proven to achieve fuel efficiency leading to a reduction of harmful gas emissions. The most effective technique for achieving lightweight vehicles is by joining dissimilar materials, predominantly aluminium alloys, with different steel grades. The main challenge encountered with production of hybrid/dissimilar vehicles by fusion welding is the creation of weak intermetallic compounds (IMCs) that undermine the mechanical response and corrosion resistance of dissimilar weld joints. Laser welding technique is regarded as the most successful method for producing dissimilar weld due to attributes such as low deformation, adjustable heat input and narrow heat affected zone (HAZ). As a result, the procedure was used for the current project.

Laser welding speed and laser welding power were varied to examine the influence of heat input on the characteristics of dissimilar weld joints between Z225 and Al 5754 with regards to microstructure, corrosion properties and mechanical properties. The optical microscope analysis, SEM/EDS, XRD, electrochemical corrosion, microhardness and tensile shear strength examinations were used to study the relationship between the microstructure, corrosion properties and the mechanical response of the dissimilar weld joints.

The results revealed that weld bead dimensions were increased by an increase in heat input, consequently increasing the interfacial layer thickness. The greatest microhardness values were recorded at the lowest speed (1.0 mm/s) owing to the development of IMC phases throughout the weld metal. The EDS composition predicted the presence of FeAl, $FeAl_2$, Fe_2Al_5, Fe_3Al_{14}, two-phased mixture of FeAl and $FeAl_2$ and Zn-Al phase. The XRD analysis however only confirmed the presence of FeAl, $FeAl_2$ and Fe_2Al_5 whose quantities increased with increasing heat input. The Z225/Al 5754 dissimilar weld joints with thicker interfacial layers exhibited better corrosion properties. The maximum tensile strength and percentage elongation of 61 MPa and 1.08 % respectively were obtained from laser power of 1500 W and 1.5 mm/s. Nevertheless, the only sample which passed the tensile strength test was produced at 1.0 mm/s and 1500 W, as it failed

at the Al5754 HAZ whereas all others failed at the weld joint interface. The highest hardness, best corrosion and tensile properties were obtained from 1.0 mm/s and 1500 W. Therefore, this combination of parameters was regarded the optimum parameters for combining Z225 and Al 5754 for car body parts.

ACKNOWLEDGEMENTS

Firstly, I thank God Almighty for bestowing me with the required perseverance and patience for successfully completing this work.

Secondly, my profound thanks go to Prof. Nthabiseng Maledi, my supervisor, for her altruistic academic guidance and assistance.

I appreciate the University of the Witwatersrand, particularly the School of Chemical and Metallurgical Engineering. Thanks to the technical staff Mr Moqabolane, Mr Mahole, Mr Mawila and Mrs Dinham for their help. I also give thanks to all my co-workers for their support.

I deeply appreciate the Council for Scientific and Industrial Research (CSIR) for sponsoring the project. I thank Mr Sam Skhosane and Mr Khoro Malabi from the Laser Department for selflessly sharing their expertise and time

.

Finally, I dedicate this thesis to my family, my late father Keabetsoe Ramaphoko, may your gentle soul continue to rest in peace. My mother Raisibe Ramaphoko, my two brothers Mokete and Lehlogonolo, as well as my younger sister Morongoa for their motivation, unconditional love, and care through the duration of the project.

LIST OF PUBLICATION

1. Nkopane Angelina Ramaphoko, Samuel Skhosane, Nthabiseng Maledi, Microstructural characterization and mechanical properties of laser beam welded dissimilar joints between A6000 aluminium alloy and galvanized steel, Mater., 15 (2) (2022), p.543. https://doi.org/10.3390/ma15020543

TABLE OF CONTENTS

DECLARATION II
ABSTRACT III
ACKNOWLEDGEMENTS V
LIST OF PUBLICATION VI
TABLE OF CONTENTS VII
LIST OF FIGURES X
LIST OF TABLES XIII
CHAPTER 1 : INTRODUCTION 1
1.1 Background 1
1.2 Research question 4
1.3 Research problem /statement 4
1.4 Hypothesis 5
1.5 Project aim and objectives 6
1.6 Significance of the research 6
1.7 Research scope 7
CHAPTER 2 : LITERATURE REVIEW 9
2.1. Introduction 9
2.2 State of the art in dissimilar materials joining 9
2.2.1 Mechanical joining methods for dissimilar materials 9
2.2.2 Welding methods for dissimilar materials 9
2.3. Overview of the laser welding process 12
2.3.1 How lasers work 13
2.3.2 Different types of laser welding 13
2.3.3 Laser welding conduction mode 16
2.3.4 Laser welding keyhole mode 16
2.3.5 Defects associated with laser welding 17
2.4 Common laser welding configurations 18
2.4.1 Laser butt welding 19
2.4.2 Laser lap welding 19
2. 5 Welding of dissimilar materials 20
2.5.1 Physical properties of parent materials 20

2.5.2 Chemical properties of parent materials 21
2.5.3 Defects associated with welding of dissimilar materials 22
2.5.4 Weldability of dissimilar materials 22
2.6.1 Single beam laser and fusion brazing welding techniques 24
2.6.2 Laser arc hybrid-fusion and fusion- braze welding techniques 25
2.6.3 Dual-beam laser fusion and fusion-braze welding techniques 26
2.7 Common challenges associated with laser welding between aluminium and steel 28
2.8. The effect of laser welding parameters on the quality of weld joints 30
2.9 Optimization of laser welding parameters 32
2.10 Microstructural and mechanical properties of weld joints between steel and aluminium 35
2.10.1. Weld bead dimensions 36
2.10.2 IMC phases and IMC layer thickness 38
2.11 Corrosion properties of dissimilar materials 43
2.12 Mechanical properties 46
2.12.1 Microhardness analysis 46
2.12.2 Tensile strength analysis 49
2.13 Progress trend in aluminium and steel laser welding 51
CHAPTER 3 : RESEACH DESIGN AND METHODOLOGY 53
3.1 Base materials 53
3.2 Experimental procedure 54
3.2.1 LBW process 54
3.2.2 Microstructural characterization 57
3.2.3 Electrochemical corrosion test 59
3.2.4 Mechanical testing 60
CHAPTER 4 : RESULTS AND DISCUSSION 62
4.1 Microstructural characterization: Optical microscopy 62
4.1.1 Morphology and defects on the weld cross sections 62
4.1.2 Weld geometry of the dissimilar weld cross sections 66
4.1.3 Grain structure of the weld metal and HAZ 68
4.2 Microstructural characterization: SEM/EDS 72
4.2.1 Effect of laser welding power on the composition of the created IMC phases 73
4.2.2 Effect of laser welding speed on the composition of the created IMC phases 76
4.3 XRD analysis of Z225 /Al 5754 dissimilar weld joints 80

4.4 Electrochemical corrosion behaviour of Z225/Al 5754 weld surfaces 82
4.4.1 Influence of NaCl concentration on the corrosion properties of the weld joints 82
4.4.2 Influence of welding parameters on the corrosion properties of the weld joints 84
4.5 Mechanical properties 87
4.5.1 Microhardness 87
4.5.2 Tensile properties 94
4.6. Summary 97
CHAPTER 5 : CONCLUSIONS AND RECOMMENDATIONS 99
5.1 Conclusions 99
5.2 Validation of hypotheses 99
5.3 Recommendations 100
CHAPTER 6 . APPENDICES 101
REFERENCES 108

LIST OF FIGURES

Figure 1.1: Binary equilibrium phase diagram of Fe and Al [6]. 2
Figure 2.1: Diagram of LBW process; (a) Conduction mode (b) keyhole mode [48]. 16
Figure 2.2: Possible laser welding configurations [58]. 19
Figure 2.3: The weldability pairs of different metals [69]. 23
Figure 2.4: Weld zone showing brittle IMCs and a crack [72]. 25
Figure 2.5: Tensile strength of the weld; (a) Varying welding current (b) Varying laser power [75]. 25
Figure 2.6: SEM image showing surface fracture of aluminium [75]. 26
Figure 2.7: Influence of welding speed on bonding width at varying roll pressures; (a) GI-A6000 joint, (b) GA-A6000 joint [8]. 31
Figure 2.8: The appearance of the weld at various laser offsets: (a) 0.1 mm, (b) 0.2 mm [88]. 32
Figure 2.9: Influence of welding parameters on the IMC thickness (a) Laser brazing speed, (b) Heat input, (c) Influence of IMC layer thickness on mechanical resistance [90]. 33
Figure 2.10: Relationship between the microstructure of welded structural steel and thermal cycle [95]. 36
Figure 2.11: EDS analysis points at varying heat input. (a) 33.3 J/mm, (b) 28.5 J/mm [104]. 39
Figure 2.12: Points of EDS performed on the micrograph [10]. 40
Figure 2.13: Various types of IMCs shown on XRD pattern of a fracture surface [105]. 41
Figure 2.14: Microsection of the IMC layer thickness [106]. 41
Figure 2.15: IMC layer thickness variation through cross section of weld joint [106]. 42
Figure 2.16: Two different IMC layers [106]. 43
Figure 2.17: Weld joint produced from $AlMg_6Mn$ filler material (a) before corrosion, (b) after corrosion and weld joint produced from $ZnAl_2$ filler material (c) before corrosion, (d) after corrosion [109]. 44
Figure 2.18: Polarization curves of joints produced at different TLP bonding temperatures [110]. 45
Figure 2.19: Schematic of a representative hardness profile of steel-Al fusion welds [111]. 47
Figure. 2.20: Hardness distribution for single pass welding at different penetration depths [32]. 47
Figure 2.21: Measurements of Vickers hardness indentations at the joint interface [8]. 48
Figure 2.22: Influence of Ar and N_2 on shear strength using single and double pass welding [117]. 50
Figure 2.23: Fracture surfaces and modes at varying heat inputs. (a) 36.3 J/mm, (b) 28.5 J/mm [1]. 51
Figure 3.1: KUKA60L30HA automated laser arm robot at CSIR, Pretoria. 55
Figure 3.2: Illustration of an overlap joint between Z225 and Al 5754 (modified from) [122]. 56
Figure 3.3: Tensile shear strength test specimen (modified from) [123]. 60

Figure 4.1: Optical micrographs for dissimilar joints produced at a constant laser welding power of 1500 and laser welding speed of (a) 1.0 mm/s, (b) 1.5 mm/s, (c) 2.0 mm/s and (d) 2.5 mm/s. 63
Figure 4.2: Optical micrographs for dissimilar joints produced at a constant laser welding speed of 3.0 mm/s and laser welding power of (a) 1400 W, (b) 1500 W, (c) 1600 W and (d) 1700 W. 65
Figure 4.3: Effect of laser welding power on the weld bead dimensions 66
Figure 4.4: Effect of laser welding speed on the weld bead dimensions 67
Figure 4.5: Microstructure created at different laser welding speeds and constant power of 1500 W: (a) 1.0 mm/s, (b) 1.5 mm/s, (c) 2.0 mm/s, 2.5 mm/s. 69
Figure 4.6: Microstructure created at constant laser welding speed of 3.0 mm/s and different laser welding powers: (a) 1400 W, (b) 1500 W, (c) 1600 W, (d) 1700 W. 71
Figure 4.7: Transition of grains from BM to WM. 72
Figure 4.8 : SEM images of IMCs at 1400 W. (a) Weld cross-section, (b) Interfacial region (A). 74
Figure 4.9: SEM images of IMCs at 1500 W. (a) Weld cross-section, (b) Interfacial region (A). 74
Figure 4.10: SEM images of IMCs at 1600 W. (a) Weld cross-section, (b) Interfacial region (A). 75
Figure 4.11: SEM images of IMCs at 1700 W. (a) Weld cross-section, (b) Interfacial region (A). 76
Figure 4.12: SEM images showing the IMCs. (a) Weld cross-section, (b) Right interfacial region (A), (c) Bottom interfacial region (B), (d) Left interfacial region (C). 77
Figure 4.13: SEM images of IMCs at 1.5 mm/s. (a) Weld cross-section, (b) Interfacial region (A). 78
Figure 4.14: SEM images of IMCs at 2.0 mm/s. (a) Weld cross-section, (b) Interfacial region (A). 79
Figure 4.15: SEM images of IMCs at 2.0 mm/s. (a) Weld cross-section, (b) Interfacial region (A). 79
Figure 4.16: XRD pattern for 1.0 mm/s showing the detected elements and IMC phases detected. 80
Figure 4.17: Polarization curves indicating the effect of NaCl concentration on the corrosion properties of dissimilar weld joints between Z225 and Al 5754. 84
Figure 4.18: Polarization curves indicating the effect (a) Laser welding speed and (b) laser welding power on the corrosion properties of dissimilar weld joints. 86
Figure 4.19: Effect of laser welding power on WM microhardness 88
Figure 4.20: Effect of laser welding speed on weld metal microhardness 89
Figure 4.21: Effect of laser welding speed on the transverse microhardness measurements. (a) 1.0 mm/s, (b) 1.5 mm/s, (c) 2.0 mm/s, and (d) 2.5 mm/s. 91
Figure 4.22 : Effect of laser welding power on the transverse microhardness measurements. (a) 1400 W, (b) 1500 W (c) 1600 W and (d) 1700 W. 93
Figure 4.23 : Stress-strain curves for constant laser power of 1500 W and varying laser welding speed. 95
Figure 4.24 : Stress-strain curves for different laser powers and constant speed of 3.0 mm/s. 96

Figure 6.1: XRD pattern for 1.5 mm/s showing the quantity of elements and IMC phases 101
Figure 6.2: XRD pattern for 2.0 mm/s showing the quantity of elements and IMC phases 102
Figure 6.3: XRD pattern for 2.5 mm/s showing the quantity of elements and IMC phases 102
Figure 6.4: XRD pattern for 1400 W showing the quantity of elements and IMC phases 103
Figure 6.5: XRD pattern for 1500 W showing the quantity of elements and IMC phases 103
Figure 6.6: XRD pattern for 1600 W showing the quantity of elements and IMC phases 104
Figure 6.7: XRD pattern for 1700 W showing the quantity of elements and IMC phases 104
Figure 6.8: Impact of NaCl concentration on the OCP values..... 105
Figure 6.9: Impact of laser welding speed on OCP values 106
Figure 6.10: Z225/Al 5754 surface before and after being exposed to different NaCl concentrations. (a) before exposure, (b) after being exposed to 2.5 % NaCl, (c) 3.5 % NaCl, (d) 4.5 % NaCl..... 107

LIST OF TABLES

Table 2.1: Comparison between LBW and FSW processes [36], [37]..... 12
Table 2.2: Various types of lasers and examples [40], [44], [45]. 15
Table 2.3: Laser welding parameters used for the tests [28]. 30
Table 2.4: Parameters used for the study of Al-steel welding process [92]. 34
Table 2.5: EDS Semi-qualitative analysis results [10]. 40
Table 2.6: Typical Fe-Al IMCs and Vickers Hardness ranges of the compounds [31]..... 46
Table 3.1: Material properties of pure metallic elements [118]. 53
Table 3.2: Chemical composition of Al 5754 base material [119]. 53
Table 3.3: Chemical composition of Z225 base material [120] [121]..... 54
Table 3.4: Dimensions of the base materials. 54
Table 3.5: System parameters for varying laser power at constant laser speed. 57
Table 3.6: System parameters for varying laser speed at constant laser power. 57
Table 4.1: Fe and Al at. % for common Fe-Al IMC phases [1]. 72
Table 4.2: Symbols used to represent the elements and IMC phases predicted from EDS analysis. 73
Table 4.3: Elements and phases detected from XRD analysis at constant laser power of 1500 W. 82
Table 4.4: Elements and phases detected from XRD analysis at constant laser speed of 3.0 mm/s. 82
Table 4.5: Effect of NaCl concentration on the electrochemical properties 84
Table 4.6: Effect of laser welding parameters on the electrochemical properties. 86
Table 4.7: Effect of laser welding speed on tensile behaviour 95
Table 4.8: Effect of laser welding power on tensile properties at constant speed of 3.0 mm/s..... 97

Nomenclature

Abbreviation	Full name
BM	Base metal
BFF	Brittle fracture fatigue
CMT	Cold metal transfer
CSIR	Council for scientific and industrial research
ED	Energy density
EBW	Electron Beam Welding
EDS	Energy dispersive spectrometer
EHT	Electron high tension
FSW	Friction stir welding
FW	Friction welding
FZ	Fusion zone
GDI	Gasoline Direct Injection
GHG	Greenhouse gases
GMAW	Gas metals arc welding
GTAW	Gas tungsten arc welding
GTS	Green Transport Strategy
HAZ	Heat affected zone
IMC	Intermetallic compound
LBW	Laser beam welding
MIG	Metal inert gas

Nd: YAG	Neodymium doped yttrium aluminium garnet
NEDC	New European Driving Cycle
NPE	Non- Proportional Elongation
OCP	Open circuit potential
PD	Power density
PFI	Port Fuel Injection
RSW	Resistance spot welding
SCC	Stress corrosion cracking
SCE	Standard Calomel Electrode
SEM	Scanning electron microscope
TLP	Transient liquid phase
TS	Travel speed
TWI	The welding institute
XRD	X-ray powder diffractometer
WM	Weld metal

CHAPTER 1 : INTRODUCTION

1.1 Background

It has become a priority for the automotive industry to produce lightweight motor vehicles with enhanced safety and fuel efficiency to decrease carbon emissions [1]. A substantial quantity of high-strength steel has previously been employed for motor vehicle body parts because of its superior characteristics in improving crash safety and decreasing mass [1]. There are specific restrictions for decreasing vehicle weight by applying thinner sheets of steel [1]. Additional enhancements may be achieved by using light alloys such as magnesium and aluminium alloys. Due to cost benchmarks, good corrosion properties and usage, aluminium alloys appear to be the most favourable candidate among other lightweight materials [2]. It has also been reported that the most efficient method for maintaining vehicle crashworthiness at reasonable costs, is using hybrid steel-aluminium constructions for motor vehicle bodies [3].

Hybrid/ dissimilar materials welding involve thermal joining of materials which are not naturally compatible with one another due to extreme discrepancies in physical and chemical properties [4]. The method allows for the creation of weld joints with suitable properties which would be almost impossible to achieve when using only one material type. Dissimilar materials welding despite its advantages, has been criticized due to the creation of intermetallic compounds (IMCs) which have hazardous consequences on the reliability and quality of dissimilar weld joints [5]. The creation of IMCs within the Fe-Al interface is unavoidable during welding because there is poor solubility between Fe and Al [1]. Figure. 1.1 shows the most probable IMCs produced from welding aluminium and steel together under varying experimental conditions.

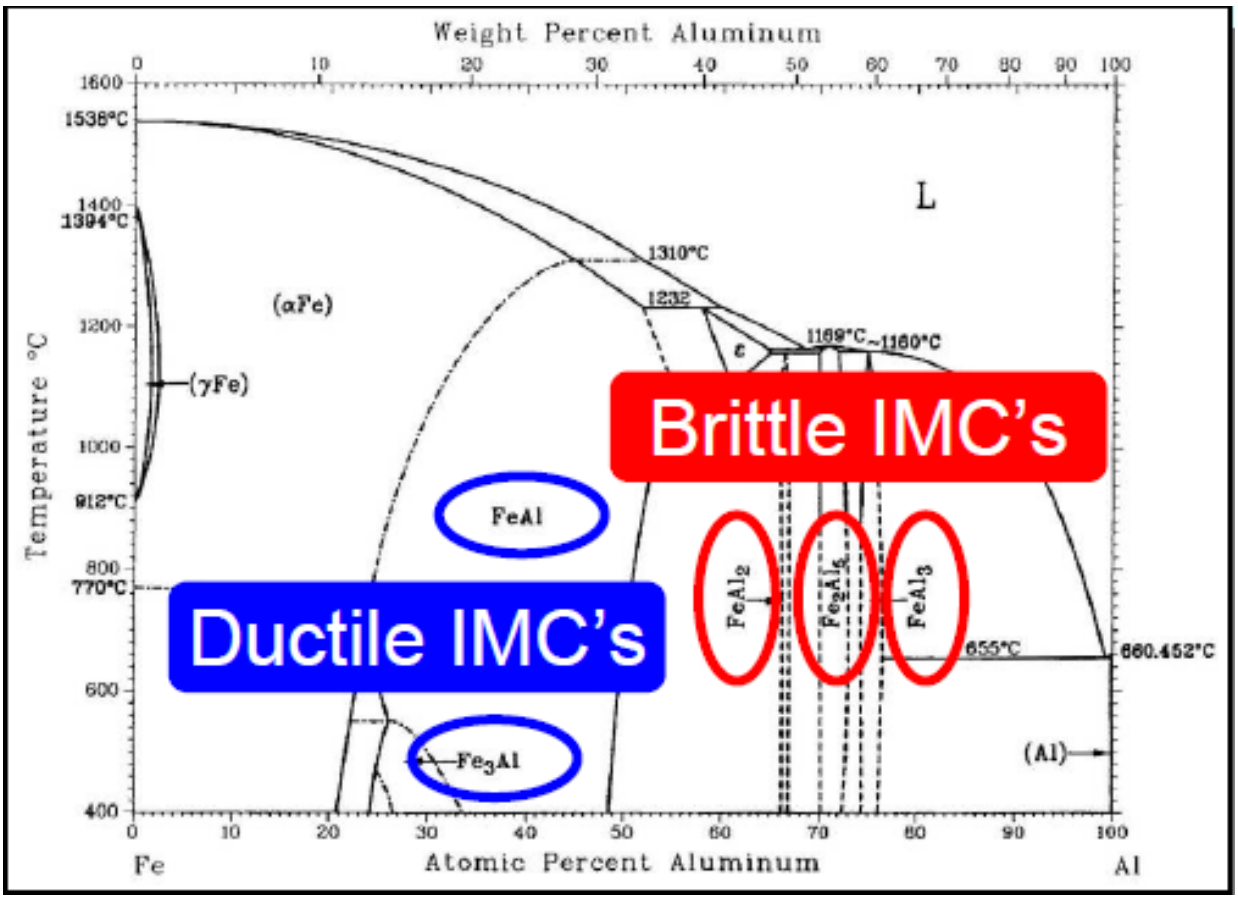


Figure 1.1: Binary equilibrium phase diagram of Fe and Al [6].

The existence of IMCs tends to decrease the toughness and plasticity of dissimilar weld joints and thus considerably increase sensitivity to cracking [7]. Literature classifies IMCs as either Al-rich (brittle) or Fe- rich (ductile) [6], [8]. To obtain improved joint functioning, particularly with regards to mechanical strength, the initiation and growth of Al- rich IMCs should be restricted as much as possible [9]. Careful selection and regulation of the heat input levels during dissimilar materials welding is thus imperative since IMC creation is principally governed by the diffusion process [10].

Numerous welding techniques have been tried and tested for successful production of dissimilar joints. The application methods such as projection, resistance spot, flash and explosion welding are not highly recommended for dissimilar metals welding because these processes are mostly limited to certain weld configurations [11]. Furnace brazing, vacuum brazing and cold metal transfer (CMT) achieve success only to some extent and result in weld joints of limited strength

[12]. Various welding techniques namely, laser beam welding (LBW), friction stir welding (FSW) and metal inert gas (MIG) welding were found to be mostly preferable for producing joints between steel and aluminium [13], [14].

Friction stir welding is a type of solid-state welding method and can create a good weld joint between steel and aluminium [15]. Application of this method is however limited by extended production periods and its need for special fitting. Also, FSW often fails to produce butts joint between aluminium and steel plates with thickness less than 2 mm due to implantation of the friction stir pin [15]. The shortcomings of the MIG method include high heat input which simplifies the creation of IMCs. In most cases, the welding methods which result in a higher standard of mechanical properties between aluminium and steel are Gas Metal Arc Welding (GMAW), electron beam welding (EBW), Gas Tungsten Arc Welding (GTAW) [16] as well LBW [12].

In relation to other welding technologies, LBW leads when it comes to combining steel to aluminium because the method possesses a couple of enhanced benefits. LBW has adjustable heat input which matches the amount required to fuse the weld metal (WM) [17]. The presence of magnetic field in laser welding restricts interference on the functionality of the laser throughout the welding process as it does in arc welding and EBW. In comparison with arc welding, weld joints between thin metals produced by LBW are less susceptible to insufficient fusion [17]. LBW has higher energy density which reduces the HAZ and can limit diffusion because of high cooling and solidification rates. Laser welding is automated. As a result, the element of human error can be reduced [17].

Even though there are numerous benefits when opting for LBW, attaining a reliable joint between steel and aluminium remains a great challenge since there is a massive disparity in coefficients of thermal conductivities, thermal expansion and melting points [11]. There are also a couple of limitations linked to the application of laser welding such as high economic aspects associated with the use and maintenance of the equipment [17]. When the process involves metals with high thermal conductivity and high reflectivity, for example aluminium, the laser wettability may be compromised. Rapid solidification related to LBW intensifies the proneness to brittleness and porosity [17].

After careful consideration of the mentioned advantages and disadvantages of LBW, it was decided that the experiments for the current project to be carried out using LBW. The decision was made based on the nature of base metals (BMs) used for the research experiments and the anticipated results. It was expected for the aluminium alloy to present problems related to its high reflectivity and thermal conductivity. This challenge was minimized by placing the steel on top of the aluminium alloy to produce an overlap joint. As a result of this arrangement, the steel was then exposed to a focused laser beam and only local heating took place for partial melting. The aluminium alloy underneath was subjected to local melting by heat conduction through steel as proposed in [18].

The current research is envisioned for application within the automotive industry. Despite high operational costs associated to LBW usage, the procedure will still be profitable because high welding speeds will allow for high production rates in great capacities as required by the sector. Since high welding speeds results in acceleration of cooling and solidification of the molten metal, cautious selection of process parameters becomes essential to minimize the extent of the challenge [19].

1.2 Research question

How do laser beam welding parameters, particularly laser welding power and laser welding speed influence the IMC creation, microstructure, corrosion resistance and microstructural properties of dissimilar joints between Z225 and Al 5754?

1.3 Research problem /statement

The state of planet Earth is under threat due to a projected hike of global greenhouse gases (GHG) from industrialization. According to an article by World Resources Institute released in February 2020, within the energy sector, the transport industry accounted for a total of 15.9 % global GHG emissions [20]. It was highlighted that 11.9 % of the total emissions resulted from road transport only [20]. As part of the global society, South Africa enhanced its approach to decarbonize the transport sector of the country through the Green Transport Strategy (GTS) in October 2018 [21]. The approach introduced vehicle fuel-efficiency specifications that

correspond to CO_2 specifications as one of the leading systems that constitute the GTS action plan.

The CO_2 emission of South Africa's passenger vehicle as measured by the New European Driving Cycle (NEDC) was 6.3 L/km in 2015 and the target was set to reduce it to approximately 5.2 L/km by 2024 [22]. There are various means of technology that may be applied within the automotive industry to address the issue. These technology compliant ways include gasoline direct injection (GDI) on fuel systems, portfuel injection (PFI), cylinder deactivation, light-weighting, hybridization, and electric vehicles [21].

It has been established that one of the most effective methods of achieving the target is by decreasing the total weight of the vehicle bodies (light-weighting) and consequently achieving fuel efficiency [23]. Reduction of the vehicle mass by 100 kg can save fuel by approximately 0.3-0.5 L/100 km. Increasing the weight of the vehicle by the same mass would result in a fuel consumption increase of 6.5 % for petrol vehicles and 7.1 % for diesel vehicles [23]. Furthermore, Jeremy Lipshaw [24] mentioned that in classical mechanics, a reduction in vehicle weight reduces energy required to accelerate it and thus reduces GHG emissions.

Therefore, car manufacturers are now focused on decreasing vehicle body mass by substituting some predominant steel parts with materials of lower specific gravity (SG) such as magnesium alloys and aluminium alloys [23]. The success of this design in most cases requires application of dissimilar materials welding methods. It is thus significant to carry out research within this area of study to produce lighter vehicles without compromising passenger safety.

1.4 Hypothesis

Up to this point, it has been established from previous research that changing heat input by either increasing laser welding power or reducing laser welding speed may affect the welding results differently. As a result, the following three hypotheses were formulated and tested through different experiments.

- Hypothesis 1: The interfacial layer thickness and the creation of IMC phases of Z225/Al 5754 joints increases as heat input increases.

- Hypothesis 2: As heat input increases, the corrosion resistance of the Z225/Al 5754 dissimilar joints decreases.
- Hypothesis 3: Decreasing heat input improves the mechanical properties of dissimilar weld joints between Z225 and Al 5754.

1.5 Project aim and objectives

The research aim was to establish laser welding process parameters which provide ideal weld joints between Z225 and Al 5754 best suitable for automotive industry application. The aim of the investigation was accomplished by addressing the following objectives.

- To examine the impact of laser power and laser welding speed on the weld bead dimensions of the Z225-Al 5754 weld joint.
- To determine the relationship between microstructural properties of Z225-Al 5754 joints with mechanical properties of the joints.
- To optimize laser power and laser welding speed to achieve minimal interfacial layer thickness and few IMCs between Z225 and Al 5754 weld joint.
- To explore the impact of laser welding parameters and NaCl concentration on the corrosion resistance of Z225-Al 5754

1.6 Significance of the research

With reference from the conducted literature review, it was discovered that various combinations of aluminium alloys and different steel grades joined by means of laser welding have been investigated. However, not much has been reported on a combination of Z225 and Al 5754 specifically by laser welding despite their great individual properties. Therefore, this research task anticipated adding to the current knowledge within the automotive sector regarding suitability of dissimilar weld joints between Z225 and Al 5754.

The success of this investigation would provide the automotive industry an extra alternative of dissimilar materials combination for manufacturing lightweight and safe materials at a reasonable production cost. Lower production costs would be achieved from substitution of heavy and expensive steel by lighter and affordable aluminium alloy parts of the vehicle body [21]. With regards to the consumers, as much as the manufacturers may sell the cars at higher

prices due to application of new and improved technology, the cost may be overshadowed by the accrued savings due to lower fuel consumption over the years of vehicle ownership [23]. The more the society members opt for vehicles with decreased mass, the total emission of GHG will subsequently decrease. This is because such vehicles utilize lesser energy and will eventually contribute positively towards the greater goal of decreasing global warming [21].

1.7 Research scope

The research project paid attention to the effect of varying combinations of laser welding parameters because these parameters yield different projected results and degrees of functionality. Focus was also given to laser welding technology because its success for usage within the vehicle manufacturing industry has been verified. The project at hand was based on combining dissimilar metals between steel and aluminium as the combination is predominantly used in the automotive sector. Therefore, it was expected that brittle IMCs will be created by thermally joining the two dissimilar materials hence attention was given to the nature of these resultant compounds.

Information acquired from literature review revealed that various laser welding parameters have an impact on the microstructural characteristics and mechanical properties of dissimilar joints. Moreover, it has been declared that laser power and laser welding speed substantially impact the absorption of energy [27], the extent in which IMCs initiate and grow [28] as well as mechanical properties [27],[29]. Therefore, laser welding speed and laser power were the principal variables of the experiments. The parameters used for the investigation were intended to fall within the ranges used in [30] whereby similar sizes of samples were used, and quality dissimilar joints were produced.

A total of eight combinations of laser welding speed and laser welding power were investigated. The first four combinations were selected to assess the effect of laser welding speed and the other four were used to establish the impact of laser welding power. Characteristically, the thickness of steel sheets used for car bodies ranges between 0.8 mm and 2.5 mm. Aluminium alloy sheets used generally have a thickness between 1 and 3 mm [3]. This information was used as guidance in selecting the thickness for BMs used for the experiments. Keyhole mode is considered the best mode for creating reliable, sound joints [3], as a result, laser welding solid-liquid keyhole mode was used.

1.8 Outline of the thesis

Chapter 1 is the introductory chapter. It gives a general outlook of what the research project is about. Chapter 2 gives a detailed literature review which paints a picture of what is presently known in the main areas relevant to the research topic. It also provides significant findings by experts and academics within the field. Chapter 3 offers thorough information about the nature of the parent materials used for the project. The chapter also describes the equipment used for preparation of samples and analysis of results. The chapter also details the methodology of the experimental tests carries out to supply acceptable results. Chapter 4 provides the findings after performing tasks in Chapter 3 and an in-depth explanation of the results. Chapter 5 is a conclusion of the vital findings in Chapter 4 and provides suggestions for forthcoming investigations.

Chapter 2 : LITERATURE REVIEW

2.1. Introduction

Welding of dissimilar metals leads to galvanic couples and increase the probability of galvanic corrosion on joints exposed to aggressive conditions [31]. The presence of IMCs increases susceptibility to cracking and the rate at which the dissimilar joints corrode. As a result, over the years, researchers have conducted extensive research around the creation and propagation of the IMC layer. This is because the IMC layer is believed to be a significant aspect that controls the mechanical response and corrosion behaviour of weld joints [31].

This chapter focuses on the metallurgical difficulties encountered during welding of dissimilar materials. It also portrays vital aspects and findings highlighted by various researchers in efforts of establishing solutions to minimize the effects of IMCs on dissimilar welds.

2.2 State of the art in dissimilar materials joining

It is important to identify other joining technologies which have been utilized for dissimilar materials before exploring laser welding method in greater detail.

2.2.1 Mechanical joining methods for dissimilar materials

Procedures which are frequently applied in joining dissimilar materials involve mechanical joining with screws, rivets, adhesive bonding, and numerous welding methods [26]. The advantage of utilizing mechanical methods is that heat transfer can be completely avoided. Consequently, the opportunity for deformation to occur is minimized although the thermal expansion coefficient of aluminium compared to that of steel is approximately two times greater. Also, mechanical joining techniques inhibit galvanic corrosion by preventing the interruption of an electrolyte [26].

2.2.2 Welding methods for dissimilar materials

There are two main classes of welding techniques which are solid-state welding and fusion welding [7]. The reactions which occur during welding of aluminium and steel can be defined by chemical, physical and statistical evaluations. During fusion welding, an irregular temperature

field which changes with time is created by a heat source when joining materials. There are thermal differences in the sections around the heat source. Inconsistent heating and solidification mechanism control the variations in behaviour of the weld bonds in terms of microstructural alterations within the fusion zone (FZ), the deformed region and HAZ [7]. The variations in heating, phase changes and solidification associated with fusion welding increase the susceptibility to IMC formation, porosity, initiation, and propagation of cracks within the weld joints [7].

There are other undesirable concerns which include residual stresses, weld distortion, weld deformations and shrinkages which may result in brittle fracture fatigue (BFF), stress corrosion cracking (SCC) and shape instabilities [7]. The creation of inevitable Fe-Al phases is the main cause for the brittleness of weld joints. The formation of IMCs is escalated by the combination of welding parameters which include temperature, pressure, time, and the environmental interactions of the material chemical composition. There are three main thermodynamic phases which control the creation of IMCs which are the chemical potential of elements, phase nucleation at the initiation of interdiffusion and movement of alloying elements as the welding process proceeds [7].

Over the past few years, the two main welding techniques that have been employed in joining dissimilar materials are FSW which is a solid-state welding method and LBW which is a fusion welding method. As a result, the two processes were further analysed.

2.2.2.1 Friction stir welding of dissimilar materials

FSW was first discovered in 1991 by The Welding Institute (TWI) which is based in England [32]. The method was invented from adjusting the friction welding method (FW). The FSW utilizes a revolving cylindrical instrument which is embraced by two adjacent materials. The materials become softer due to the friction heat which reduces the material resistance to plastic deformation [32]. After stirring of the materials, a solid-state joint is created. FSW is mostly appropriate for combining materials with higher thermal conductivity, high reflectivity, and lower melting temperatures. Therefore, the technique has been widely applied in joining aluminium alloys, both similar and dissimilar [32].

Some of the reported work for application of FSW includes research conducted by the Korea Advanced Institute of Science and Technology which was intended for the automotive industry. A lap joint was successfully created between a 0.6 mm thick low carbon steel to a 1 mm thick Al alloy [33]. Srinivasan *et al*. [34] employed the FSW method to weld two 5 mm thick dissimilar aluminium alloys. Chen *et al*. [35] conducted an experiment between Zn coated steel and an aluminium alloy in a lap joint from FSW technique.

2.2.2.2 LBW of dissimilar materials

Laser welding methods in the past involved the principle of welding aluminium only while the steel plate was brazed [25]. An investigation by the Chair of Metals and Alloys at the University of Bayreuth improved the technique by adding a zinc filler material to directly fuse the aluminium sheet by using a dual-spot laser head [25].

LBW is an alternative method used for joining dissimilar materials in various industries because of characteristics which include, rapid heating and cooling rates, higher energy density and low heat input [32]. The technique has been used to join different combinations of dissimilar materials with success. The main issue regarding laser welded dissimilar joints is the creation of IMC phases. An example of successful application of laser welding between dissimilar materials was between DX54 Zn-coated steel and EN-AW-5754 aluminium alloy. Both sheets were 1.0 mm thick and were arranged in a lap joint [32].

2.2.2.3 Comparison between FSW and LBW of dissimilar materials

The difference between FSW and LBW is that the latter is characterized by higher welding efficiency. FSW is mostly applied to aluminium alloy and magnesium alloy dissimilar joints because both the materials have high reflectivity and thermal conductivity [32]. On the contrary, it is challenging to manufacture sound weld joints between the two alloys through laser welding. A thinner HAZ and a significant reduction in interdiffusion of materials can be achieved by LBW even though FSW can achieve a lower creation of brittle IMC phases. Table 2.1 compares FSW method and LBW method. Generally, it can be observed that laser welding offers more advantages in joining dissimilar metals than FSW. Despite the ability of both methods in restricting the creation of IMC phases in dissimilar joints, there is still extensive work required to develop the application of both techniques around this area [32].

Table 2.1: Comparison between LBW and FSW processes [36], [37].

	Laser beam welding (LBW)	**Fusion stir welding (FSW)**
Joining efficiency	+	_
High aspect ratio	+	_
Little heat affected zone	+	_
Great processing speed	+	_
Weld bead appearance	+	_
Weld low melting point materials	_	+
Weld high reflective materials	_	+
Weld high conductive materials	_	+
Weld thinner materials	+	_
Weld without porosity	_	+

2.3. Overview of the laser welding process

Laser welding was designed with an intention to generate weld joints without defects frequently encountered in most welding methods [25]. Laser welding also produces weld joints with required characteristics such as narrow HAZ, high weld strength and enough reliability required for materials sensitive to elevated temperatures. Advantageous properties of laser welding include the capability of automation, high throughput, and reduced distortion because of low heat input [25].

Other reasons for laser welding to be considered as one of the procedures for combining aluminium alloys to steel involve the ability to exactly locate the source of heat which precisely situates the energy spot. This leads to minimal thermal distortion and reduced operational periods as required by industries for mass production [7]. Even with all these advantages, there are some concerns connected to laser welding such as sensitivity to cracking due to fast cooling and solidification of the melt. This can however be manipulated by careful choice of welding parameters [19],[38]. Some laser types may be costly due to production in small quantities. Also, the successful application of laser welding technique in a more flexible and easily accessible manner requires a working area which is appropriately protected and isolated [7].

2.3.1 How lasers work

For a laser to be fully functional, it requires three main elements which are a thermal excitation source, a gain medium, and an optical cavity [39]. A neodymium-doped yttrium aluminium garnet (Nd: YAG) crystal in the form of a rod acts as a light amplifier and a rod-shaped flash lamp in the exterior provides a light pulse functioning as a stimulator [40]. A high-yielding reflector guarantees usage of light from the lamp and ensures that it is integrated to the laser crystal effectively. In order to allow the laser radiance to be discharged in the magnified path, two mirrors creating the resonating chamber are assembled on the exterior of the crystal for light to be reflected. Since one of the mirrors is usually partially translucent, it allows laser radiation which is extremely directional to be extracted from the resonator. The wavelength of the radiation is narrow and has a value of 1064 nm. The high concentration of laser energy towards the workpiece is permitted through the narrow wavelength range and high directionality [40]. The concentration achieved through laser is way higher compared to those of other regular sources of light. Rapid vaporization of material and the creation of high-velocity plume are caused by high power density of a laser beam [39]. For laser pulse, the workpiece in the spotlight scale is heated beyond the melting temperature of the welding materials. After melting, the materials diffuse into each other and compact to create a solid compound. Due to greater and short-term intensity offered by laser energy to a restricted capacity, production of heat occurs only at the position where it is required. This attribute thus makes laser a brilliant means for application in laboratory and industry [40].

2.3.2 Different types of laser welding

Different laser types such as fiber lasers, solid-state gas, gas, or semiconductor may be used in laser welding [41]. Fiber laser welding utilizes an optical fiber as the principal medium for laser welding processes. This type of laser welding is mostly applied in robotic industrial welding and can use powers with a maximum of 50 kW [41]. Solid-state welding is conducted at wavelengths of about 1µm which are shorter compared to those of gas laser welding. In cases whereby Nd: YAG laser is applied, the laser welding process can be conducted in either continuous or pulsed mode. Some solid-state laser sources are only restricted to a pulsed mode. Gas laser welding can function in both continuous and pulsed mode. It operates at high voltage and low current power sources to intensify the mixture of gases which act as the main medium in gas laser welding [41].

The laser type which offers the greatest advantages including high output power, high beam quality, high laser efficiency and low noise in comparison to other laser types is fiber laser [42]. The application of fiber laser enables the beam quality to be enhanced as it provides better thermal control and circular single mode wavelength. Additionally, the surface-to-volume of the fiber can be magnified as there is easy heat dissipation [42]. The beam in fiber laser welding can also be focused to an extremely tiny focus [43]. As a result, fiber laser welding results in energy which can be focused on a small spot and thus results in low dilution and consequently strong weld joints [43].

The first practical exhibition of lasers was by Theodore Harold Maiman in the 1060s [43], where fiber laser was examined and proposed as the most assuring laser arrangement. From there on, fiber lasers have played an important role in the fast-growing photonics sector which has entirely changed the industrial and scientific field. Regardless of all the advantages offered by fiber laser welding, the method is associated with limitations due to fiber non-linearities and other impacts such as photo-darkening, transverse modal instabilities and optical damage [41]. It is thus highly recommended for fiber operators to wear special protective eyewear to prevent damage of the eye retina. Table 2.2 summarizes the different types of lasers and examples of lasers.

Table 2.2: Various types of lasers and examples [40], [44], [45].

Laser type	Description and example
Gas laser	Helium-neon laser, Argon laser, Krypton laser, Xenon ion laser, Nitrogen laser, Carbon dioxide laser, Exciter laser, Helium-neon laser.
Chemical laser	Hydrogen fluoride laser, Deuterium fluoride laser, COIL (Chemical oxygen-iodine laser), AGIL (All gas-phase iodine lasers)
Metal vapour laser	Helium-cadmium (HeCd), Helium-mercury (HeHg), Helium-selenium (HeSe), Helium-silver (HeAg), Strontium Vapor Laser, Neon-copper (NeCu), Copper vapor laser, Gold vapor laser.
Solid-state laser	Ruby laser, Nd:YAG laser, Er:YAG laser, Neodymium YLF (Nd:YLF), Neodymium doped yttriumorthovanadate (Nd:YVO4) laser, Neodymium doped yttrium calcium oxoborate $Nd:YCa_4O(BO_3)_3$ or just Nd:YCOB, Neodymium glass (Nd:Glass) laser, Titanium sapphire (Ti:sapphire) laser, Thulium YAG (Tm:YAG) laser,
Semi-conductor	GaN, AlGaInP, AlGaAs, InGaAsP, lead salt, Vertical cavity surface emitting laser (VCSEL), Quantum cascade laser.
Nd: YAG	The ND: YAG laser is the most frequently used solid-state laser in numerous areas of study due to its excellent thermal properties and that it can easily be repaired. ND: YAG laser contains single Neodymium. The triply ionized dopant Neodymium substitutes a tiny segment of the yttrium ions in the host crystal form of the yttrium aluminium garnet because of a tiny amount.

Laser welding tests may be conducted in either conduction mode or keyhole mode. For conduction mode to be attained the penetration to weld thickness ratio should not exceed 0.5 and the applied power density must not exceed10^6 W/cm^2 [43]. The benefit of using conduction mode is that it offers an opportunity for appropriate temperature gradients to be obtained during welding of Al to steel because only Al is liquefied and steel remains in a solid state. Generally, when a lap joint arrangement is applied, the laser beam is positioned on top of the steel sheet for heat conduction to occur which subsequently melts Al resulting in the connection of the two. When conduction mode is applied, the extent of interaction between Fe and Al can be lessened because the Fe-Al interface temperature becomes less relative to the melting point of steel. The steel plate remains in a solid state which reduces the formation of IMCs [43].

Laser welding method is a non-equilibrium process. Therefore, rapid cooling and solidification can generate a weld with a fine microstructure and raised hardness levels [46]. Conduction mode is classified by a ratio less the 0.5 and has a semi-circular structure. Keyhole mode has a ratio

greater than 0.5 and has a much deeper weld penetration [32]. The factors which govern the resultant mode during laser welding are thermo-mechanical characteristics of the BMs and the level of supply by the laser beam [47]. The surface of the melt pool for conduction mode cannot be broken into. For keyhole mode, the molten pool can be broken to achieve a keyhole which permits radiation of the laser beam through the melt pool [36]. The two mechanisms are portrayed in Figure. 2.1.

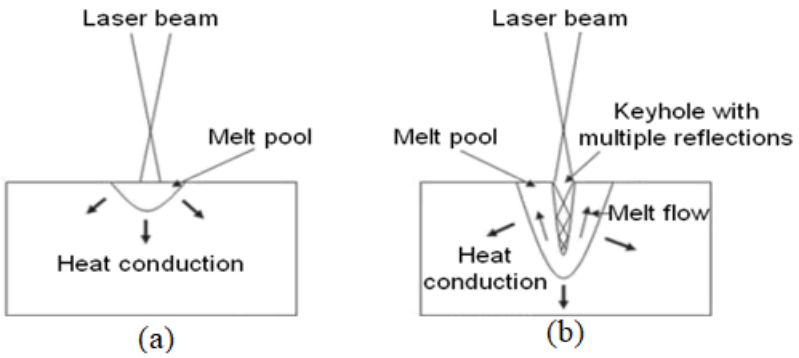


Figure 2.1: Diagram of LBW process; (a) Conduction mode (b) keyhole mode [48].

2.3.3 Laser welding conduction mode

A defocused laser beam or low levels of heat input result in a conduction mode characterized by a semi-circular appearance, shallow weld penetration depths, increased heat losses and inefficiency in welding [49]. The maximum temperature applied is typically less than the boiling temperature of the base materials. Conduction mode welding is appropriate for combining thin materials due to its ability to maintain stability of the molten pool and produce WM without defects. Conduction mode mechanism is generally practiced in the automotive, medical, electronics, and aerospace industries [49].

2.3.4 Laser welding keyhole mode

For keyhole mode, the geometry of the WM is associated with laser power density and the laser beam focal spot size. The mechanics is categorised by high heat input, deep weld penetration, high energy density and higher efficiency [50]. In keyhole mode, the WM can be separated into two sections which are the semi-circular shape at the upper part of the weld and a parallel-sided region which progressively narrows from the upper surface to the bottom [37]. During keyhole

mode welding, there is a high possibility for the base materials to be heated way over the boiling temperatures of the base materials. This results in evaporation on top part and inside of the keyhole. The keyhole depth may be increased by replications of the laser beam occurring in the keyhole. Overall, keyhole mode is more efficient in welding compared to conduction mode because of a decrease in losses by thermal conduction as the laser beam is reflected within the keyhole [51].

2.3.5 Defects associated with laser welding

The changes which occur within materials during laser welding may result in defects which impact the resultant weld quality. The alterations of microstructure, chemical composition, and residual stresses within the FZ and HAZ are caused by high rates of cooling and heating in laser welding [52]. Phase transformations and defects such as cracking, porosity, oxidation, and deficiency of elements can negatively influence the corrosion resistance and mechanical properties [32]. Some of the most common causes of laser welding defects were further studied to understand the circumstances of the occurrence of these defects.

2.3.5.1 Porosity

One of the most common defects which occur in welding of light materials, particularly aluminium alloys, titanium alloys and magnesium alloys is porosity/cavity [32]. The existence of bubbles within the laser weld may result from the keyhole collapse. In cases whereby the interaction period between the keyhole wall and occurrence of laser beam is extended, the low surface tension of the melt instantly persuades the keyhole breakdown [32]. Zhou *et al*. [53] mentioned that porosity readily occurs in keyhole mode welding relative to conduction mode welding provided that the weld width remains constant. Katayama *et al*. [54] further indicated that the collapse of the keyhole wall due to the presence of bubbles readily occurs at the top of the keyhole for lower laser welding speed. Therefore, at higher welding speeds, creation of porosity is lesser on the tip of the weld. This observation is attributed to a slower flowrate at the base of the keyhole and the breakdown of the wall is thus restricted by rapid solidification [54].

2.3.5.2 Cracking

Cracking usually occurs when the strain within the weld is greater than the strain which can be endured by the tensile stress of the material [32]. The creation of cracking within the weld may be influenced by welding parameters, chemical composition of BMs and weld features. Other factors which govern the formation of cracks include the grain structure, phases, quantity of liquid phases within the weld and the range of solidification temperature [55]. Sometimes cracking occurs when the residual stresses in the weld exceed the yield strength of base materials or due to the existence of contaminants [56]. Increasing the rate of heating in laser welding may be applied as a measure of restricting solidification cracking. This is made possible by the fact that rapid heating rates commonly result in rapid cooling rate especially if the heat source is in motion. High cooling rates lead to a finer microstructure which decreases the degree of segregation and thus promotes restriction of crack formation [32].

2.3.5.3 Spatter

Spatter is created by rapid progression of metal vapour which results in the discharge of molten metal droplets from the keyhole which scatters around the surface of the workpiece and inside the chamber [17], [32]. The occurrence of spatter can influence corrosion properties of the weld and can also contaminate the appearance of the weld. Vapour pressure, boiling temperature of welding materials, the magnitude of the melt and processing parameters are connected to the quantity of spatter formed. Larger molten pools generally lead to less amount of created spatter [32]. Kuo *et al.* [55] and Kataoka *et al*. [57] agreed that a few measures may be implemented to limit the creation of spatter. These procedures include increasing welding speed, decreasing laser power, choosing an appropriate shielding gas, applying a defocused laser beam, and including a filler material [55],[57].

2.4 Common laser welding configurations

One remarkable benefit that laser welding has over other fusion welding techniques is flexibility. Laser welding is appropriate for combining sections in various geometries and can create sound weld joints for industrial application [58]. The different configurations possible in laser welding

are demonstrated in Figure 2. 2. The most common geometries for weld joints are butt joint welding and lap joint welding, especially for dissimilar welding.

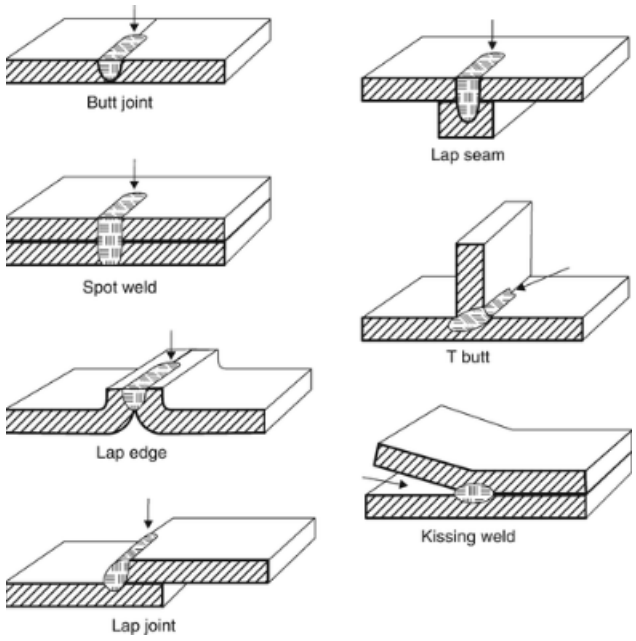


Figure 2.2: Possible laser welding configurations [58].

2.4.1 Laser butt welding

Butt joint geometry may either be linear, annular or circumferential [17]. The configuration is usually applied in keyhole mode welding method. The melt surrounding the keyhole breaks down and fills the keyhole to a point where solidification takes place [32]. Both base materials can be entirely combined after going through the melting and solidification stages. Laser butt welding is prevalently applied in the manufacturing sector. The efficacy of butt welding depends on the gap between the base materials. Sometimes it is acceptable for root opening to be about 3% of the metal plate thickness but if the opening is too wide, underfilling may occur [17]. If laser butt welding is used to join dissimilar materials, it is possible for the temperature profiles to be different at opposite sides of the weld. This outcome depends on different properties which include melting points, thermal conductivity, and boiling points [32].

2.4.2 Laser lap welding

Another common laser welding joint type is lap joint which is mostly applied for joining thin pieces, specifically in the automobile industry [32]. There are three classes of laser lap welding

namely, liquid-liquid, solid-liquid and solid-solid state welding. In liquid-liquid state welding, the two parent materials are completely liquefied to achieve complete mixing as in conventional fusion welding techniques. As a result, regulating the creation of IMCs is a challenge when this type of lap welding process is applied for dissimilar materials. For solid-liquid state welding process, the joint is created by melting only the base material positioned on top and then a liquid layer is created between the melting surfaces through conductive heat transmitted from the top [32]. Therefore, the principal advantage of solid-liquid phase state welding is that accurate control of heat input and rate of diffusion is achievable. Additionally, solid-liquid phase state welding is mostly applied when joining two materials whose melting temperatures are considerably different. Solid-solid state welding on the other hand offers a similar physical mechanism of diffusion welding. The solid-solid state welding technique relies on strict supervision of the creation of an oxide film between the joining surfaces and constant pressure [32].

2. 5 Welding of dissimilar materials

2.5.1 Physical properties of parent materials

The key physical properties of parent materials which affect laser welding of dissimilar materials include thermal conductivity, density, thermal expansion coefficient, specific heat capacity and melting temperature [59]. Materials which have high thermal conductivity such as copper and aluminium tend to disperse energy quickly, which makes it a challenge to sustain a molten weld bead. If there is unequal heat dissipation within a weld joint between base materials with extensively different thermal conductivities, an asymmetric weld bead may result. Also, there is a chance of omission of the joint line at the weld root [59]. Laser welding offers a higher energy density and greater degree of accuracy of energy input control compared to other conventional fusion welding techniques. As a result, laser welding has a higher probability of resolving the above-mentioned challenges. Nonetheless, metals with high thermal conductivity usually have low absorptivity, specifically for CO_2 laser radiation of 10.6 µm wavelength. For such cases, extra aspects such as preheating might have to be considered for the beam to be absorbed more quickly [59].

Welding of dissimilar materials with a great difference in thermal expansion creates considerable residual stresses that have negative consequences on the joint strength and fatigue properties [60]. Laser welding technology has the potential of decreasing the HAZ thickness when operated at low energy input which leads to a decrease in residual stresses. An addition of a filler material with an in-between thermal expansion coefficient is considered a sensible solution for laser welding as it accommodates thermal discrepancies to some degree.

A focused laser beam of elevated energy density is enough to dissolve almost all engineering metals [60]. Nevertheless, huge variations in melting temperatures and the closeness of boiling temperature of one BM to the melting point of the other BM can promote difficulties. These problems can be decreased by accurate regulation of the positioning and amount of laser welding energy input. This can restrict the melting of the material with the lowest melting point, permitting the creation of a brazed joint [60].

2.5.2 Chemical properties of parent materials

Mismatches in chemical properties between BMs can increase diffusion of elements, which can result in the creation of unwanted phases weakening mechanical properties of dissimilar weld joints [59]. The crystal structure, atomic size, relative valency, and chemical affinity govern the miscibility of materials in both liquid and solid states. This further determines the phase transformations. Metal combinations which are soluble in liquid state but insoluble in solid states create a eutectic system. Low melting eutectics particularly, present challenges because such eutectics add towards the solidification cracking mechanism [59].

Since laser welding offers high heating rates, it has the potential of restraining the period available for segregation to occur [59]. The high cooling rates on the other hand results in the creation of fine solidification microstructures. Both these mechanisms decrease the probability of solidification cracking. In some cases, intermediate phases occur in the form of IMCs. Generally, such compounds have a complex crystal shape and are mostly hard and brittle. Weld joint with such compounds commonly present high sensitivity to cracking and low ductility [59].

2.5.3 Defects associated with welding of dissimilar materials

Several researchers have explored laser welding of both ferrous and non-ferrous dissimilar materials. These include joining aluminium alloy STO4Z to galvanized steel sheet [61], AISI 304 to AISI 420 stainless steel [62] and aluminium alloys to steel [63]. The principal issue is that dissimilar metals welding has become one of the most complicated yet vital duties that manufactures encounter nowadays. Farabi *et al*. [64] reported that mechanical properties of dissimilar ferrous metals are largely dependent on base materials used and a combination of welding parameters [64].

Then again, welding of non-ferrous dissimilar materials was mostly characterized by microcracks which increased the opportunity for crack initiation and propagation [64]. Also, the principal challenge associated with welding of non-ferrous dissimilar materials is the increased probability of IMC creation. These compounds are created when several BM elements are diluted into the weld region during fusion and results in destructive side effects to mechanical properties of the weld joints [38]. The large variations in electro-chemicals of these IMCs escalate the probability of galvanic corrosion which results in failure of weld joints when applied under a corrosive environment. In previous research, it has been discovered that careful control of the heat input can decrease the creation of IMCs and thus improves the functionality of weld joints under corrosive environments [65],[66].

An additional obstacle related to dissimilar metals welding is the variance in coefficient of thermal expansion [67]. Thermal contraction generates residual stresses within the WM and the adjacent BM which creates inconsistencies in the magnitudes of residual stress distribution throughout the weld joint. Under circumstances whereby the difference in coefficient of thermal expansion is pronounced, internal stresses may result within the HAZ causing failure during application [67].

2.5.4 Weldability of dissimilar materials

Weldability refers to the ability of materials to go through a welding process without cracking or severe embrittlement [68]. It is imperative to predict the weldability of dissimilar metals before the welding process commences. This can be done by predicting the most possible IMCs in the

transition zone between the potential BMs and solubility from the phase diagram to check the feasibility of producing weld joints with minimal defects. This can also assist to determine the joint behaviour such as susceptibility to corrosion, sensitivity to cracking and ductility [69].

Figure 2.3 can also be used as an additional guidance especially when the welding process involves Al as one of the BMs [69]. The selection chart is based on eight most important properties to be considered during welding which are susceptibility to fracture, strength properties, toughness, corrosion properties, behaviour at high temperatures, ductility, post- weld heat treatment and colour match after anodizing. This table also assists in terms of selecting the most suitable filling materials or buttering layers to achieve a smooth transition between dissimilar materials during welding [69].

	Al	Ag	Au	Cu	Pt	Ni	Fe	Ti	W
Al	–	C	X	C	X	X	X	X	X
Ag	C	–	S	C	S	C	D	C	D
Au	X	S	–	S	S	S	C	X	N
Cu	C	C	S	–	S	S	C	X	D
Pt	X	S	S	S	–	S	S	X	X
Ni	X	C	S	S	S	–	C	X	X
Fe	X	D	C	C	S	C	–	X	X
Ti	X	C	X	X	X	X	X	–	X
W	X	D	N	D	X	X	X	X	–

Metals: Al: aluminum; Ag: silver; Au: gold; Cu: copper; Pt: platinum; Ni: nickel; Fe: iron; Ti: titanium; and W: tungsten.
Keys: C: Complex structures may exist; **X:** Inter-metallics compounds formed undesirable combination; **S:** Solid solubility exists in all alloy combination; **D:** Insufficient data for proper evaluation; and **N:** No data available.

Figure 2.3: The weldability pairs of different metals [69].

Various technologies have been tested to tackle the challenges which result from welding of dissimilar materials using laser technique. The focus of such methods is to restrict the creation of brittle IMCs within the weld. The methods involve the application of pulsed wave lasers, pre or post heat treatments of materials and offsetting the laser beam on distinct locations [32]. The advantage of pulsed-wave welding over continuous-wave laser is that it has a greater ability to

regulate heat input, rate of solidification and the extent of material mixing [70]. The heating and cooling processes take place simultaneously in pulsed wave laser welding. As a result, the welding materials are not solidified individually. Suitable choice of laser welding parameters including welding speed, average power, peak power, and pulse frequency supposedly enhances the quality of dissimilar materials weld joints [70].

2.6 The advancements in aluminium and steel welding research

There has been so much development in laser welding over the recent years in terms of achieving precision by changing wavelength, laser power, welding speed and power density. Laser fusion-brazing is a welding process whereby laser thermal energy is correctly controlled [11]. This assists in attaining partial fusion of the base material with the lowest melting temperature to wet the BM with the higher melting point for a dissimilar weld joint to be produced. If the technique is used to join aluminium and steel, the joint near aluminium is fusion welded and the one close to steel is braze welded. The application of weld-braze process offers the benefit of decreasing the development of IMCs at the point of contact between steel and brazed seam by providing high cooling rates and rapid process time [71],[72]. There are different arrangements of the laser beam for fusion-braze welding, for example, single beam laser, dual beam laser and laser arc hybrid [11].

2.6.1 Single beam laser and fusion brazing welding techniques

Laser brazing method has been highly recommended for welding of dissimilar metals between steel and aluminium alloys. The method permits localized fusion which subsequently regulates the development of IMCs [73]. In one investigation by Torkamany *et al*. [72], a pulsed Nd: YAG single beam laser was applied to produce a dissimilar weld joint between a 0.8 mm thick ST14 low-carbon steel structural steel and a 2.0 mm thick aluminium alloy 5754. The effect of laser power and pulse period on the weld joint was scrutinized. IMC phases were detected within the weld zone as depicted in Figure 2.4 [72]. The results also indicated that raising laser power and pulse duration intensified the quantity of the IMCs within the weld section, the degree of spatter and the presence of cracks and other defects. Reduction of these parameters resulted in insufficient penetration and decreased weld joint strength [72].

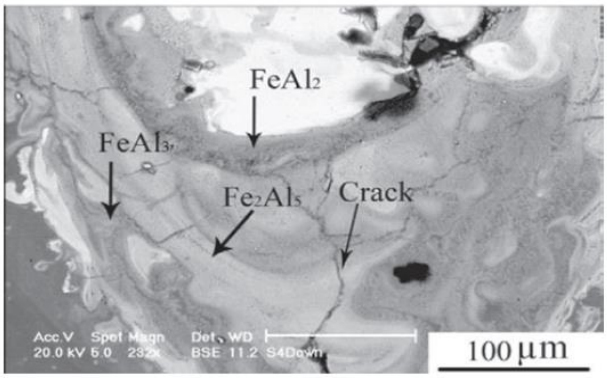


Figure 2.4: Weld zone showing brittle IMCs and a crack [72].

2.6.2 Laser arc hybrid-fusion and fusion- braze welding techniques

Laser arc hybrid procedure offers complete stability of the welding process. This is achieved through enhancement of the arc ignition, re-ignition, consistency of the arc, homogeneous and deep penetration [74]. Qin *et al*. [75] investigated the hybrid Nd: YAG laser-GMAW method by applying it to galvanized steel of 2 mm thickness and 6013-T6 aluminium alloy of 1 mm thickness. At first, when the arc current and laser power were elevated, the brazed joint tensile strength increased until it reached a peak and then started to decrease as demonstrated in Figure 2.5.

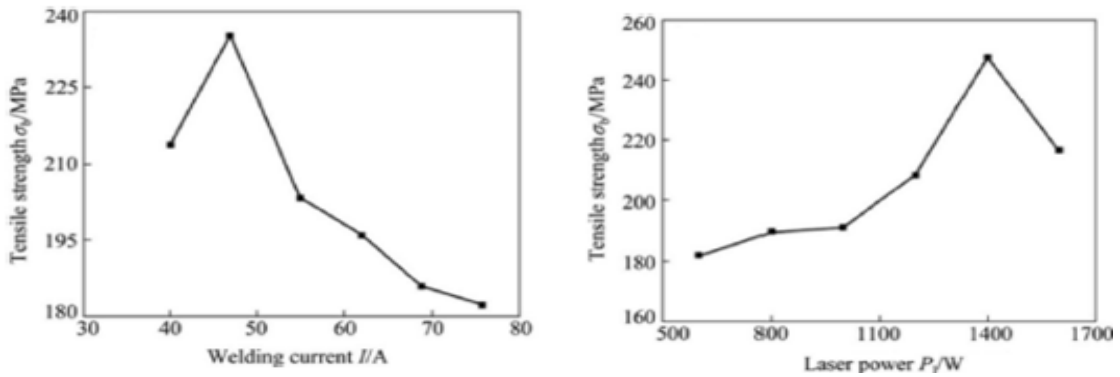


Figure 2.5: Tensile strength of the weld; (a) Varying welding current (b) Varying laser power [75].

The greatest tensile strength of 247.3 MPa was reached for an arc current of 62 A, laser power of 1400 W and travel speed of 1 m/min. The IMC layer principally consisted of $FeAl_2$, Fe_2Al_5 and Fe_4Al_{13}. The layer thickness ranged between 2 and 4 µm. Microhardness measurements showed

a steady increase from the steel side towards the aluminium side. A maximum value was recorded at the weld interface of the steel side and then the microhardness decreased gradually towards the aluminium alloy.

Results from the tensile test failure analysis showed that fracture of the sample mainly occurred in the aluminium alloy HAZ, far from the weld interface area. The analysis also revealed that both ductile and brittle fracture modes were present in Figure 2.6.

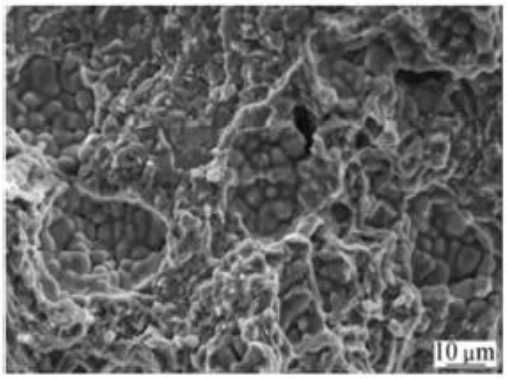


Figure 2.6: SEM image showing surface fracture of aluminium [75].

In another research by Liu *et al*. [76], laser-GAMW hybrid welding technique was used to combine an aluminium alloy AA6061 with a high-strength steel. There was an added explosively welded steel-Al transition joint between the BMs. A finite element simulation and regulation of heat input resulted in the temperature circulation at the transition zones. It was discovered that restricting temperature of the Al-steel explosion welded interface to less than 315 $^{\circ}$C significantly decreased the creation of Fe-Al IMCs. The presence of microcracks at the IMC layer was detected. Tensile tests results disclosed that the strength of the weld joint went as high as 220 MPa and failure occurred within the HAZ of aluminium parent metal [76]. Comparable results were reported by Qin *et al*. [75].

2.6.3 Dual-beam laser fusion and fusion-braze welding techniques

The application of dual laser beams was regarded as a means of enhancing weld strength, creating smoother weld surfaces and deeper weld penetrations compared to single beam laser welding [11]. Ma *et al*. [77] suggested the application of a double pass laser welding method as a measure of eliminating the laser welding related flaws between zincs coated steels and aluminium alloys. As a result, an aluminium alloy 6061 T6 of 1.00 mm thickness was welded to

a dual phase zinc coated high strength steel DP590 of 0.75 mm thickness [77]. A lap joint was created from a two-pass laser beam. The purpose of the first pass was to partly liquefy and evaporate the zinc covering using a defocused laser beam as supply for preheating. The second pass was then applied to perform the actual welding process with a focused laser beam. It was noted that the thickness of both BMs and that of the zinc coating influence the choice of process parameter combinations used for both the first and the second pass of the laser beam.
For the first pass, both laser welding power and travel speed should be regulated so that the heat input is enough to vaporise the galvanized steel coating however, it must not be too high to avoid extreme laser-induced plasma. The results showed that for thicker zinc coatings, laser-induced plasma is easily created for certain heat inputs. As a result, merely increasing the laser power during the first preheat pass may not necessarily be useful for vaporising thick zinc coatings. For instances where the quantity of the coating evaporated is not enough during the first laser pass, laser energy may be trapped by laser-induced plasma during the second laser pass which inhibits penetration of the upper section of the plate [78].

Too much laser-induced plasma creates instabilities during the process and leads to imperfections including creation of pores, zinc splashing and irregular weld penetrations. For zinc coatings which are too thin, the amount of zinc necessary for producing adequate Zn-Al phases becomes limited and thus allows for the creation of high amounts of Fe-Al based IMCs which negatively affect the joint strength. The EDS examination revealed that the Fe-Al IMC layer next to the steel side mainly contained Fe_3Al and FeAl whereas the layer next to the aluminium side mainly contained $FeAl_2$ and Fe_2Al_5. Accurate control of laser welding parameters maintained the IMC layer thickness at approximately 5 μm, confirming the claims made by Ma *et al.* [77].

It was stated that the method was successful in creating a lap joint with partial penetration and no defects [77]. It was further reported that no spatter, cracks, and blowholes were detected in the weld joint, and that the method was extremely stable. It was also stated that the optimal parameters for the study were 4.0 kW laser power and 50 mm/s travel speed for the first pass and for the second pass the optimal parameters were laser power of 3.2 kW with welding speed of 100 mm/s. On average, the joints strength was 158 MPa [77].

It was therefore concluded that correct selection of double-pass laser welding parameters and a regulated preheating process of Zn coated steel and aluminium can restrict the Al-rich IMC thickness to approximately 5 µm. It was discovered that extremely high amounts of heat input can completely evaporate the Zn coating and increase the weld's susceptibility to the creation of Fe-Al layer. It was mentioned that the availability of Zn in the IMCs has the potential to enhance the strength of a lap joint between Zn coated steel and aluminium alloys [77].

.

From another research by Yan *et al*. [79], a dual beam YAG laser with both continuous wave and pulsed wave modes was employed to join aluminium alloy A6111-T4 to steel JS270CC. It was stated that a shearing strength of 128 MPa was achieved and there was a semi-circle shaped IMC layer of 10 µm formed at the base of the weld zone. In another case, a silicon-based filler alloy A4047 was used to weld AA6022 and two different types of galvanized steels. It was reported that the strength of the resultant joint did not exceed 55 to 75% of the aluminium alloy strength as IMCs were created [80].

2.7 Common challenges associated with laser welding between aluminium and steel

Generally, fusion welding between aluminium alloys and various grades of steel is confronted with complications such as the creation of brittle IMC phases along the interface, vast differences in chemical, physical and mechanical characteristics which makes the welding process extremely challenging. For instance, if welding temperature is kept between the melting points of aluminium and steel which are 660 $^{\circ}$C and 1538 $^{\circ}$C respectively, the former completely melts while the latter remains in a solid form since laser power required to dissolve steel is extreme for aluminium [14]. The formation of liquid on the aluminium surface escalates the rate at which laser energy is absorbed and thus forms laser induced plasma resulting in instabilities during the welding process. The problem of different melting points in laser welding can however be minimized by a combination of welding and brazing process as confirmed by Laukant *et al*. [71].

Aluminium is very reactive and thus readily reacts with oxygen to generate high melting temperature Al_2O_3 film on the aluminium surface which makes the melting process of aluminium quite challenging. The melting point of Al_2O_3 is 2050 $^{\circ}$C and thus traps humidity quickly and

easily [81]. The presence of moisture on the weld zone decomposes into oxygen and hydrogen which results in porosity [81]. Additionally, the Al_2O_3 film has a tendency of creating slag which damages mechanical properties by creating a cover above the melting pool surface and thus prevents the liquid metal from flowing freely and eventually consolidates [81]. Aluminium and steel have different thermal expansion coefficients and thermal conductivities which exacerbates welding difficulties [82], [83]. This leads to the formation of complex residual stresses created by thermal stresses at room temperature throughout the welding process and consequently affects the fracture strength and fatigue failure of weld joints [84]. The solid solubility of Fe and Al is approximately 0.053 wt% and occurs at the eutectic temperature of 645 $^{\circ}$C. As solidification progresses, the probability of creation of hard and fragile Fe-Al based IMCs increases because these compounds greatly rely on temperature and time [85],[86]. The density of aluminium is 2.69 g/cm^3 whereas that of steel is 7.80 g/cm^3. This difference in density makes aluminium to float on top of steel if both aluminium and steel are melted [33].

Corrosion behaviour of laser welded joints between Zn coated steel and aluminium alloys are crucial. Factors that mostly influence corrosion resistance are the initiation and development of IMC phases, micro-segregation, defects, and the loss of Zn through evaporation. Corrosion performance diminishes at the HAZ and FZ [32]. Oxidation and degradation of alloying elements in the molten pool can be lowered by the application of high-density inert gases. It has been stated that the application of Ar shielding gas for a laser welding process presents improved resistance to corrosion compared to N_2 gas. This is possibly attributed to the higher density of Ar that helps protect against oxidation of parent metals more effectively [32].

Kashani *et al*. [87] also stated that the susceptibility of weld joints between zinc coated steels and aluminium alloys to porosity may be aggravated by using higher density shielding gases. The probability of such shielding gases to be entrapped within the keyhole area and the weld joint upon solidification is higher.

2.8. The effect of laser welding parameters on the quality of weld joints

The importance of laser welding parameters was highlighted by research performed by Sierra *et al.* [28]. It was discovered that different combinations of welding parameters govern the IMC layer thickness. The findings of the experiment are displayed in Table 2.3. The outcome indicated that the lowest thickness value of the IMC layer obtained was 3.8 µm and the highest was 22.2 µm.

Table 2.3: Laser welding parameters used for the tests [28].

Beam diameter, D_{beam} (mm)	**Power, P (kW)**	**Power density, PD (kW/m^2)**	**Travel speed, TS (m/min)**	**Interaction time, t_i (s)**	**Specific point energy, $E_{sp.}$ (kJ)**	**IMC thickness (µm)**
13	4	3.01×10^4	0.20	3.90	15.60	22.2
13	4	3.01×10^4	0.25	3.12	12.48	6.6
13	4	3.01×10^4	0.30	2.60	10.40	3.8
13	5	3.77×10^4	0.30	2.60	13.00	21.6
13	5	3.77×10^4	0.35	2.23	11.14	10.7
13	5	3.77×10^4	0.40	1.95	9.75	4.7

Dharmendra *et al*. [74] performed similar research to explore the impact of laser welding process parameters which include power, laser brazing speed and wire feed speed on the thickness of the IMC layer and mechanical properties. Laser welding-brazing technique was applied between an aluminium alloy and dual phase steel with an addition of Zn type filler material. The IMC layer thickness differed between 3 and 23 µm subject to different combinations of welding parameters employed, corroborating observations made by Sierra *et al*. [28]. It was also noted that the IMC layer thickness was inconsistent as it was higher at the middle of the seam and decreased toward the edges of the braze seam [74].

Qianqian *et al*. [4] researched the impact of fiber laser welding parameters on the mechanical response of an overlap weld joint between low carbon steel and 6016 aluminium alloy at welding velocity ranging from 1.5-2.5 m/min. It was revealed that there was a deficiency of material on

the weld joint when the lowest welding velocity of 1.5 m/min was employed [4]. On the other hand, a similar behaviour was detected when powers as high as 1450 W were applied with high welding velocities. This observation was attributed to the fact that the samples were produced at high energy absorption under low welding velocities. Another reason given for this behaviour was that higher laser input resulted in intense convection and consequently caused metal splashing [4]. The bead thicknesses obtained from the experiment were between 1.1 and 2 mm whereas the mean penetration depth ranged between 1.1 to 2.2 mm [4].

Laser roll welding between an aluminium alloy A6000 and two types of zinc coated steels namely hot-dip galvanized steel (GI) and hot-dip galvannealed steel (GA) was conducted by Ozaki *et al*. [8]. The impact of welding speed on the IMC layer thickness under the middle of the laser beam spot was examined. It was concluded that there was a noticeable reduction of the IMC layer thickness as the welding speed was elevated from 5.0 to 11.7 mm/s irrespective of the applied roll pressure for both types of steel in Figure 2.7 (a) and (b). The reason behind this observation was that increasing welding speed lowers the heat input and thus decreases diffusion of elements. As a result, these deviations in welding parameters can be used as a measure of suppressing the IMC layer thickness [8].

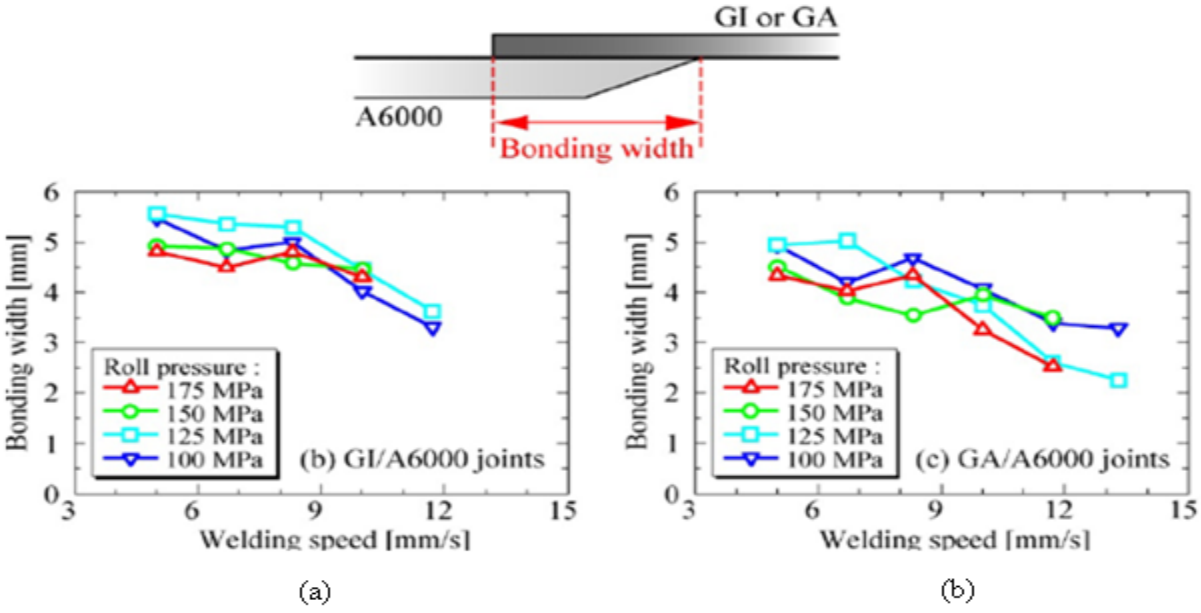


Figure 2.7: Influence of welding speed on bonding width at varying roll pressures; (a) GI-A6000 joint, (b) GA-A6000 joint [8].

Dissimilar materials offset laser welding was performed between 5052 aluminium alloy and press hardened steel by Cao *et al*. [88]. The intention of the experiment was to analyse the impact of various laser offsets (0.1, 0.2, 0.3 and 0.5 mm) on the weld surface appearance and mechanical properties. For a laser offset of 0.1 mm displayed in Figure 2.8 (a), there was evidence of spatter and solidification cracking (SC). An explanation given for the observation was that there was an increment of Al elements volume fraction within the molten pool which escalated the vulnerability to SC. The defects observed for 0.1 mm offset were not present for 0.2 mm offset and a denser weld texture was achieved as shown in Figure 2.8 (b). Further increase in laser offset to 0.3 and 0.5 mm resulted in a reduction of the density of the weld texture. Also, the weld seam appearance was inconsistent which became detrimental to the quality of the weld joint [88].

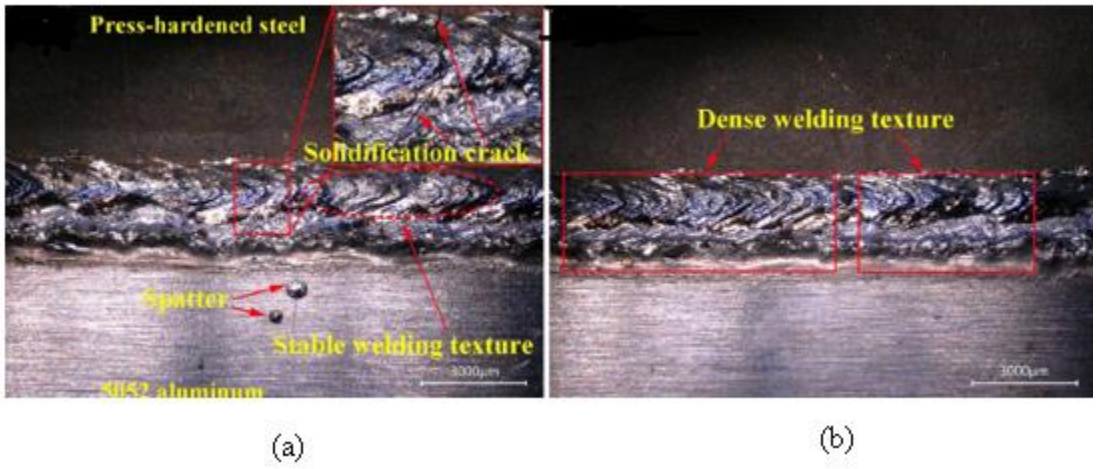


Figure 2.8: The appearance of the weld at various laser offsets: (a) 0.1 mm, (b) 0.2 mm [88].

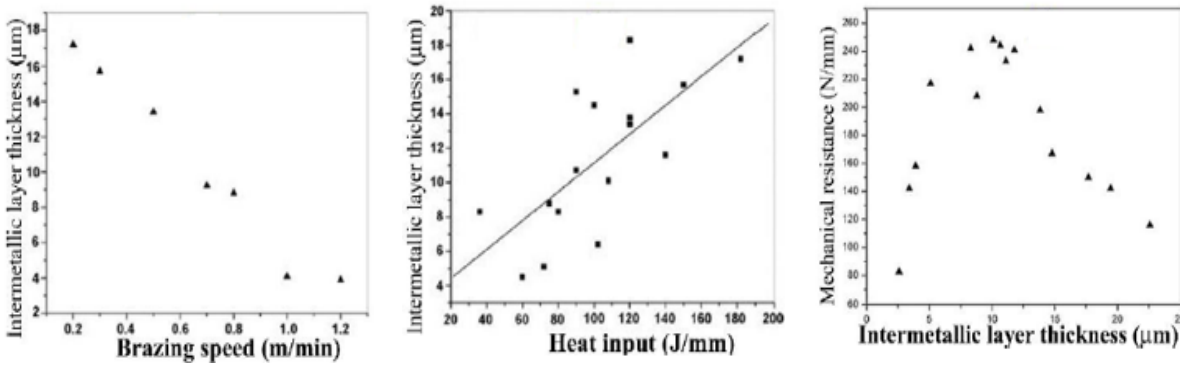
2.9 Optimization of laser welding parameters

Numerous attempts have been made to optimize the welding parameters, various filler materials, heat input rate and metallurgical inconsistencies such as the creation of oxide film that deter the weld joint eminence and wettability. This is significant in laser welding experiments for producing weld joints with high quality, good geometry, reduced roughness of the surface, uniform microstructure, and desirable mechanical properties [89],[90]. Laser welding speed has been proven to be the parameter which plays an imperative role in this regard [85], [91]. For

continuous laser welding, the most important parameters are laser power, welding speed and focal position [91]. From an experiment by Mathieu *et al*. [73], a filler wire with 85 % Zn and 15 % Al composition was utilized to combine aluminium to steel. The Taguchi method was applied to optimize the process parameters. It was revealed that a 200 MPa tensile strength was attained. However, a noticeable fracture was detected within the HAZ [73]. The IMC thickness was between 3 and 23 µm.

Information attained from research by Kim *et al*. [30], highlighted that the welding parameter with the highest impact on tensile strength is welding speed, followed by laser power and focal point. Nearly all laser welding experiments which produced the required microstructural and mechanical properties were performed using laser power ranging between 0.6 to 2.4 kW, welding speed between 0.82 and 3 m/min and focal point position between -0.8 and 0.2 mm. The shielding gas flowrate ranged between 5 to 15 L/min [30].

Krishnaja *et al*. [90] reviewed the progress of research of dissimilar laser weld-brazing for automotive applications and concluded that based on diffusion mechanism, the fusion period seems to have the greatest effect on the reduction of brittle phases of the reaction layer thickness as it controls the brazing speed. It was also discovered that the reaction layer thickness was reduced by an increase in both brazing speed and a reduction in heat input as depicted in Figure 9 (a) and (b).



(a) (b) (c)

Figure 2.9: Influence of welding parameters on the IMC thickness (a) Laser brazing speed, (b) Heat input, (c) Influence of IMC layer thickness on mechanical resistance [90].

Another revelation was that the mechanical resistance was initially enhanced by an increase in IMC layer thickness and started declining after reaching a maximum of approximately 243 N/mm for an IMC layer of about 12 µm as shown in Figure 2.9(c). This further proved that the IMC layer thickness should be restricted to avoid compromising tensile behaviour [90].

Pereira *et al*. [92] conducted an investigation to determine ideal laser welding parameters with respect to the resultant microstructural and mechanical properties. A pulsed Nd:YAG laser was used to create a lap joint between DP1000 steel and aluminium 1050 H11. Laser parameters which were under consideration are laser beam power and pulse duration recorded in Table 2.4. Laser beam diameter and superposition were kept unchanged at 1 mm and 60% respectively. From the results, it was concluded that laser powers exceeding 7.20 kW would result in full penetration of the aluminium plate. Diffusion of elements increased, exacerbating the weld joint brittleness. The best tensile test results were observed for a laser power of 6.48 kW and pulse duration of 14 ms, (for sample viii) from Table 2.4.

Table 2.4: Parameters used for the study of Al-steel welding process [92].

Sample number	Power (kW)	Pulse duration (ms)
i.	8.40	14
ii.	7.20	14
iii.	7.08	14
iv.	6.96	14
v.	6.84	14
vi.	6.72	14
vii.	6.60	14
viii.	6.48	14
ix.	6.36	14
x.	6.24	14
xi.	6.12	14
xii.	6.00	14

In one research by Peyre *et al*. [93], the impact of flux on the microstructural and mechanical characteristics of weld joints between galvanized steel and an aluminium alloy was inspected. The findings revealed that liquid flux obstructed the vaporization of the zinc covering as the welding process proceeded and thus constrained the creation of IMCs, voids, and fractures. These results were attributed to appropriate modifications of parameters that include laser welding speed, laser power and wire feed rate [93]. This increased the potential for regulation of the wetting angle of braze and IMC creation which subsequently improved the joint strength. Therefore, it was assumed that the wetting angle was reduced by an increase in heat input. Moreover, for small braze wetting angles, the wetting and distribution of the filler material becomes greater [93] Then again, at high heat inputs, the IMC layer thickness becomes greater which is unfavourable for mechanical behaviour. The outcome proved that optimization of laser welding parameters can limit the IMC layer thickness to between 3 and 23 μm, as observed in research by Sierra *et al*. [28] and Dharmendra *et al*. [74]. For welding speeds between 0.55 and 0.85 m/min yielding heat inputs from 60 to 110 J/mm, failure of the weld joint happened at the HAZ next to the aluminium parent metal achieving 220 MPa average tensile strength [93]. Additionally, it was recorded that the braze material geometry has a major impact on the mechanical strength expressed as mechanical resistance which is linear to L/θ whereby.

L = the braze length through the weld joint

θ = braze wetting angle

2.10 Microstructural and mechanical properties of weld joints between steel and aluminium

The welding process is considered a metallurgical procedure. Therefore, the quality of the joints is intensely influenced by the chemical, physical, thermal, and mechanical characteristics of the materials used for welding [94]. In general, the weld microstructure is governed by the heat transfer and thermal cycles which take place during laser welding process [95]. Figure 2.10 shows the interaction between thermal cycle and the microstructure of a laser welded structural steel. Micro-segregation and non-equilibrium phase changes which take place during solidification can also affect the development of microstructures within the weld. In laser welding, the anticipation is for micro-segregation to be lesser compared to other fusion welding procedures because of rapid heating and cooling rates [95].

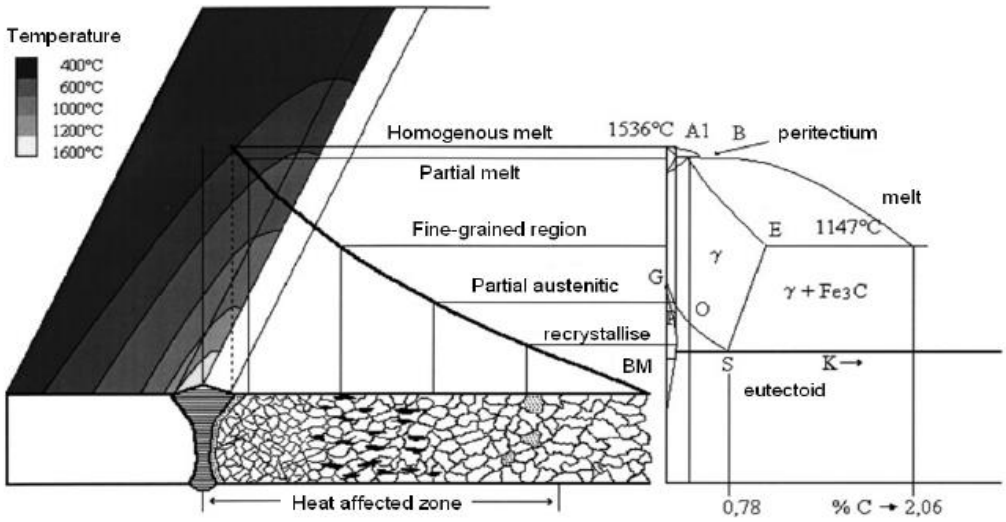


Figure 2.10: Relationship between the microstructure of welded structural steel and thermal cycle [95].

2.10.1. Weld bead dimensions

Weld penetration (area and depth) as well as bead geometry (width and bead height) are vital physical properties of a weldment [96]. The coarseness and breadth/thickness of the weldment are often used to express the quality of the weld joint [97]. It has been established that a few welding parameters influence both the weld penetration and bead geometry [96]. Several studies have proven that weld penetration depth can be regulated by laser welding parameters which greatly impacts the creation of weld defects, IMC layer thickness and mechanical properties of the weld joint [28], [72], [82].

Laser welding parameters which mostly influence these weld properties are heat input, welding speed, position of focal point as well as the rate of gas flow [97]. Ruggiero *et al*. [97] studied the weld bead profile and optimization of CO_2 welding of austenitic AISI 316 and low carbon steel. The parameters used were laser power (1.1 to 1.43 kW), welding speed (0.25 to 0.75 m/min) and focal position (-0.8 to 0.2 mm). It was deduced that the welding parameter which mostly affects the weld bead dimensions is welding speed [97].

An orthogonal design and a range evaluation were applied to establish the impact of laser parameters towards the bead profile between aluminium and steel joint by Qianqian *et al*. [4]. The thickness of the bead and the welding penetration were assessed using varying welding velocities and laser powers. The findings indicated that energy absorption was improved by

increasing laser power and reducing welding velocity [4]. Therefore, a high degree of penetration and a greater bead width was gained for lower welding velocities and high laser powers. The highest degree of penetration and greatest bead width were observed at laser power of 1450 W and welding velocity of 1.5 m/min whereas the lowest degree of penetration and lowest bead width were obtained for 1300 W and 2.4 m/min.

The concentration of aluminium within the weld bead and the heat input governs the creation of IMC phases, weld bead hardness, geometry of the weld and consequently the thickness of the IMC layer [98]. The weld bead geometry determines the structural stiffness. For this reason, it is imperative to regulate the geometry by modifying the laser welding parameters to accomplish good weld joints [98]. Sierra *et al*. [28] and Kouadri-David [99] agreed that the mechanical strength should be improved by constraining the penetration depth to reduce the IMC layer from high dilution of aluminium and steel. Seffer *et al*. [100] reported that moderately low weld penetration depths result in high mechanical strength and added that these results can also be achieved by an increase in weld width of the seam.

The aim of a research by Yuce *et al*. [1] was to inspect the microstructure and mechanical characteristics of an aluminium alloy and a high strength galvanized steel laser weld joint. It was disclosed that there is a connection between weld penetration, creation of IMC layer and fracture morphology. It was also reported that previous research showed that heat input levels below 27.5 J/mm resulted in inadequate penetration and at heat input above 40 J/mm there was destruction of BMs. As a result, heat input between 28.5 J/mm and 36.3 J/mm was used. Another revelation was that increasing heat input result in larger weld penetration and larger weld width for most samples [1].

The microstructural examination by Narsimhachary *et al*. [101] on a laser weld brazed joint between AA6082 and galvanized steel showed the relationship between various bead profile parameters and laser power. The results disclosed that an increase in laser power increased the penetration depth. The lowest laser power utilized (2.5 kW) resulted in a braze penetration of 1800 µm whereas the highest laser power (4 kW) produced a greater penetration of 1925 µm. This behaviour is attributed to an increased degree of melting as laser power increases [102]. These results corroborate those obtained by Torkamany *et al*. [72].

Liu *et al.* [76] performed laser fusion-brazing between a 1.5 mm thick A5052-H34 aluminium alloy to a 0.8 mm thick STO7Z galvanized steel using a 4 kW Nd:YAG. The metal plates were arranged in a lap joint and a filler material in the form of a pure Al powder was added. The higher the laser power, the greater the weld width when the power feed rate was kept constant. This occurs due to an enhanced moistening and distribution of the filler material throughout steel base surface as heat input increases [76]. Additionally, at low powder feed rate, the degree at which aluminium base melts increases as the powder feed rate increases. However, a further increase of powder feed rate results in inadequate melting of both aluminium base plate and Al powder which reduces the heat transfer towards the steel plate, reducing the filler wetting and thus reduces the weld width.

2.10.2 IMC phases and IMC layer thickness

The soundness of the weld joint is principally controlled by the creation of IMC phases since these compounds influence the vulnerability to SC [32]. Therefore, it is imperative to deeply understand and efficiently regulate the creation of brittle IMC phases in laser welding of dissimilar metals.

Liu *et al*. [76] stated that at extremely low powder feed rates the galvanized steel surface easily traps laser power and creates evaporation of Zn which increases the production of pores at the weld base. An XRD analysis performed along the steel-braze interface revealed that the most prevalent IMC detected was $Fe_2Al_5Zn_{04}$. Similarly, Shabadi *et al*. [102] discovered the presence of a 10 µm thick $Fe_2A_{15}Zn_x$ IMC at the bond area. The results were acquired from a laser brazing process used to fuse low carbon galvanized steel and an aluminium alloy AA6016 with an addition of a zinc-based aluminium alloy filler material [102]. The chemical composition of the IMC layer observed by Vrenken *et al*. [103] for the analysis of fluxless laser brazing of Superlite ^{R} 200 AA6016 aluminium alloy to galvanized steel EN10292, did not show any presence of Zn. Instead, only Fe, Al and Si were found. This means that the resultant weld joint was a true aluminium-steel joint [103].

Yuce *et al*. [104] combined DP600 galvanized steel with an aluminium alloy 6082-T6 in a zero-gap lap joint alignment using an automated laser arm robot. The influence of heat input and weld

penetration depth on the creation and thickness of IMC layer was examined. EDS analysis was performed on the dissimilar weld joint to obtain the atomic percentage of Fe and Al at varying heat input levels and weld penetration depth. SEM image for 33.3 J/mm heat input level and 412.8 µm penetration depth is displayed in Figure 2 .11 (a). The corresponding EDS analysis showed that the average composition of Fe and Al at the FZ were 76.48 % and 13.61 % respectively. The results showed that the weld seam depth increased with an increase of aluminium quantity [104]. The results also indicated the presence of Fe-rich IMCs namely, Fe_3Al and FeAl within the weld bead and Al-rich IMCs ($FeAl_2$ and Fe_2Al_5) were created adjacent to the borderline of the weld bead in the Al sheet. A microcrack was spotted near the Fe_2Al_5 phase which was found to be the most brittle phase detected and had the highest hardness value of 1144 HV.

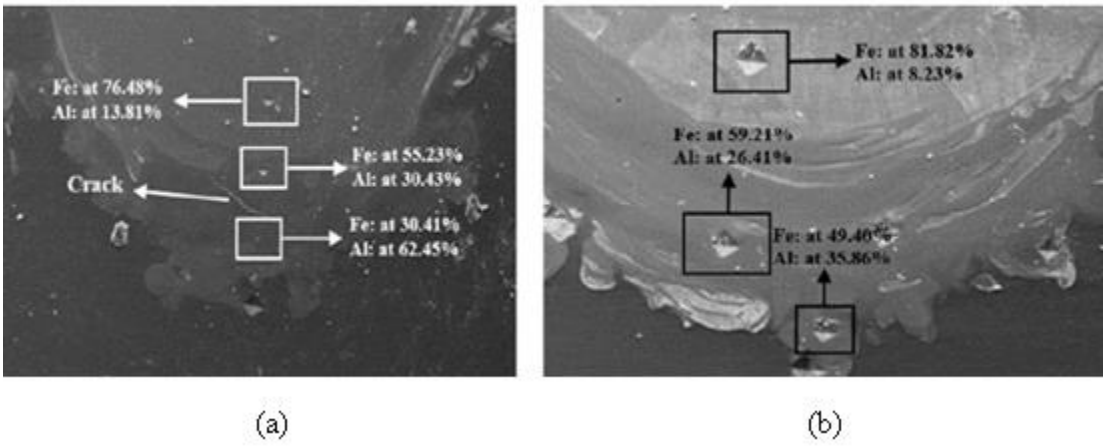


Figure 2.11: EDS analysis points at varying heat input. (a) 33.3 J/mm, (b) 28.5 J/mm [104].

The boundary morphology was transformed for lower parameters that is, heat input level of 28.5 J/mm and penetration depth of 212 µm as shown in Figure 2. 11 (b). No Al-rich IMC phases were detected on the weld bead edges. The greatest Al content obtained from EDS was 35 %. Less brittle Fe-rich IMC phases (Fe_3Al and FeAl) were detected. It was concluded that increasing heat input levels increases the weld penetration and weld width which consequently increases the Al composition and Al-rich IMCs along the weld seam and boundary [104].

An overlap joint between different combinations of steel and aluminium from a conduction mode laser welding was created by Meco *et al*. [10]. The first trial was between XF 350 steel and

AA5083-H22 aluminium alloy. The second test was between a low carbon galvanized steel and AA2024 aluminium alloy. For a spot size of 10 mm, the thickness of the IMC layer at the centre was approximately 12.6 µm and was much greater in comparison to 3.5 µm detected at the edges of the weld. This behaviour could have resulted from the shorter thermal cycle that occurs at the weld edges compared to the central section of the weld joint [10]. The SEM analysis revealed that the weld interface constituted of varying IMC phases. At first, $FeAl_3$ was spotted close to the aluminium side and then changed stoichiometrically to Fe_2Al_5 after the layer increased to a specific quantity as shown in Figure 2.12. The weight and atomic percentage distinctions for Fe and Al for both components at different positions are displayed in Table 2. 5. It was discovered that for Zn coated steel, the creation and development of the IMC layer resulted in a more uneven distribution configuration and the later was more regular for uncoated steel whose phases also displayed stoichiometric relations [10].

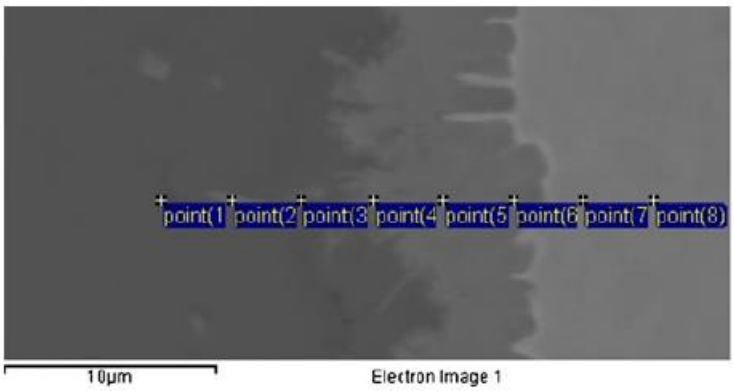


Figure 2.12: Points of EDS performed on the micrograph [10].

Table 2.5: EDS Semi-qualitative analysis results [10].

	Al (wt %)	**Fe (wt %)**	**Al (wt %)**	**Fe (wt%)**	**Remarks**
Point 4	67.36	32.64	81	19	$FeAl_3$
Point 5	58.22	41.78	74	26	Fe_2Al_5

Lee *et al*. [105], welded together an aluminium alloy A6111 to a low carbon steel SPCC in an overlap arrangement. The deepness of the melt was retained at approximately 90 % of the steel plate's thickness and thus resulted in melting of the top aluminium surface into a semi-elliptical structure. The greatest attainable tensile shear strength was almost 70 % that of the aluminium

BM. XRD analysis displayed in Figure 2.13 confirmed the presence of Fe_4Al_3, Fe_2Al_5, $FeAl_2$, Fe_3Al and $FeAl_{16}$ phases within the melt which were represented by needle-like IMCs [105].

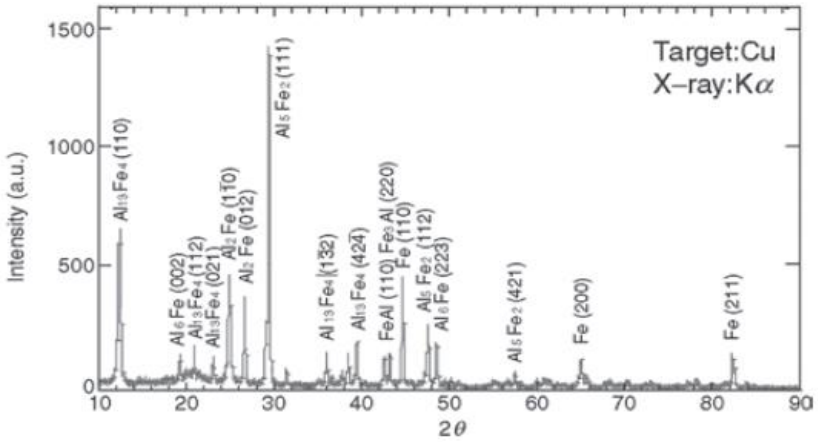


Figure 2.13: Various types of IMCs shown on XRD pattern of a fracture surface [105].

Meco *et al*. [106] studied the use of LBW between aluminium and steel for application in structural parts. The results revealed that there was incomplete melting near the top part of the steel sheet where it was exposed to laser as it was noticed from the weld cross section presented in Figure 2.14. It was also clear that the steel near the Fe-Al interface did not change its solid phase [106].

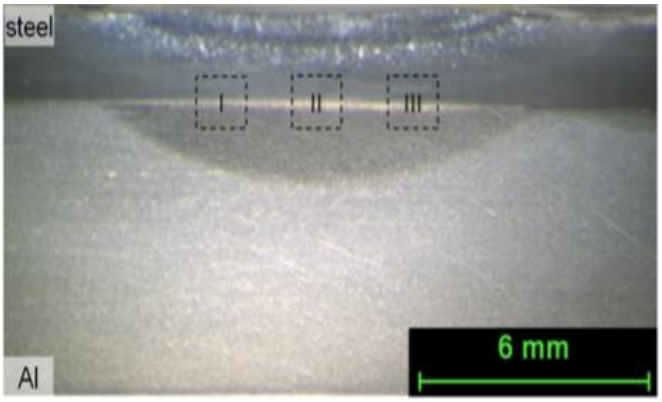
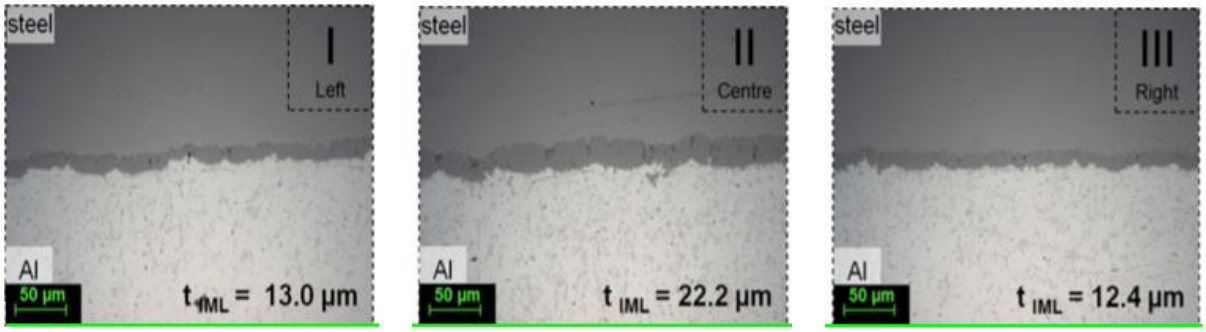


Figure 2.14: Microsection of the IMC layer thickness [106].

Similar behaviour was also noticed under various welding conditions such as when the specific point energy [Esp.] was at its minimum value of 9.75 kJ [106]. The intention was for the temperature at the Fe-Al interface to exceed the melting point of aluminium. This can be obtained by sustaining the temperature gradient through the steel plate thickness at high levels during heating of the top steel surface [106].

It was also detected that the IMC layer thickness varied through the cross section of the weld. The IMC layer thickness was lower at the sides of weld as depicted in Micrograph 1 and 3 and then increased adjacent to the centre of the weld demonstrated in Figure 2.15. These findings correspond with those obtained by Dharmendra *et al*. [74]. Also, Ozaki *et al*. [8] recorded the IMC layer thickness averages as 4.1, 13, and 4.9 µm for steel edge, laser beam spot centre and aluminium edge respectively. The thickest IMC layer was measured at the middle part. These variations in thickness could be credited to the fact that temperature closer to the middle section of the weld is greater and the cooling rates are slower whereas the temperature at the boundaries of the weld is lower and there is rapid cooling rate [106],[107]. There are three main aspects which could be influencing this behaviour: (a). the material around the weld zone consuming heat from the weld zone; (b). the laser beam which induces elevated temperatures around the weld centre due to its intensity profile and (c).at the centre, there is high reaction time compared to the interaction at the weld edges. According to literature, the formation of the IMC layer is governed by diffusion and thus largely depends on time and temperature conditions amid the welding process [106].



(a) (b) (c)

Figure 2.15: IMC layer thickness variation through cross section of weld joint [106].

The optical micrograph depicted in Figure 2. 16 revealed two separate layers which make up the IMC layer [106]. The layer close to the aluminium sheet was found to be $FeAl_3$ and was thin whereas the layer close to the steel sheet was Fe_2Al_5 which is wider and largely determined by temperature and time [107]. Since low temperatures are experienced at the edges, only the $FeAl_3$ layer was detected. This is mainly subject to free energy of formation of $FeAl_3$ is low which

makes the phase readily thermodynamically feasible. On the other hand, the formation of Fe_2Al_5 is mostly dependent on kinetics of the process hence its uneven thickness through the weld interface [107].

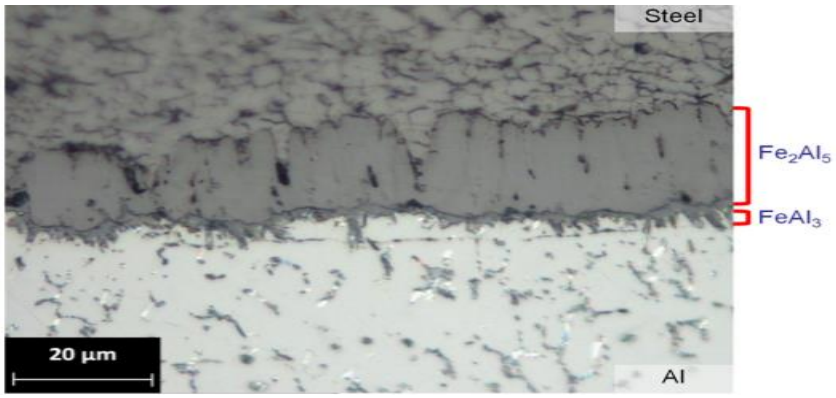


Figure 2.16: Two different IMC layers [106].

2.11 Corrosion properties of dissimilar materials

Corrosion is most likely to happen between the transition region of two dissimilar materials [69]. For two welding metals that are at vastly different locations of the electrochemical scale, the degree of susceptibility to corrosion is much higher which imposes challenges for the dissimilar joint [69].

Shi *et al*. [108] examined the corrosion properties of 1060 aluminium alloy and galvanized steel lap joint produced by GMAW. Aluminium silicon and aluminium magnesium filler materials were added in different tests. Both electrochemical and immersion corrosion tests were employed. The findings revealed the presence of galvanic corrosion for immersion corrosion experiments. It was also discovered that increasing heat input increased the rate of corrosion of the weld joints. Corrosion rate was much higher when aluminium-silicon filler material was used compared to aluminium-magnesium filler material. The region on the weld joints which was Zn-rich was more susceptible to corrosion [108]. The outcomes confirm those obtained by Wloka *et al*. [109] on the corrosion behaviour analysed by salt spray test on laser beam welded joints between steel and aluminium. The two filler materials used for the experiment are $AlMg_6Mn$ and $ZnAl_2$. It was reported that welding process formed a Zn-rich region exhibited Figure 2.17 which was found to be most sensitive to corrosion. The high amount of Zn at the runout resulted in

creation of Zn-aluminium microstructure that has the most negative potential and was the first to melt away [109]. It was further noted that improved corrosion resistance was obtained when $ZnAl_2$ filler material was used.

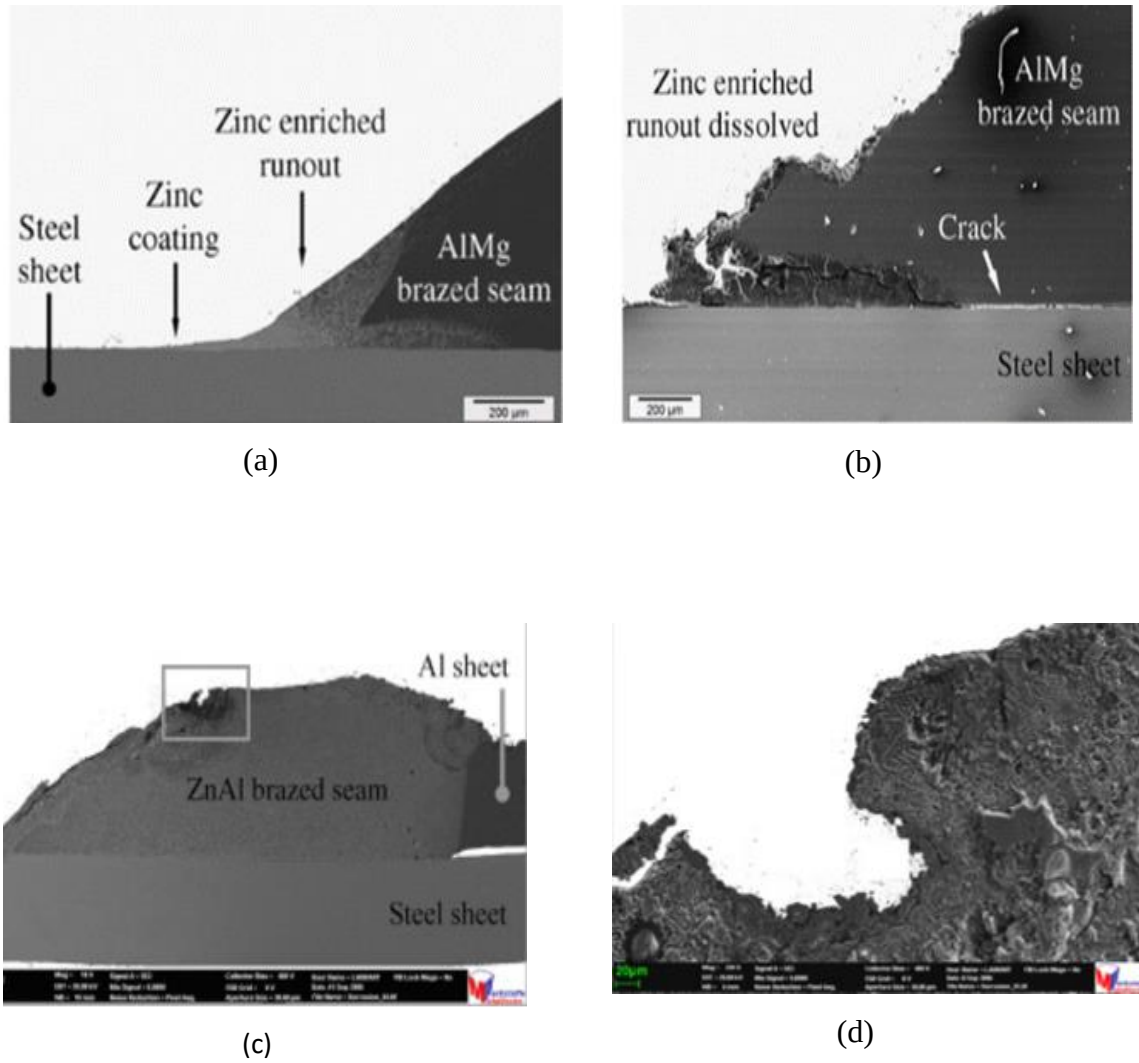


Figure 2.17: Weld joint produced from $AlMg_6Mn$ filler material (a) before corrosion, (b) after corrosion and weld joint produced from $ZnAl_2$ filler material (c) before corrosion, (d) after corrosion [109].

Shi *et al*. [108] further reported that the presence of IMCs at the interfacial region resulted in scattering of the nearby weld seam and thus quickened galvanic corrosion. As the IMC layer thickness increased, the corrosion resistance of the weld was reduced. These results contradict those obtained by Saleh *et al*. [110] from using Transient Liquid Phase (TLP) bonding to join 6063 aluminium alloy and Duplex alloy 2304 stainless steel. The findings demonstrated that as

the bonding temperature increased, the reaction layer thickness also increased. Increased heat input led to higher corrosion current density. It was deduced that the corrosion resistance of the dissimilar joints upgraded as the reaction layer became thicker. Figure 2.18 showed that, as the bonding temperature extended from 550 ^{0}C to 570 ^{0}C, the polarization curves moved towards a more positive potential which denoted improvement in corrosion resistance [110].

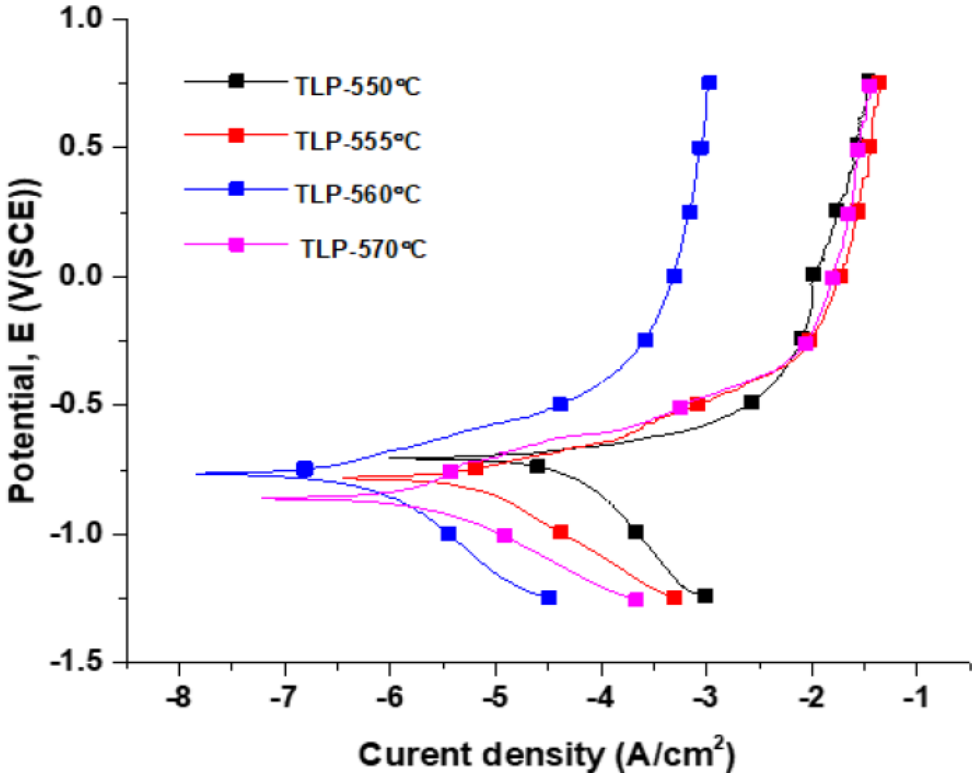


Figure 2.18: Polarization curves of joints produced at different TLP bonding temperatures [110].

Chen [32], investigated the impact of N_2 and Ar shielding gases on the corrosion resistance of laser-welded joints between EN-AW-5754 Al alloy and DX54 Zn coated steel. Electrochemical polarization analysis was performed on the joints using 3.5 % NaCl electrolyte at 25 ^{0}C. The results indicated that the appearance of the top surface produced from N_2 gas was mostly affected by corrosion. It was discovered that for weld joints produced from Ar, the critical current densities were higher, and the corrosion potentials were less negative than those produced with N_2 gas. The same behaviour was observed for all combinations of laser power and laser welding speed for single passing welding [32].

2.12 Mechanical properties

2.12.1 Microhardness analysis

LBW is characterized by rapid cooling and solidification rates coupled with non-equilibrium processes. As a result, it is expected for finer microstructures to be produced which consequently lead to increased hardness values [46].

Meco *et al*. [10] identified that, not only the IMC layer thickness is accountable for the weld joint strength. The composition, alignment, diffusion and bonding mechanism of Fe and Al elements also plays a part in the mechanical strength of weld joints. The hardness of the interfacial region is elevated by the recrystallizes [31]. The ranges of hardness values of typical Fe-Al intermetallic phases at 25˚C are demonstrated in Table 2. 6.The hardness values of the IMCs were much greater than those of Fe and Al. A schematic diagram in Figure 2.19 represents a characteristic hardness profile of dissimilar weld joint between steel and aluminium.

Table 2.6: Typical Fe-Al IMCs and Vickers Hardness ranges of the compounds [31].

Phases	**Vickers Hardness (9.8 N)**
Fe (Steel)	180-480
FeAl	491-667
$FeAl_2$	1058-1070
$FeAl_3$	772-1017
Fe_2Al_5	1000-1158
Fe_3Al	344-368
Al (5×××, 6×××)	35-150

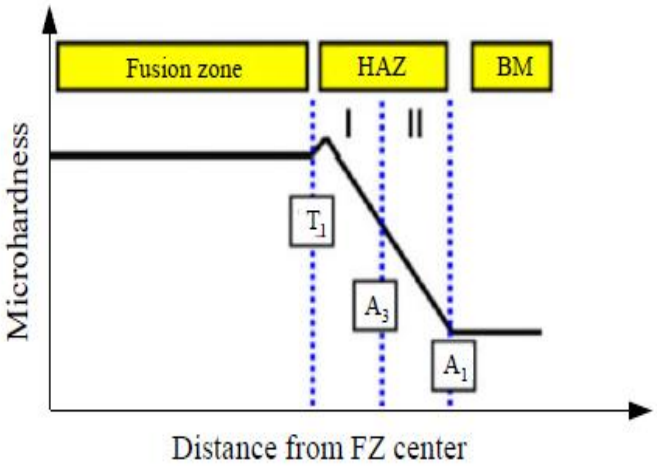


Figure 2.19: Schematic of a representative hardness profile of steel-Al fusion welds [111].

The hardness declines from the FZ towards the parent metal. Maximum hardness is experienced within the FZ and the HAZ. A steady reduction of hardness takes place from the FZ to the BM.

The hardness results obtained by Hui-Chi [32] are shown in Figure 2.20. The BMs used for the experiment were a DX54 Zn-coated steel and EN-AW-5754 aluminium alloy both of 1.0 mm thicknesses. Single mode continuous wave IPG fiber laser was used to create a weld seam. The hardness profiles were performed at three different levels of penetration namely 250, 750 and 1100 µm.

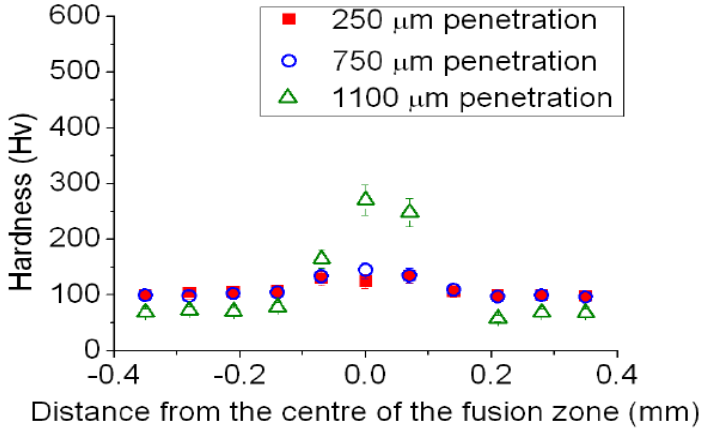
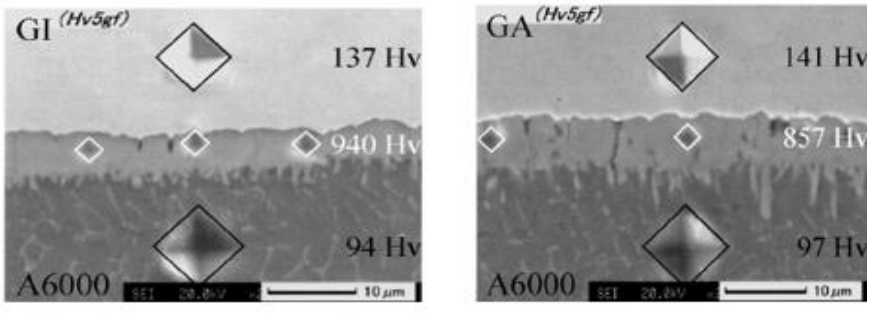


Figure. 2.20: Hardness distribution for single pass welding at different penetration depths [32].

The average hardness of steel base material was about 101.3 HV whereas that of aluminium was approximately 67.9 HV. The hardness profiles for 250 and 750 µm exhibited a similar behaviour.

The highest hardness was recorded close to the FZ confirming the claims made in [31]. For 1100 µm, the hardness at the middle of the FZ was higher than for both 250 and 750 µm penetration levels.

In a similar manner, Sierra *et al.* [112] joined 6000 series aluminium alloy and low carbon steel in a lap joint using a key-hole laser welding mode for optimization of the process, characterization of material and testing of mechanical tests. Hardness profiles were done at three different levels of penetration namely 120, 380 and 640 µm. It was discovered that there were small differences in hardness values and the average increased with an increase in penetration depth. Subsequently, the aluminium ratio increased due to a good relationship between aluminium content and joint hardness [112]. At 120 µm penetration level, the average hardness was 220 HV at 5 at. % Al. Weld penetration of 380 µm corresponded with an average hardness of 260 HV and 8 at. % Al whereas 640 µm had an average hardness of 360 HV and aluminium content of 20 at. %. The greatest hardening effect for individual values greater than 400 HV was due to the impact of steel quenching. It was also noted that the steel HAZ hardness increased from 180 to 270 HV due to refining of grains amid recrystallization process and the effect of quenching which caused a fine acicular microstructure [112]. Ozaki *et al*. [8] carried out a Vickers hardness test across the weld interface to predict the IMC phases created between two different grades of zinc coated steel and A6000 aluminium alloy. The average hardness values for steel, IMC layer and aluminium are displayed in Figure. 2.21. In both cases, the hardness of the IMC was greater than the hardness of the BMs. Referring to Table 2.6, it is safe to assume that the created IMC phase was mainly $FeAl_3$.



(a) (b)

Figure 2.21: Measurements of Vickers hardness indentations at the joint interface [8].

Meco *et al.* [106] performed a microhardness analysis through a vertical line across steel, through the weld joint to the aluminium side. There was an irregular hardness curve on the steel side because of incomplete dissolution which took place near the top part of steel which resulted in the formation of different metallurgical phases. The maximum hardness value was detected on the IMC layer and had a value of 1145 HV.

2.12.2 Tensile strength analysis

Often, structures are constructed in such a way that when subjected to stress, only plastic deformation should occur [68]. Therefore, it is necessary to understand the stress level whereby plastic deformation of the structure commences or at a point where the yielding phenomenon occurs. As a result, tensile tests are conducted in engineering materials to establish the maximum tensile strength that materials can endure before fracture occurs [68].

In dissimilar metals welding, the creation of intermetallic phases is crucial as it plays a role in the reduction of weld toughness. Hirose *et al*. [113] investigated the defect structure of Fe_2Al_5 IMC by deforming it through compression at elevated temperatures. The findings revealed that at temperatures less than 500 ^{0}C, Fe_2Al_5 was brittle and as temperature was further increased above 600 ^{0}C, Fe_2Al_5 phase displayed plastic behaviour when subjected to tensile test [113]. The plastic deformation which occurred above 600 ^{0}C was said to have been governed by the Peiels mechanism which incorporates the correlation between applied stresses, strain rate and temperature on the probability for dislocation slip [113]. As temperature is increased, the energy necessary for slip to take place decreases which increases the potential for slip to occur at lower force applied at equal strain rate [114]. Kang *et al*. [115] reported that Fe_3Al exhibited higher yield strength that ranged between 450 and 600 MPa at room temperature and achieved elongations as high as 8-12 %. On the contrary, depending on the applied heat treatment process, the yield strength of FeAl was found to be 350 MPa with elongation ranging between 6 and 17 % [114].

From research by Narsimhachary *et al*. [101], the highest joint efficiency of 80 % was acquired for a sample produced at a laser power of 4 kW. Tensile failure occurred on the aluminium side. A similar type of failure was observed by Su *et al*. [116] for a braze joint between zinc coated steel and 5052 aluminium alloy with an addition of 4047 Al-12Si filler wire. The maximum

achievable strength was 205 MPa and the created IMC layer thickness ranged between 4 and 7 µm [116]. Laukant *et al*. [71], also stated comparable results when AA6061 aluminium alloy was brazed with galvanized steel. The results from Narsimhachary *et al*. [101] further revealed tiny depressions and coarse irregular surface of a ductile type of fracture for 4 kW. The joint efficiency lowered to between 70 and 75% for lower laser powers between 3.0 kW and 3.5 kW. A mixture of both brittle and ductile fracture mode was exhibited at the galvanized steel interface whereas an irregular ductile failure morphology was observed on the aluminium side.

A significant decrease of the IMC was observed by Chen *et al*. [117] and it was attributed to the application of N_2 as a shielding gas for fiber laser welding between Zn coated steel and Al alloy. To support the claims, it was also reported that the application of N_2 decreased the hardness differences across the FZ and that the shear strength was higher than when Ar is used presented in Figure 2.22. This could have been because N_2 has a higher thermal conductivity in comparison to Ar. This benefit can result in an increase of the melt and rate of cooling during the laser welding process [117]. Consequently, the diffusion and mixing of Fe and Al elements is restricted hence the reduction of IMC development. Another advantage of selecting N_2 as a shielding gas is that the N_2 plasma reacts with the evaporated Al to create aluminium nitride (AlN) which substitutes the formation of Fe-Al IMCs.

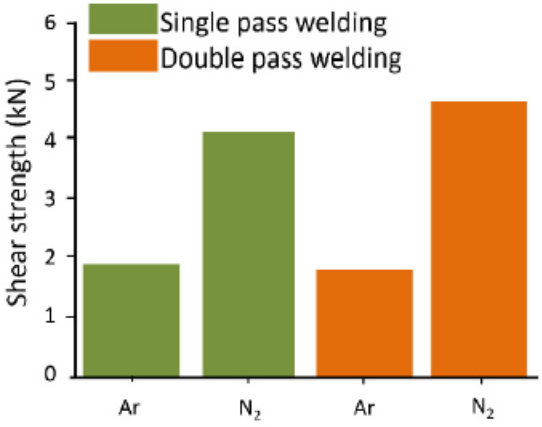
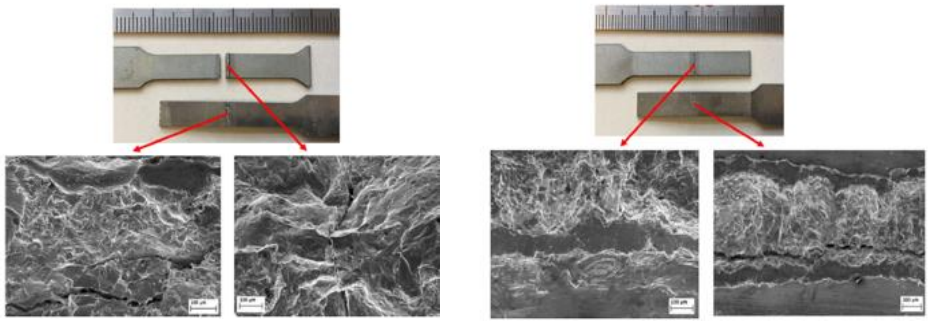


Figure 2.22: Influence of Ar and N_2 on shear strength using single and double pass welding [117].

Tensile tests performed by Yuce *et al*. [1] revealed that two distinct failure modes were detected. The failure morphology for weld joints produced at the lowest and highest inputs are displayed in Figure 2.23. It was stated that at the greatest heat input, failure took place within the fusion

borderline of the steel side. The reason for this observation was attributed to the intensification of aluminium content within the weld seam which is driven by an increase in weld penetration depth [116]. Figure 2.23 (a) shows that cracks were created in the IMC layer because of low elasticity at this region which increased fracture susceptibility when subjected to tensile force. On the other hand, for low heat inputs with low weld penetration depths, crack propagation occurred in the IMC region on the Al-weld interface as exhibited in Figure 2.23 (b).



(a) (b)

Figure 2.23: Fracture surfaces and modes at varying heat inputs. (a) 36.3 J/mm, (b) 28.5 J/mm [1].

Laser roll welding was suggested by Ozaki *et al*. [8]. The aim of the technique was to decrease the creation of Al-rich IMC phases by reducing the heat cycle and increasing the rate of heat transfer between the two surfaces which are under pressure contact. It was revealed that the maximum shear strength attained from the experiments was 162 N/mm for a roll pressure of 150 MPa and welding speed of 8.3 mm/s. The results also showed that the shear strength was reduced when the IMC layer thickness exceeded the 10 µm mark. Also, it was noticed that for IMC layer thicknesses less than 10 µm, the tensile shear strength test fracture of the samples happened at the BMs and not in the weld joints [8].

2.13 Progress trend in aluminium and steel laser welding

There has been so much progress in laser welding of aluminium and steel over the past few years in terms of its precision by application of various wavelengths, laser welding speed, laser welding power, and power density. Nevertheless, the incapability of the process to generate weld joints with characteristics suitable to meet the standards of function sometimes restricts the

widespread application for aluminium and steel welding [11]. Laser welding does however provide benefits such as adjustable heat input, high energy density, limited deformation, and the ability to be used for complicated welding positions and shapes due to extraordinary levels of automation. A combination of these advantages, deep weld penetration and required mechanical properties can be achieved by laser-arc hybrid welding.

Both laser welding and laser arc hybrid have the ability of combining zinc coated and uncoated steels to aluminium alloys successfully and will thus garner investigation and advancement attention in the future. At present, the creation of inevitable Fe-Al IMCs and unacceptable quality of mechanical properties limit the broad application of fusion welding and fusion-brazing between aluminium and steel. As a result, the principal research topic currently is based on the regulation and reduction of the nucleation and growth of IMCs. This is because IMCs are a chief hindrance to overcome in dissimilar materials welding [11].

Focus should also be on the minimization of other welding flaws such as porosity, cracking, and weld penetration discrepancies [11]. There has been progress in terms of the enhancement of weld joint mechanical properties by utilizing laser-arc hybrid fusion welding and braze welding by correct selection, addition, and management of a filler material. Currently, a large extent of the work is still in trial stage, the dominant philosophies and technologies are still developing. More work still needs to be done to address various combinations of different grades of steel and aluminium alloys and different types of joints to discover new techniques for improvements of weld joint properties [11].

Chapter 3 : RESEACH DESIGN AND METHODOLOGY

The design of each research project is important as it determines whether the objectives of the project are achieved or not. Chapter 3 describes the nature and properties of base materials used for the project. This chapter also provides details on the procedures followed in different experimental tests. The laser machine operational settings and parameters of the equipment used are also given in this chapter.

3.1 Base materials

The two dissimilar materials that were selected for the present study were Zn coated steel Z225 and aluminium alloy Al 5754. The material properties of pure metallic elements which are the principal constituents of both base materials are provided in Table 3.1.

Table 3.1: Material properties of pure metallic elements [118].

Property	Fe	Al	Zn
Melting point (˚C)	1538	660	419
Boiling point (˚C)	2861	2520	907
Thermal conductivity	80	238	113
Coefficient of expansion	12.1	23.5	30.2
Specific heat	449	897	388
Density	7.87	2.70	7.14
Yield strength	540	90	90

The chemical composition of Al 5754 and Z225 are displayed in Table 3.2 and Table 3.3 respectively

Table 3.2: Chemical composition of Al 5754 base material [119].

Chemical composition (%)	**Al**	**Mg**	**Si**	**Ti**	**Mn**	**Fe**	**V**	**Cu**	**Zn**
Al 5754	Bal.	3.03	0.02	0.25	0.18	0.27	0.01	0.003	0.002

Table 3.3: Chemical composition of Z225 base material [120] [121].

Chemical composition (%)	V	Cu	Fe	Mn	Zn	Sl	P	S	Mo	Ni
Z225	0.071	0.250	99.50	0.370	Bal.	0.270	0.014	0.009	0.016	0.012

3.2 Experimental procedure

The experiments performed in the current study explored the practicability of joining Z225 and Al 5754 by LBW without adding a filler material. A succession of tests such as metallographic examinations, electrochemical experiments and mechanical tests were conducted. The focus was to obtain weld joints which meet the automotive industry requirements regarding hardness variations, weld strength and surface finish. The details of the tests and the methodology are given in the subsequent sections.

3.2.1 LBW process

A CO_2 laser cutter was used to cut the two base materials namely Z225 and Al 5754 into metallic plates with dimensions presented in Table 3.4.

Table 3.4: Dimensions of the base materials.

Material	Length (mm)	Breadth (mm)	Width (mm)
Zn-coated steel (Z225)	30	50	0.8
Al alloy (A1 5754)	30	50	1.2

The Council for Scientific and Industrial Research (CSIR) laser department in Pretoria, South Africa offered the equipment used for the LBW experiment. The automated laser welding system was operated from a KUKA60L30HA arm robot connected to a Precitec YW 50 welding head. The equipment assembly is presented in Figure 3.1. The laser welding robot used a IPG continuous wave fiber heat source with a wavelength of 1.06 µm and 3000 W maximum laser power. A focusing lens with a constant laser beam diameter of 0.4 mm was used. Helium gas released at 10 L/min flowrate was applied as a shielding gas.



Figure 3.1: KUKA60L30HA automated laser arm robot at CSIR, Pretoria.

3.2.1.1 Laser welding configuration

A lap joint alignment was created between the dissimilar base materials. The steel plate was situated above the aluminium plate and a 3 mm overlap width was maintained throughout the experiment. The schematic representation in Figure 3.2 portrays the arrangement. A clamping system was used to avoid a microscopic opening between the base materials during welding.

Key-hole mode laser welding approach was applied. Heat was subjected to steel and the flow descends to the aluminium plate because of a positive gradient on thermal conductivity. A 12 mm gap between the work piece and the laser head was kept constant throughout the experiment. All the experiments were conducted in the absence of a filler material was used in all the experiments.

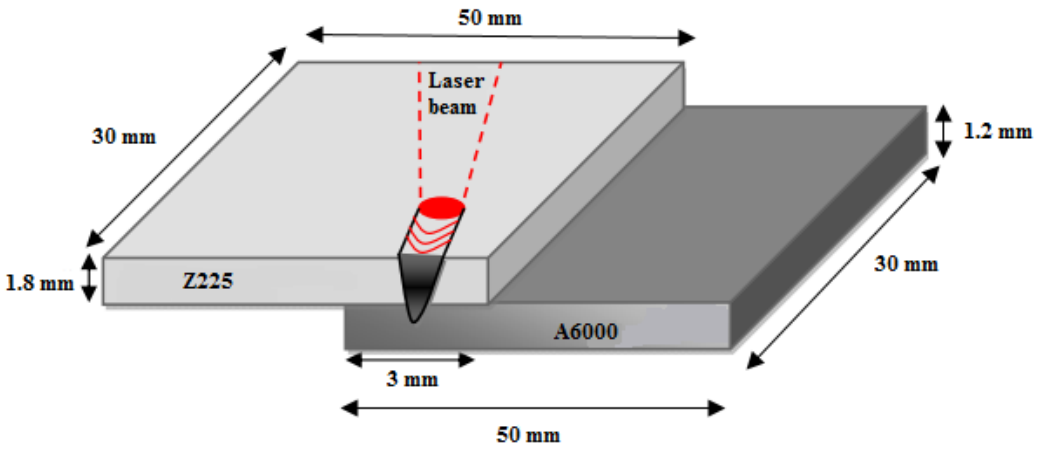


Figure 3.2: Illustration of an overlap joint between Z225 and Al 5754 (modified from) [122].

The process parameters which were controlled during the process are.

- Laser welding speed
- Laser welding power

Table 3.6 and 3.7 depict the exact combinations of laser welding speed and laser welding power used to produce the samples for the study. It is important to note that there are various tests which were initially executed before reaching the optimised laser welding parameters displayed in Table 3.5 and 3.6. The preliminary experiments produced unacceptable results characterized by either incomplete fusion or over-penetration. Laser powers of 1300 W and below, and laser welding speeds greater than 3 mm/s were not enough to melt and fuse Z225 and A5754. On the other hand, laser welding speed less than 1 mm/s resulted in excessive penetration and caused a collapse of the aluminium surface. Laser power of 1500 W was chosen to study the effect of laser speed because one of the objectives of the project was to limit the creation of brittle IMCs as much as possible. The idea was to achieve the most desirable properties at the lowest possible heat input. At 1400 W, joints were created however most samples failed due to insufficient fusion. The calculations of power density from equation (1) presented in Table 3.5 and 3.6 have proven that the experiments were performed in keyhole mode as all the values were greater than 10^6 W/cm^2.

Power density (W/cm^2) = $\frac{Laser\ power}{Area_{beam}}$ ..... (1) [43].

During laser welding process, it was observed that at laser welding speed below 3.0 mm/s, there were sparks that usually indicate too much mixing. However, this behaviour was not observed at 3.0 mm/s. As a result, 3.0 mm/s was used as the constant speed for exploring the impact of laser welding power.

Table 3.5: System parameters for varying laser power at constant laser speed.

Sample	Laser welding power (W)	Laser welding speed (mm/s)	Power density (W/cm^2)
1	1400	3	1114085
2	1500	3	1193662
3	1600	3	1273240
4	1700	3	1352817

Table 3.6: System parameters for varying laser speed at constant laser power.

Sample	Laser welding power (W)	Laser welding speed (mm/s)	Power density (W/cm^2)
1	1500	1	1193662
2	1500	1.5	1193662
3	1500	2	1193662
4	1500	2.5	1193662
5	1500	3	1193662

3.2.2 Microstructural characterization

Different metallographic methods were conducted to characterise BMs and the dissimilar joints.

3.2.2.1 Sample preparation

Before conducting the metallographic techniques, the samples were subjected to a Struers Secotom-10 abrasive cutting machine which was set at 3400 r/min wheel speed, 0.020 mm/s feed speed and cut length of 43 mm. The machine used a diamond cut-off wheel of 127 mm diameter and 0.4 mm thickness to cut the welded samples through the cross section. A black Phenolic resin was then used to mount the samples in a hot mounting press OPAL 410 at 200 ˚C for 5 min. The mounted samples were ground using 220, 800 and 1200 SiC paper grades respectively

and were polished with a Struers MD-Dur 250 mm diameter polishing cloth to obtain a scratch free and smooth surface. The process was performed from a Saphir 520 single wheel grinder/polisher attached to a Rubin 500 head. The samples were etched with a 3 % Nital solution composed of 3 % HNO_3 and 97 % ethyl alcohol to attack the grain boundaries and expose the microstructure of the dissimilar weld joints.

3.2.2.2 Optical microscopy

Optical microscopy was conducted to study the microstructure of the weld joints. An Olympus SC optical microscope at varying magnifications ranging between 10 × and 50 × was used to analyse the grain size of the weld joints and the HAZ. Micrographs of the samples were captured from digital analysis Olympus Stream Essentials software installed on a PC connected to the microscope. The software was also used to measure the weld bead dimensions namely, weld width, weld penetration and HAZ.

3.2.2.3 SEM-EDS

The SEM and EDS techniques were incorporated. The SEM examinations were conducted using Zeiss Sigma 300 VP instrument with a field emission gun and ZEISS Smart SEM Software for analysing data. The EDS detector used was OXFORD INSTRUMENT x-act PentalFET Precision which examines data using Oxford INCA software. The equipment was set at 20 kV Electron High Tension (EHT). SEM was utilized for examining the morphology and qualitative chemical composition of the dilution zone. EDS was used to determine the presence of various elements at different regions of the weld surface.

3.2.2.4 X-ray Diffraction Analysis

The surfaces were also assessed using the XRD technique. The purpose of the test was to characterise the existing phases in the samples. A Bruker D8 Advanced diffractometer with a monochromator which uses a solid detector and Cu kα radiation characterized from 2θ by a scan ranging between 0 to 90° and a wavelength of 1.5406 was employed. Voltage and current were adjusted to 40 kV and 40 mA respectively. The Match! and FullProf Suite software were used to analyse the raw data. The former was used to detect and characterize the different peaks on the diffractograms whereas the latter was used to quantify the detected phases. The quantitative

analysis was automatically done by the FullProf Suite software from the peaks produced by the Match software.

3.2.3 Electrochemical corrosion test

Electrochemical techniques were used to study the corrosion properties of dissimilar welds between Z225 and Al 5754. Chemical composition, weld bead appearance and polarization curves were used to analyse the impact of laser welding parameters and electrolyte concentration on the corrosion resistance of dissimilar weld joints.

3.2.3.1 Sample cleaning

The samples were placed inside a beaker with 100 ml acetone. The beaker was inserted inside a Digital Heated Ultrasonic Cleaner with half-full cold water at 25 $^{\circ}$C. The machine was operated for 10 minutes to remove the grease and dirt on the surfaces. After degreasing, the samples were rinsed with cool water and air-dried.

3.2.3.2 Electrochemical corrosion analysis

The corrosion properties of the samples were gauged from the electrochemical technique using an Autolab potentiostat PGSTAT20 controlled from a computer installed with NOVA 2.4 software. The samples were screwed to a cylindrical three-electrode Pyrex glass cell of 500 ml volume. An electrolyte made from NaCl solution was poured inside the cell before inserting electrodes. The concentrations used for the test were 2.5, 3.5 and 4.5 % NaCl. The electrodes namely, the Standard Calomel Electrode (SCE) (reference electrode), graphite (counter electrode), and the connected sample (working electrode) were placed inside the solution. Before the potentiodynamic polarization readings were taken, the system was run for 2 hours to allow the open circuit potential to stabilize. The area of the sample weld surface exposed to the electrolyte was 2.834 cm^2. Although the ASTM standard scan rate is 0.1667 mV/s, a constant scan rate of 1 mV/s was used for the sake of comparing the obtained results in the current work to those in literature under similar corrosion test conditions for similar materials. The scanning potential ranging between -1.5 and 1.5 V were used throughout the tests. The Tafel plots (log t vs Eplot) were extrapolated to determine the corrosion potential (E_{corr}), corrosion current (I_{corr}) and corrosion current density (i_{corr}).

At the completion of each test, the samples were rinsed with clean water and ethanol and were air-dried. The samples were analysed from SEM-EDS technique to evaluate the surface aspects and the chemical composition of both prior and post corrosion test to track the change in Zn composition as the NaCl concentration was varied. The tests were conducted 3 times for each combination of parameters.

3.2.4 Mechanical testing

With the intention of determining whether the produced dissimilar weld joints will be suitable for application within the automotive industry, the hardness and tensile behaviour of the joint were assessed.

3.2.4.1Tensile shear test

Tensile assessments were completed to assess the impact of various welding conditions on weldability. The tensile shear test specimens were cut into a "dog bone" shape by means of a water jet cutting device. The welded samples were in accordance with the ASTM E8 geometry standards as illustrated in Figure 3.3.

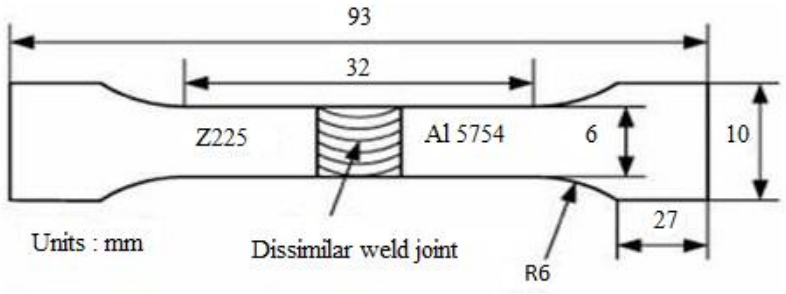


Figure 3.3: Tensile shear strength test specimen (modified from) [123].

A Zwick/Roell electro-chemical machine was used to perform the tensile tests. The equipment was set at a test speed of 0.0067 L/s and 5 MPa pre-load. The experiments were performed at 25 ˚C temperature. The machine was linked to a computer which captures the test data using TestXpert II software. Focus was also given to the position in which failure occurred for each sample. The possible locations of failure are on either of two BMs, the HAZ or along the weld joint. The benchmark for the test was for the weld joints to be as tough as the weakest base meaning that fracture should occur at the weakest BM which was Al 5754.

3.2.4.2 Microhardness testing

Hardness tests are a valuable means of evaluating the properties of a material. The tests were performed from a Vickers FM-700 microhardness tester conducted in accordance with ASTM E384:11^{E1} specifications. The machine was set at a load of 300 gf and 10 s dwell time. Pyramid shaped diamond indentations with an average of 125 µm increments were subjected to the sample surfaces. Microhardness readings were taken in the transverse direction from one base material, through the weld joint and towards the other base material. The average number of indentations in the transverse direction was 29 indentations. The readings were also taken from the weld surface through to the weld root with an average of 14 indentations. The microhardness profiles were used to study the hardness variations at different zones through the weld joints.

Chapter 4 : RESULTS AND DISCUSSION

The results attained from performing experiments in Chapter 3 are presented and analysed in this chapter. The results were compared to those obtained from previous research. This chapter is divided into three sections, that is, microstructural analysis, electrochemical corrosion behaviour and mechanical properties.

4.1 Microstructural characterization: Optical microscopy

4.1.1 Morphology and defects on the weld cross sections

The optical microscope was utilized to analyse the exterior of the weld bead. The weld penetration depth, weld width and HAZ measurements of the weld cross section were determined. The micrographs were also used to explore the structural characteristics related to grains within the weld metal.

4.1.1.1 The effect of laser welding speed on the appearance of the weld cross section

Figure 4.1 displays the cross-sectional morphologies of Z225/ Al 5754 laser welded joints at constant laser power of 1500 W and laser welding speed of 1.0 mm/s, 1.5 mm/s, 2.0 mm/s and 2.5 mm/s, respectively.

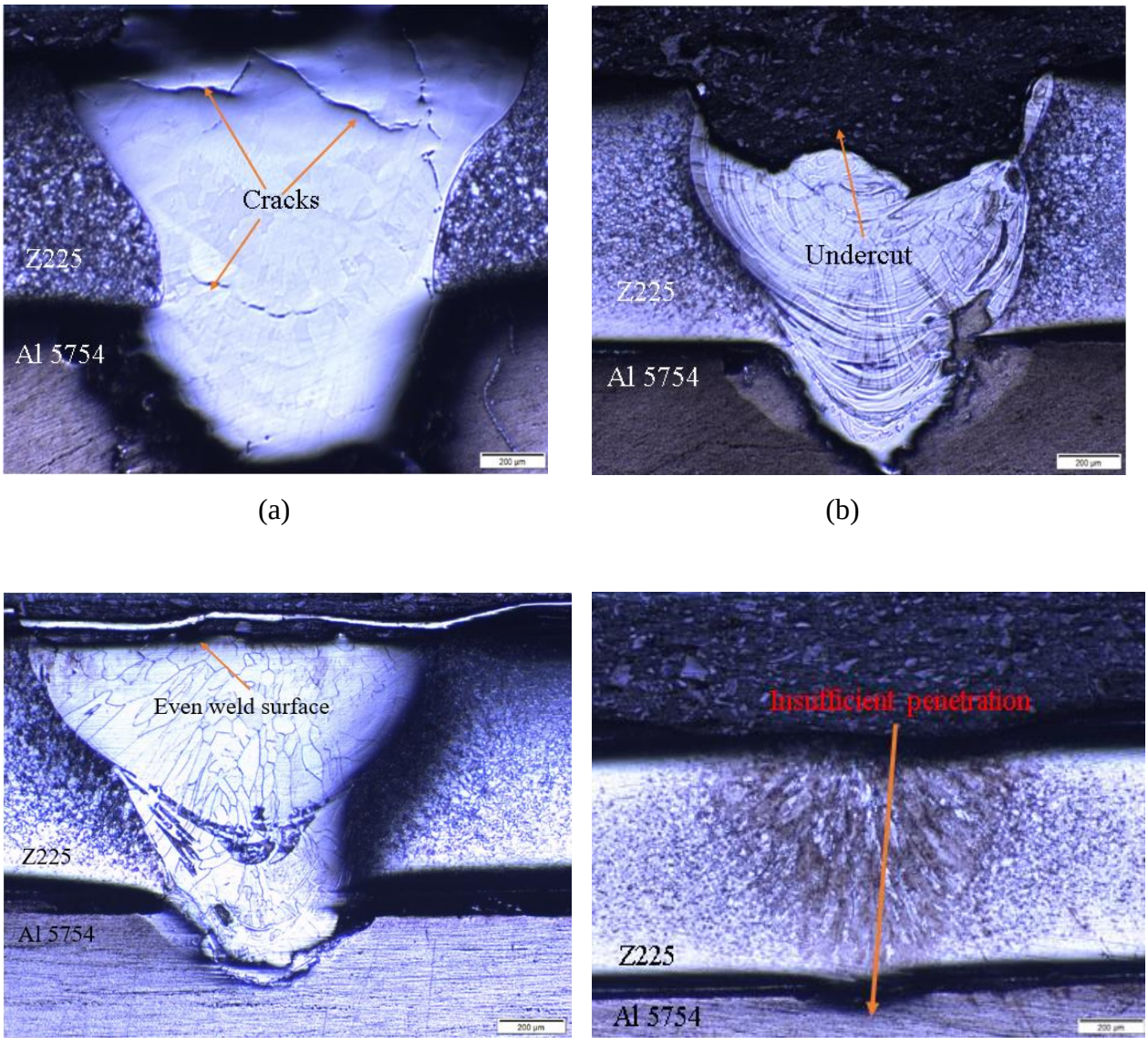


Figure 4.1: Optical micrographs for dissimilar joints produced at a constant laser welding power of 1500 and laser welding speed of (a) 1.0 mm/s, (b) 1.5 mm/s, (c) 2.0 mm/s and (d) 2.5 mm/s.

It was evident that for the lowest laser welding speed of 1.0 mm/s there was deeper penetration of the WZ (Figure. 4.1(a)). Multiple cracks were identified on the WM. Schimek *et al* [63] mentioned that high weld penetration depths indicate high levels of mixing between Fe and Al atoms and may lead to crack initiation. At high heat inputs, there are high levels of mixing between Fe and Al atoms. Therefore, the formation of brittle intermetallic phases increase, intensifying susceptibility of the weld metal to cracking. As the welding speed was increased to 1.5 mm/s, the degree of penetration decreased and undercut defect was observed (Figure 4.1(b)).

The most common cause of undercut is high levels of welding speed [32], [124]. Another reasonable explanation behind this observation could be that the evaporated Zn-coating accumulated pressure during laser welding [125]. The pressure caused by zinc vapour often evokes extreme disturbances towards the flow of the molten metal and creates the undercut [125]. The abrupt change in geometry which originates in the undercut then causes potential high stress concentration [126]. The stress concentration is commonly created by the height differences between the BMs and the WM [127]. When laser welding speed was increased to 2.0 mm/s, a much even weld surface was obtained (Figure 4.1 (c)). Penetration of the WZ to aluminium was slightly reduced. A further increase of speed to 2.5 mm/s resulted in a weld joint with insufficient penetration (Figure 4.1 (d)). This observation can be alluded to the fact that, rapid laser welding speed results in lower heat input levels which are often not sufficient to cause penetration of the steel [128].

Generally, the results indicated that as laser welding speed was increased, the weld pool decreased. The weld penetration depth also decreased with an increase in speed. The susceptibility of the weld joints to defects seemed higher at slower speeds.

4.1.1.2 The effect of laser welding power on the appearance of the dissimilar weld cross sections

Figure 4.2 presents the micrographs for the welds produced at constant laser welding speed of 3.0 mm/s and laser powers of 1400 W, 1500 W, 1600 W and 1700 W respectively.

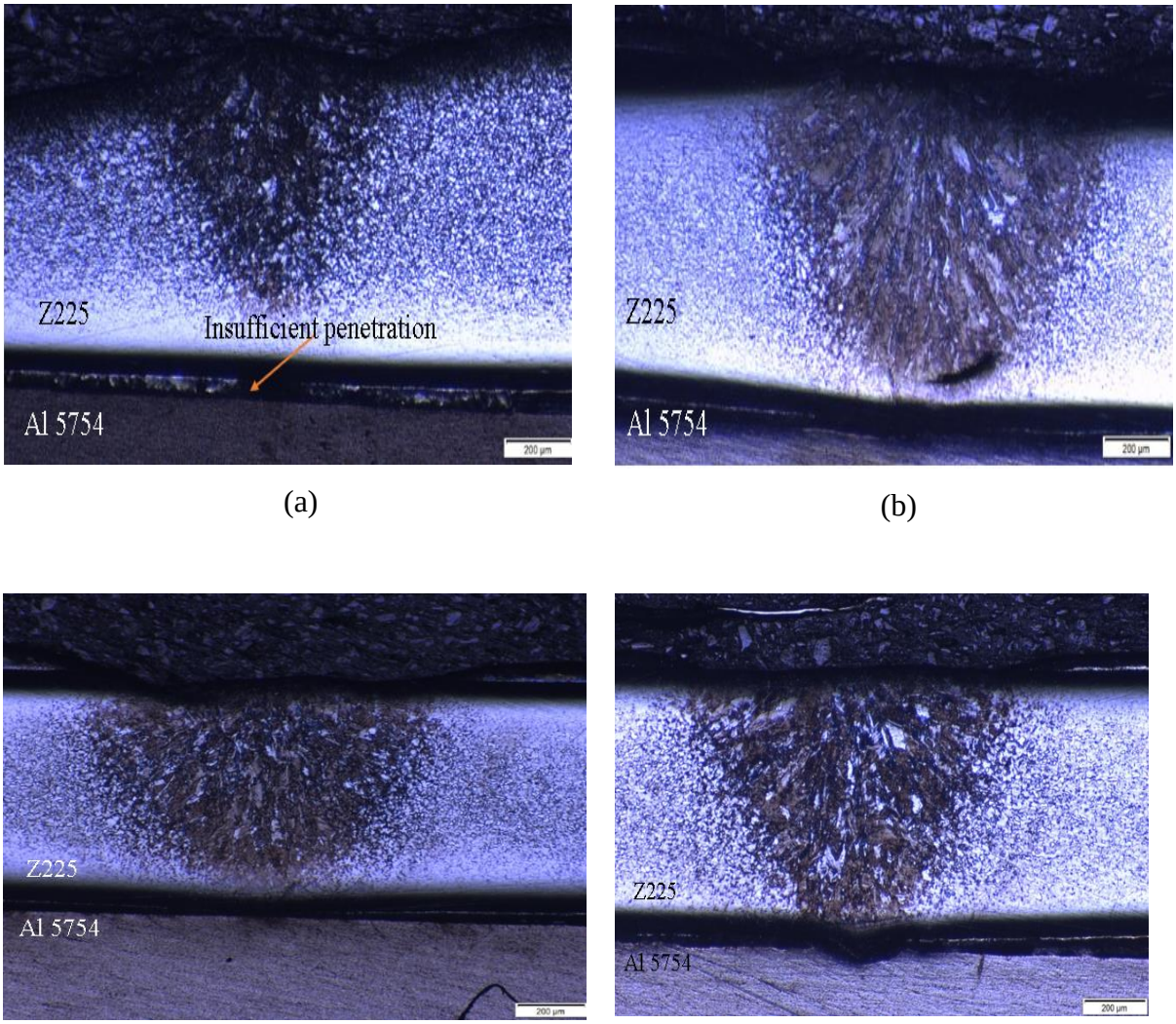


Figure 4.2: Optical micrographs for dissimilar joints produced at a constant laser welding speed of 3.0 mm/s and laser welding power of (a) 1400 W, (b) 1500 W, (c) 1600 W and (d) 1700 W.

For the lowest laser welding power of 1400 W, there was lack of penetration (Figure 4.2 (a)). The weld bead size was the smallest. Increasing laser power to 1500 W (Figure 4.2 (b)) did not make a huge difference in the morphology of the weld. There was however a marginal increase in the size of the weld bead. At 1600 W, there was a slight increase in penetration of steel and generally, the weld bead size increased (Figure 4.2 (c)). A much more visible penetration was detected at the highest laser power of 1700 W (Figure 4.2 (d)). Generally, the WMs produced at a constant laser welding speed of 3 mm/s had an even weld surface and had few weld defects. The weld pool size increased with an increase in power.

4.1.2 Weld geometry of the dissimilar weld cross sections

The weld bead geometry plays a significant role in the firmness of the structure. As a result, it is crucial to appropriately adjust the laser welding parameters to control the weld bead geometry which leads to sound weld joints [1].

The weld width was measured as the top plane surface whereas the weld penetration depth was defined as the longest distance from the weld surface to the weld root.

4.1.2.1 The effect of laser welding speed on weld bead dimensions

The weld bead dimensions for constant laser welding speed of 3.0 mm/s and laser power varying between 1400 W and 1700 W are presented of in Figure 4.3.

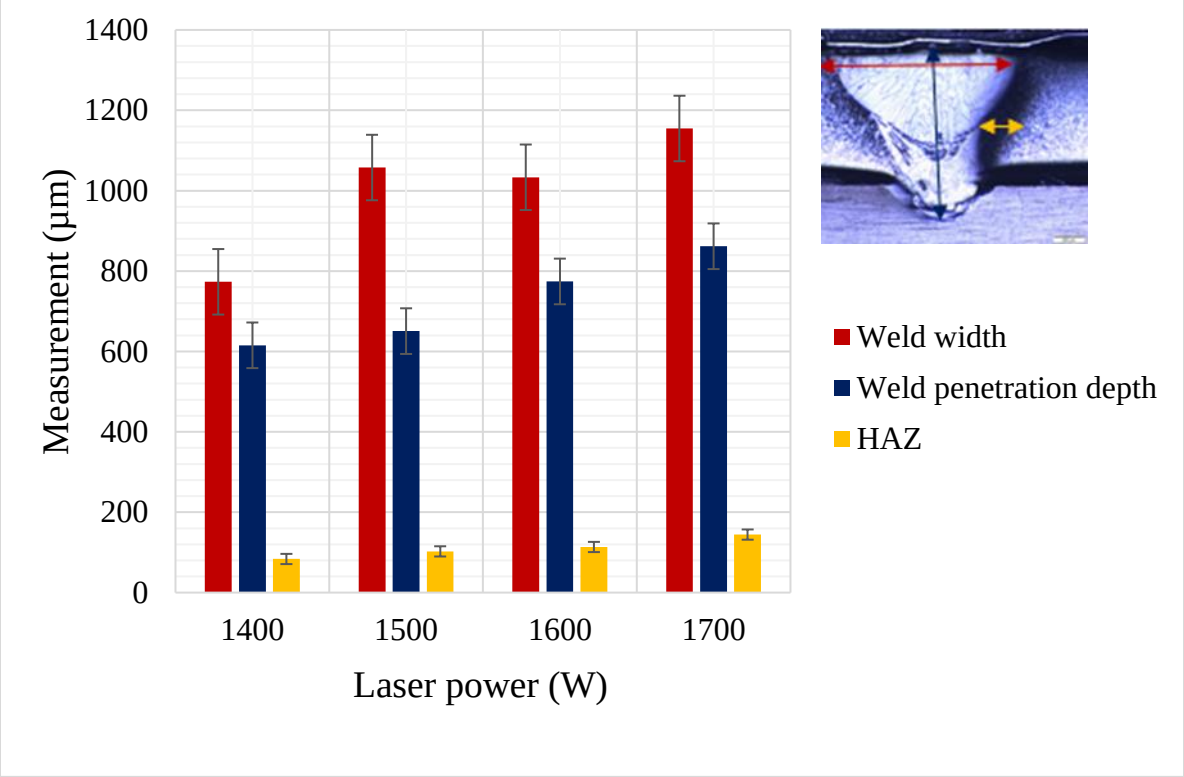


Figure 4.3: Effect of laser welding power on the weld bead dimensions

The weld bead dimensions increased with increasing laser power. At the lowest laser power of 1400 W, the weld penetration depth, weld width and HAZ values were 773.29 µm, 615.30 µm and 83.64 µm respectively. The values increased to 1154.83 µm, 861.78 µm and 144.37 µm respectfully when laser welding power increased to 1700 W. Comparable observations were made by Qianqian *et al*. [4]. Their results revealed a linear increase in both weld width and weld penetration as laser power was increased from 1300 W to 1450 W at a constant speed of 25 mm/s. The weld width increased from 1.766 mm to 1.916 mm whereas the weld penetration increased from 1.747 mm to 2.141 mm. The proportional link between weld penetration depth and laser welding power was because as the laser beam power increases, the energy absorbed by the material increases [4]. Therefore, greater extent of weld penetration depth was observed for higher values of laser power. Benyounis *et al* [129] also discovered that heat input has a directly proportional relationship with laser power. As laser power increases, the heat input also increases resulting in high amounts of melt which leads to deeper weld penetration [129].

4.1.2.2 The effect of laser welding speed on weld bead dimensions

Figure .4.4 displays the change in weld bead dimensions as laser welding speed increases.

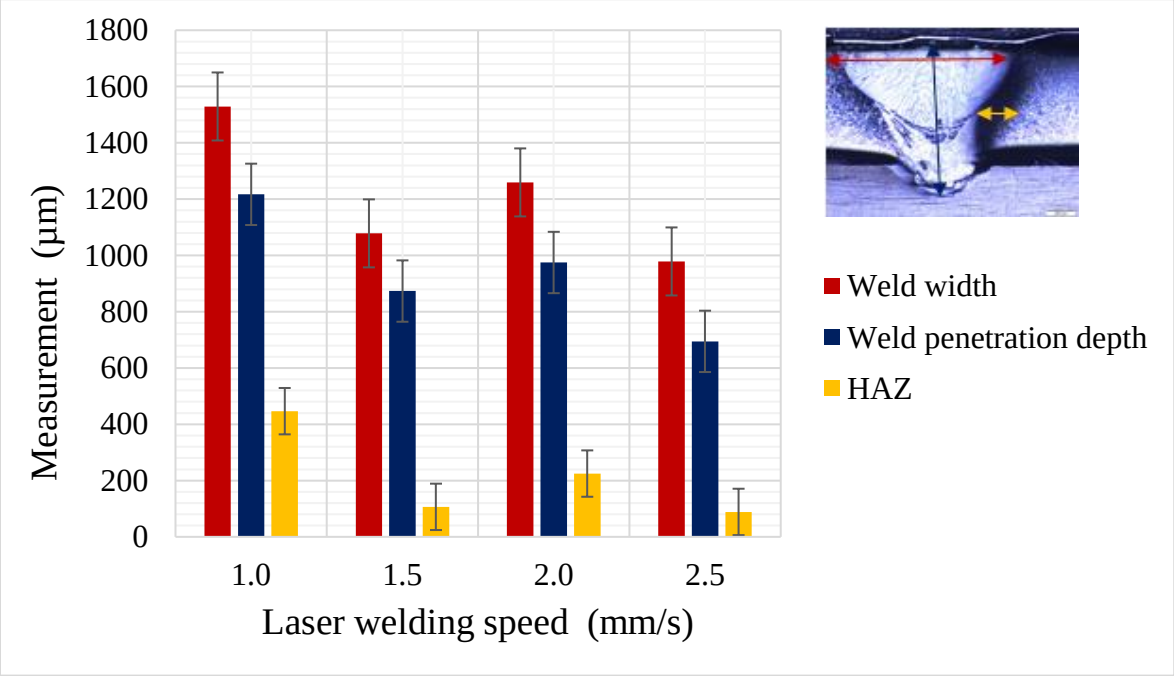


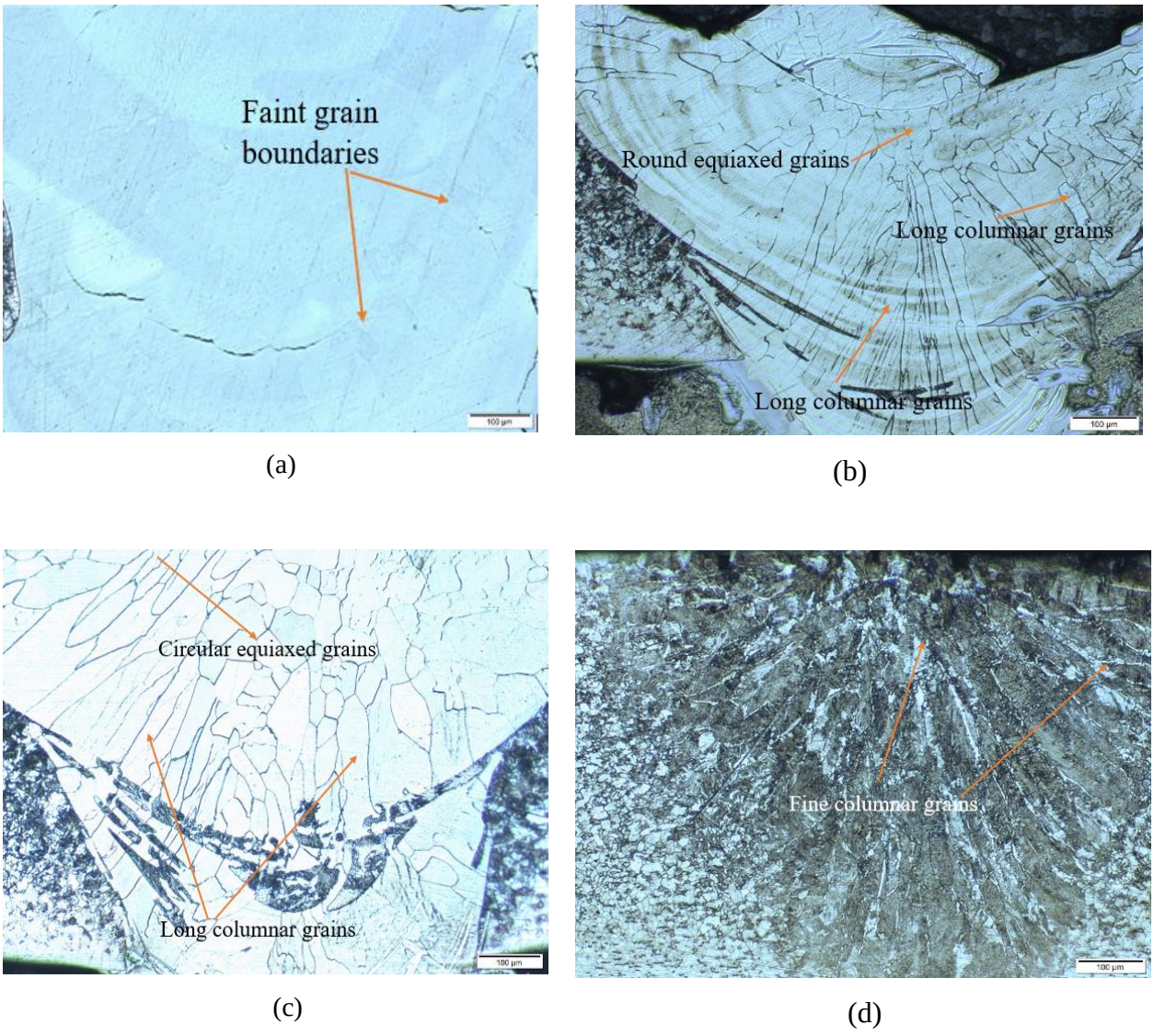
Figure 4.4: Effect of laser welding speed on the weld bead dimensions

At constant laser power of 1500 W, the weld width, weld penetration depth and HAZ dimensions varied randomly as laser welding speed increased from 1 mm/s to 2.5 mm/s (Figure 4.4). The fluctuation of the values was due to the undercut which was detected at 1.5 mm/s. The presence of this defect resulted in weld bead dimensions which were much lower than expected. Yuce *et al*. [1] also observed fluctuations in weld bead dimensions at the same heat input level. They reported that the discrepancies were most likely due to evaporation of zinc or the differences in gap opening size between the base metal plates during the welding process [1]. Overall, the weld width, weld penetration and HAZ dimensions were much higher for the lowest laser welding speed of 1.0 mm/s and were lowest for the highest welding speed of 2.5 mm/s. The weld penetration depth, weld width and HAZ average values for 1.0 mm/s were 1216.99 µm, 1529.17 µm and 446.54 µm respectively. The values decreased to 694.63 µm, 698.41 µm and 88.62 µm respectively at 2.5 mm/s. This tendency was observed because at slower laser welding speeds, temperature within the FZ increases which results in deeper weld penetrations [4]. The highest laser welding speed of 2.5 mm/s produced the smallest size of the molten pool. At higher laser welding speed levels, the BMs tend to have low absorptivity of the laser beam which results in lower weld penetration depths [4]. Also, at faster laser welding speed, the weld bead dimensions were smaller because the high speed at which the beam travels result in insufficient interaction time between the beam and BMs. Therefore, only a small amount of the BMs dissolve and the weld bead dimensions decrease [129]. Yuce *et al*. [1] also noticed a reciprocal connection between heat input and bead geometry. The results revealed that at constant laser power, the weld width and weld penetration depth decreased with an increase in laser welding speed [1].

4.1.3 Grain structure of the weld metal and HAZ

The impact of laser welding speed on the grain structure of the FZ is displayed in Figure 4.5. At 1.0 mm/s, the grain structure was undefined. The grain boundaries were very faint, and the grain size was too large (Figure 4.5 (a)). The weld microstructure is controlled by the welding speed which determines the size and shape of the weld pool [52], [68], [130]. The greater the weld pool, the coarser the grain structure [68]. The size of grains within the weld metal is larger for slow laser welding speed and decrease as welding speed increases. High heat input by means of slow laser welding speed results in slower cooling rates which drastically increases grain growth due to a slower solidification rate within the weld pool [133]. Large grains have a tendency of

producing weak microstructures, with the alloy losing its toughness and becoming more brittle and susceptible to cracking. The weak microstructure also depends on other factors such as chemistry of BMs, peak temperatures, and dilution percentage [133].



(a) (b)

(c) (d)

Figure 4.5: Microstructure created at different laser welding speeds and constant power of 1500 W: (a) 1.0 mm/s, (b) 1.5 mm/s, (c) 2.0 mm/s, 2.5 mm/s.

Similar microstructures were observed at laser welding speeds of 1.5 mm/s and 2.0 mm/s (Figure 4.5 (b) and (c)). At the fusion boundary, columnar grains were formed and stretched from the bottom and edges towards the middle of the WM. At the middle of the WM, a coarse, equiaxed microstructure was detected. The rate of solidification in the weld played an imperative role in this observation. The solidification rate is governed by the cooling rates and the extent in which material mixing occurs [32]. In LBW, immediately when the laser beam is removed from the WZ after welding, the molten WM temperature quickly decreases to room temperature over a short time interval. As a result, the melt rapidly changes from liquid to solid state [131]. Each section of the weld then experiences different solidification rates that lead to the creation of different microstructures at the edges and middle of the weld joint. Haboudou *et al*. [132] also observed similar results from microstructures of laser beam welded dissimilar joints between A356 and AA5083 aluminium alloys. Their results revealed the creation of columnar grains at the bottom and edges of the weld whereas at the centre and top of the weld an equiaxed grain structure was obtained [132]. At 2.5 mm/s, a fine columnar grain structure was observed (Figure 4.5 (d)). The microstructure had very fine and consistent grains throughout the entire WM. A fine grain structure created at high welding speeds occurs due to limited time for coarsening of grains to take place [89].

Changing laser welding power at constant laser welding speed of 3 mm/s did not have a great effect on the grain structure of the weld metal. The grain structures for WMs produced at 1400 W, 1500 W, 1600 W and 1700 W in Figure 4.6 were similar. This could be attributed to cooling rates that remained constant due to the laser welding speed that was kept constant, and thus resulted in similar microstructure [87].

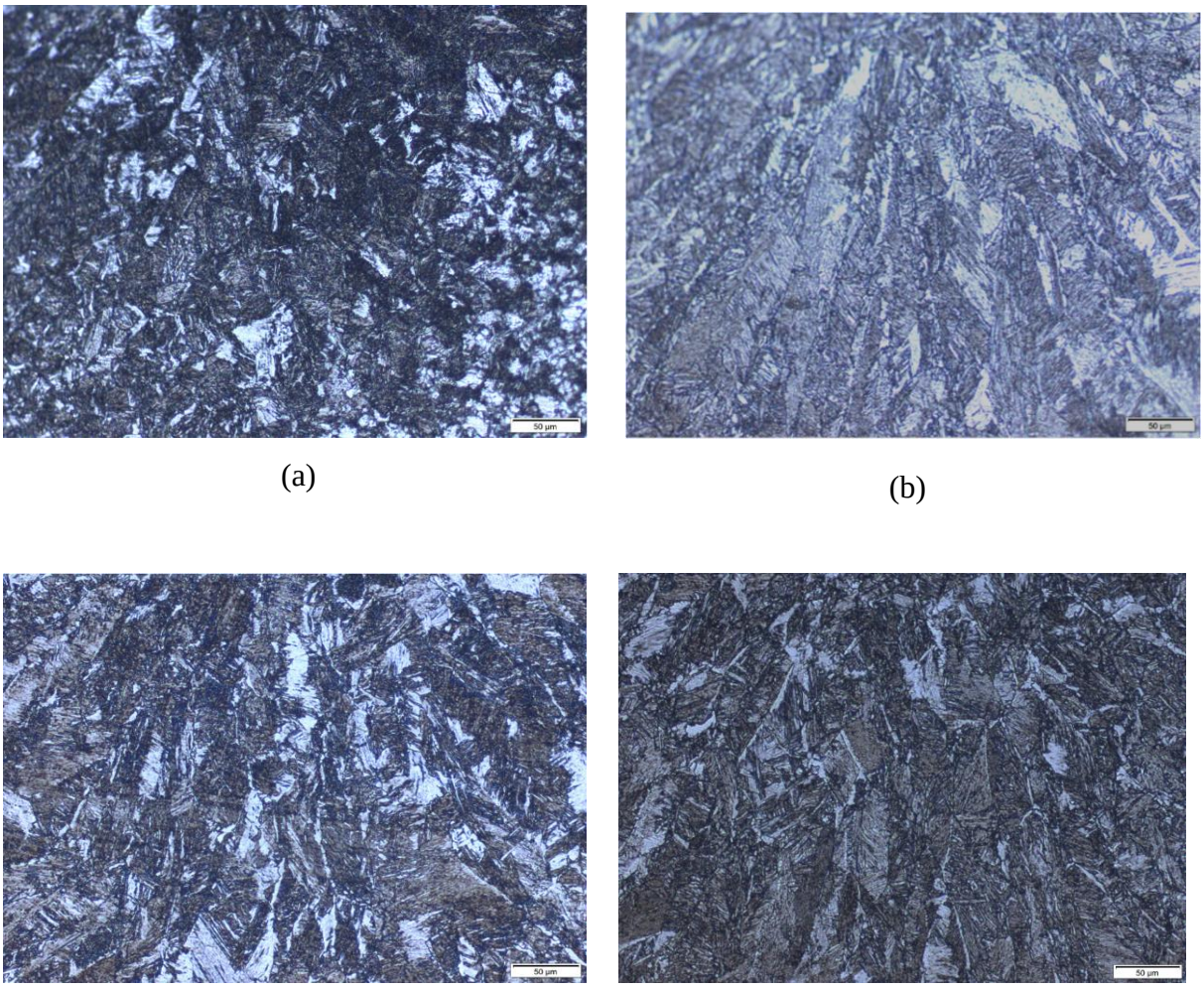


Figure 4.6: Microstructure created at constant laser welding speed of 3.0 mm/s and different laser welding powers: (a) 1400 W, (b) 1500 W, (c) 1600 W, (d) 1700 W.

The WM for all welding conditions was made of a fine columnar microstructure. Increasing laser power from 1400 W to 1700 W did not have a massive impact on the grain size and shape. The microstructure of the HAZ was also similar. The Z225 BM displayed an equiaxed grain microstructure (Figure 4.7) which transitioned to the microstructure observed at the HAZ for all conditions. A microstructure created by solidification developed from the weld pool towards the HAZ. At the HAZ, the microstructure was transformed to an inhomogeneous grain size which demonstrated grain growth because of heating and cooling cycles within the weld [127]. Larger columnar grains were detected at the HAZ. This grain growth occurred due to recrystallization [4].

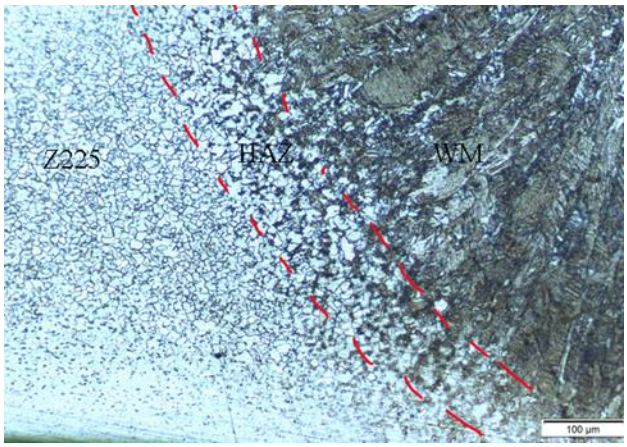


Figure 4.7: Transition of grains from BM to WM.

4.2 Microstructural characterization: SEM/EDS

It has been reported that the creation of intermetallic phases can generally take place when the quantity of Al element is greater than 12 wt. % on the Fe-Al phase diagram [32], [134].

The cross sections of the welded samples were studied using the SEM-EDS technique. The EDS composition was used to predict the presence of IMC phases by comparing the atomic percent of Fe and Al with data provided in literature. The analysis was done on the WM and the interface for different combinations of welding parameters. The Fe-Al phase diagram in Figure 1.1 and data provided in Table 4.1 were used as reference for predicting the IMC phases from the composition obtained through EDS analysis.

Table 4.1: Fe and Al at. % for common Fe-Al IMC phases [1].

	Fe-Al phases	**Al (at. %)**	**Fe (at. %)**
Al-rich IMC	$FeAl_2$	51-65	47-61
	Fe_2Al_5	51-74	26-37
	$FeAl_3$	76-79	18-20
Fe-rich IMC	FeAl	41-45	52-55
	Fe_3Al	12-28	66-80

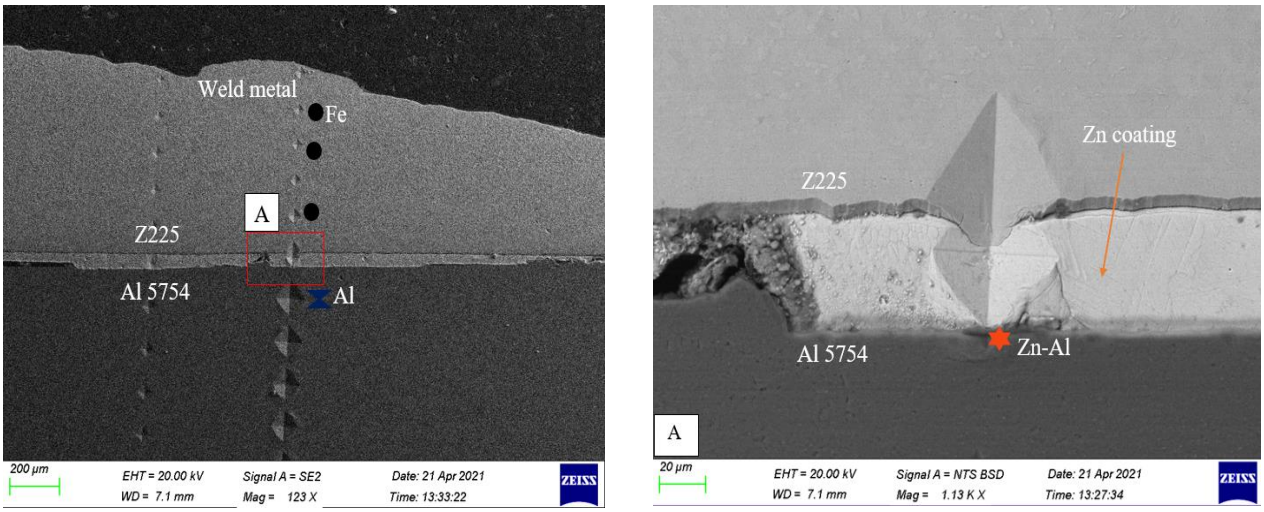
The IMC phases predicted from the EDS analysis and the symbols used to represent them on the SEM images are exhibited in Table 4.2.

Table 4.2: Symbols used to represent the elements and IMC phases predicted from EDS analysis.

IMC phase	Symbol
Fe	
FeAl	
$FeAl_2$	
FeAl + $FeAl_2$	
Fe_2Al_5	
Fe_4Al_{13}	
Zn-Al	
Al	
Zn	

4.2.1 Effect of laser welding power on the composition of the created IMC phases

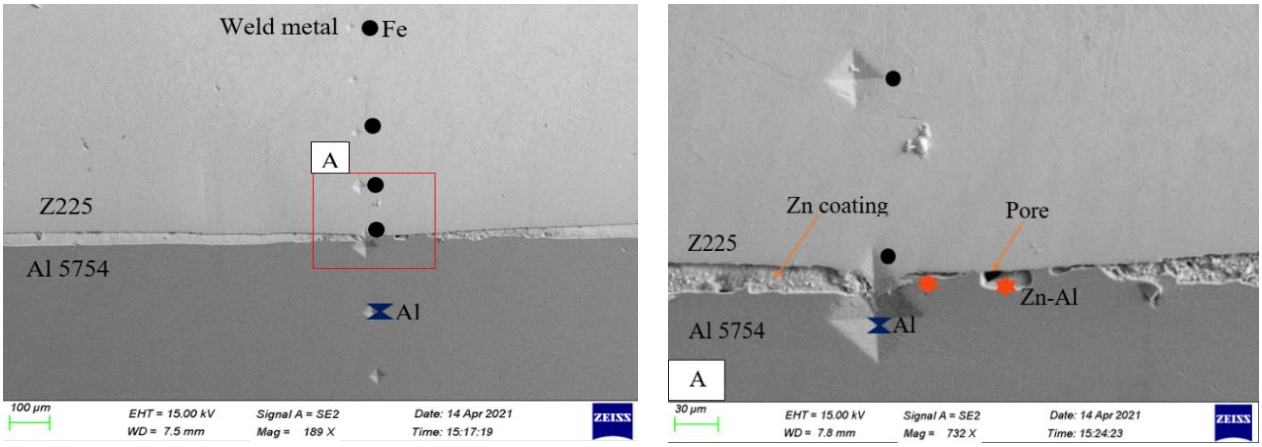
The SEM images shown in Figure 4.8 indicate the impact of laser welding power on the growth of IMC phases within the weld metal and at the interfacial region. At 1400 W, the EDS analysis did not identify any Fe-Al intermetallic phases on the WM from weld surface to the weld root (Figure 4.8 (a)). The only phase predicted on the WM was Fe. This may be an indication that there was no excessive mixing between Fe and Al elements. It should be mentioned that the laser welding experiments were performed in the absence of a filler material. At the interfacial region (Figure 4.8 (b)), it was observed that there was very little diffusion between the elements due to low heat input. The Zn coating was still visible and not severely affected by heat during welding. However, Zn-Al phase was detected along the interface next to the Al 5754 base metal. This observation could mean that the heat input generated by 1400 W was only sufficient for partially melting the Zn-coating as it has a lower melting point compared to Al and Fe. According to Marder *et al*. [135], the presence of Zn-Al phases that occur due to the preferential reaction between the Zn-coating and aluminium BM limits the development and extent of Fe-Al phases.



(a) (b)

Figure 4.8 : SEM images of IMCs at 1400 W. (a) Weld cross-section, (b) Interfacial region (A).

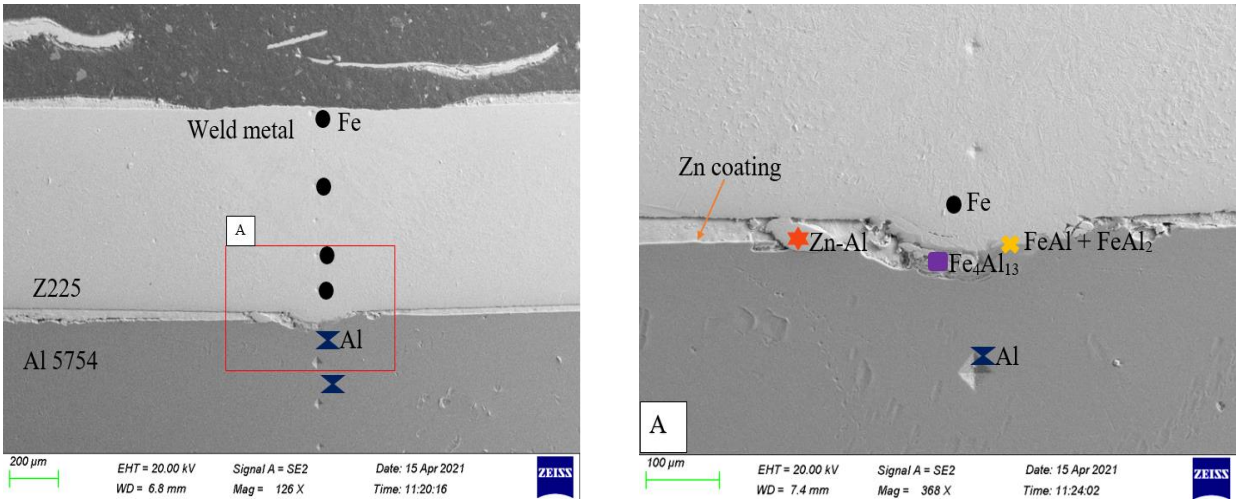
As laser power increased to 1500 W, no major changes were noted in the composition of the WM (Figure 4.9 (a)). No Fe-Al phases were detected within the WM. The extent at which Zn dissolved seemed to have faintly increased. The Zn-Al phase was detected at the interface next to aluminium where a pore was spotted (Figure 4.9 (b)). The pore was most probably created by evaporation of Zn when the vapour was trapped during solidification [76].



(a) (b)

Figure 4.9: SEM images of IMCs at 1500 W. (a) Weld cross-section, (b) Interfacial region (A).

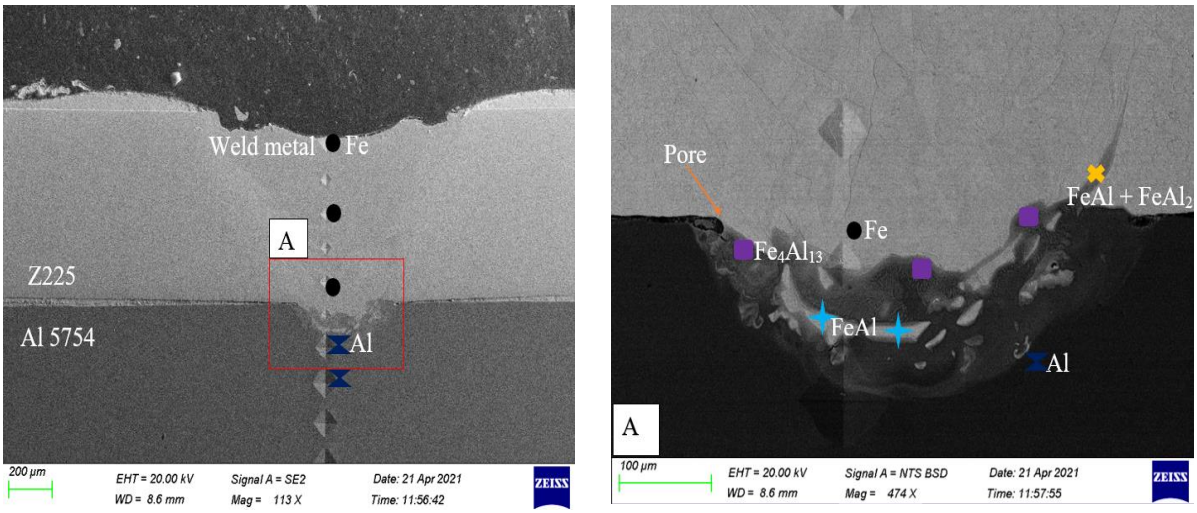
A further increase of power to 1600 W did not have much effect on the composition from the surface to the root (Figure. 4.10 (a)). At the interfacial region though, there was a marginal increase in the thickness of the interfacial layer which was due to the increase in heat input. Some IMC phases were detected. The two-phased mixture of FeAl and $FeAl_2$ IMC was detected on the steel side whereas the Fe_4Al_{13} was detected on the aluminium side (Figure (4.10(b)). The Zn-Al phase was also observed. Diffusion between Al and Fe atoms occurs when the steel matrix makes contact with the molten metal [5]. The diffusion coefficient of aluminium atoms into the steel matrix ($D_{Al_,\ solid_{Fe}}$ =1.8 $\times 10^{-4}$ m^2/s) is much lower compared to the diffusion coefficient of Fe atom in aluminium ($D_{Fe_\ Al}$ =53 $\times 10^{-4}$ m^2/s) [5]. As a result, a higher quantity of Fe atoms can diffuse deeper into the molten metal, away from the interface. On the other hand, few Al atoms can diffuse into the shallow steel surface and then build-up in the narrow band [5].



(a) (b)

Figure 4.10: SEM images of IMCs at 1600 W. (a) Weld cross-section, (b) Interfacial region (A).

At maximum laser power used (1700 W), the thickness of the interfacial layer was much more visible (Figure 4.11(a)). The EDS analysis portrayed similar IMCs to those obtained for 1600 W with an addition of FeAl phase. Again, the two-phased mixture of FeAl and $FeAl_2$ IMC was spotted on the steel side whereas Fe_4Al_{13} was spotted on the weld-aluminium interface (Figure 11(b)).



(a) (b)

Figure 4.11: SEM images of IMCs at 1700 W. (a) Weld cross-section, (b) Interfacial region (A).

4.2.2 Effect of laser welding speed on the composition of the created IMC phases

The lowest laser welding speed of 1.0 mm/s revealed the presence of IMCs within the WM from the surface to the weld root (Figure 4.12(a)). At 1.0 mm/s, the deep weld penetration led to excessive reaction between Fe and Al which results in brittle IMCs [63]. The most prevalent phase in the WM was the two-phase mixture of FeAl and $FeAl_2$ IMC. FeAl was also present and had a bright shade of grey. $FeAl_2$ and Fe_2Al_5 were then spotted towards the Al 5754 BM. Tiny dendritic structures were also created as the composition of Al increased and were identified as the Fe_4Al_{13} phase (Figure 4.12(b) and (c)). A pore was detected where the concentration showed the presence of Zn-Al phase. The Zn-Al phase was characterized by thicker dendrites compared to those of Fe_4Al_{13}.

Heat input applied during laser welding can govern the chemical components of the weld metal and the cooling rate [32]. High cooling rates may lead to thermal strains which increase the rate of crack initiation. High thermal gradients may create strong Marangoni fluid flow which facilitates the creation of brittle IMC [32].

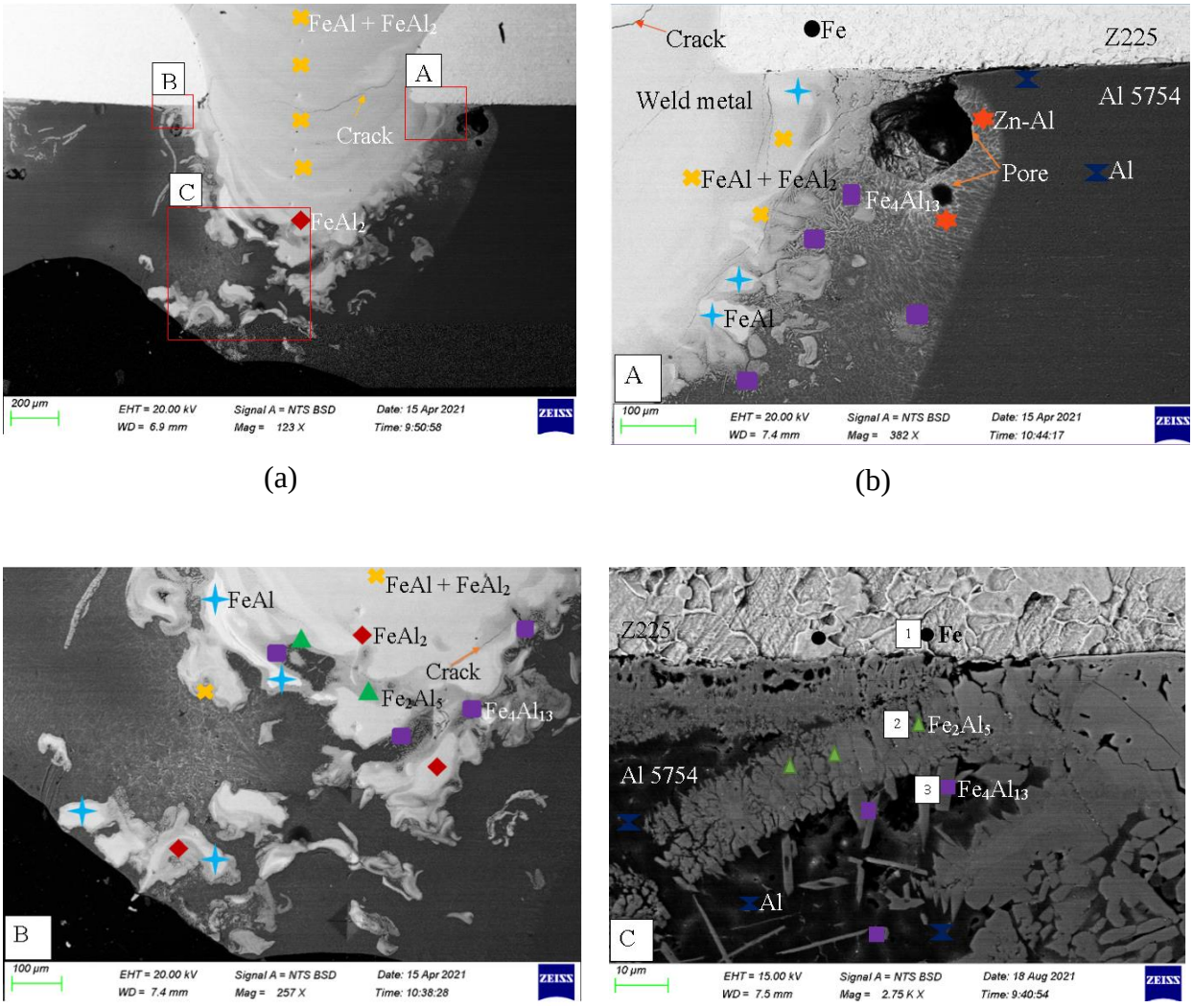


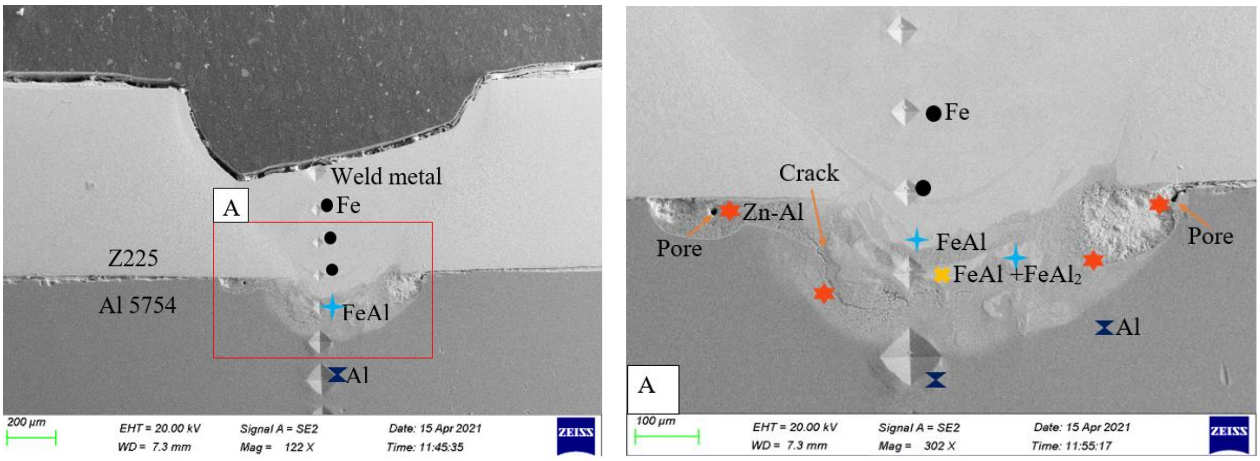
Figure 4.12: SEM images showing the IMCs. (a) Weld cross-section, (b) Right interfacial region (A), (c) Bottom interfacial region (B), (d) Left interfacial region (C).

The extent of plastic deformation is influenced by welding speed, which consequently influences the quantity of the IMC nucleation, stored energy, and atomic diffusion rate. The level of heat input controls the type of Al/Fe IMC phase created [136].

Figure 4.12(d) illustrates the mechanism in which Fe_2Al_5 was created and developed to Fe_4Al_{13} between steel and aluminium for 1 mm/s and 1500 W through developmental stages explained by Karim *et al*. [31]. As the welding process commences, the temperature first reaches the

aluminium liquidus line while steel remains solid (Point 1). Diffusion of Al atoms to the steel begins which results in the nucleation of plate-like $FeAl_5$ IMCs near the interface of steel and aluminium (Point 2). As a result, a double-layered IMC is formed between steel and aluminium creating an interface between steel and Fe_2Al_5 layer and another interface between Al and Fe_2Al_5. The development of the Fe_2Al_5 IMC is anisotropic and may contain 30 % vacancies beside the c-axis. Therefore, Fe and Al atoms are transferred by the IMC layer and solid-state diffusion mechanism. Since Al atoms have high diffusivity in the Fe_2Al_5 layer, the growth rate of Fe_2Al_5 along the c-axis direction is thus accelerated [31]. The Fe_2Al_5 layer performs as a boundary between solid steel and molten aluminium. The thickness of the Fe_2Al_5 slowly increases to a point where it nearly hinders the connection between solid steel and molten aluminium. Because the size of Fe atoms is much larger than those of Al, the transmission of Fe atoms through the Fe_2Al_5 IMC declines. Needle-like shaped Fe_4Al_{13} IMCs (Point 3) are then created between Fe_2Al_5 and Al. As Al liquid rapidly cools, Fe_4Al_{13} forms disturbing Al atom diffusion to steel and thus alters the structure and crystal alignment of Fe_2Al_5 [31].

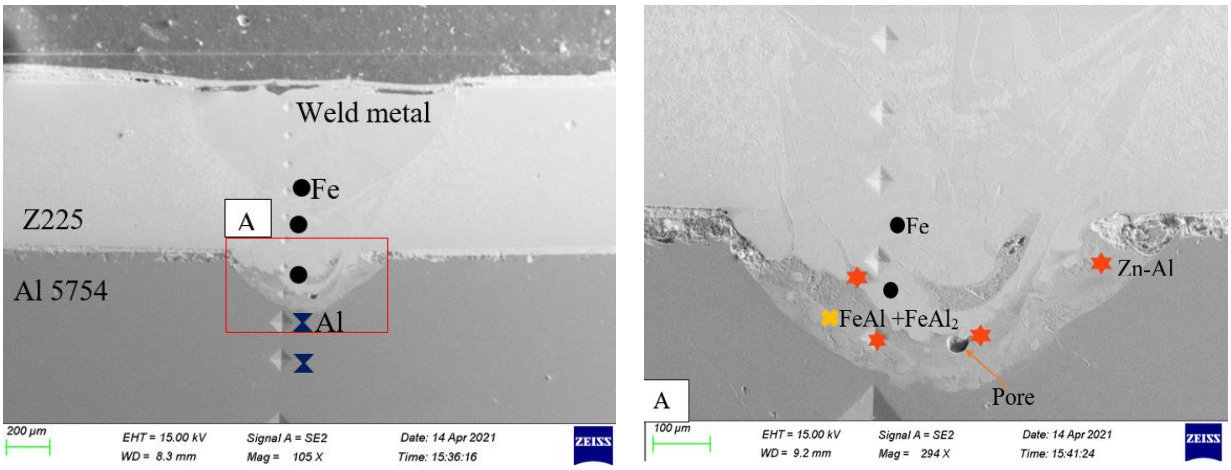
At 1.5 mm/s, the FeAl IMC was detected (Figure 4.13 (a)). Zn-Al phases were detected around a crack and next to a pore (Figure 4.13 (b)). FeAl and $FeAl_2$ two phase IMC mixture was also spotted at the interfacial region.



(a) (b)

Figure 4.13: SEM images of IMCs at 1.5 mm/s. (a) Weld cross-section, (b) Interfacial region (A).

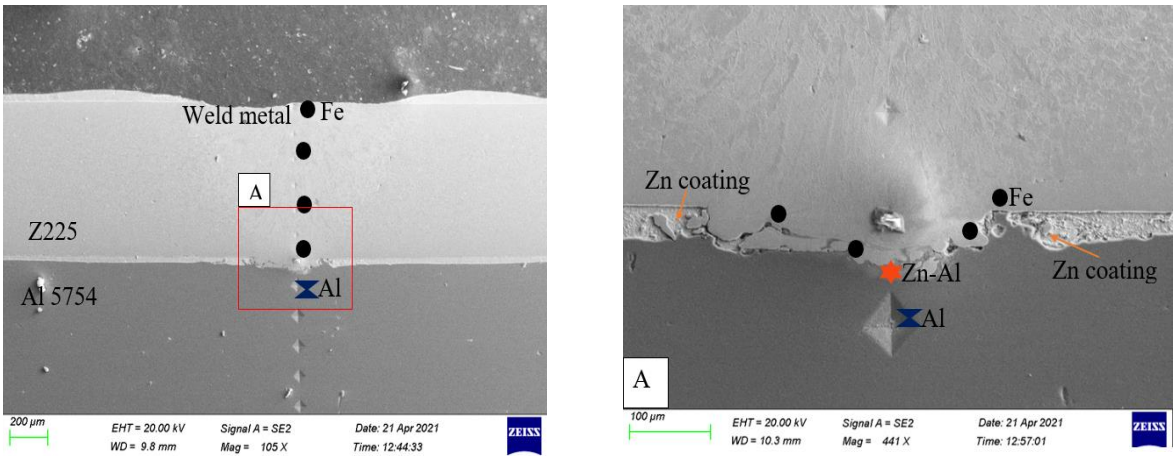
A further increase in laser welding from 1.5-2.0 mm/s decreased the thickness of the interfacial layer (Figure 4.14(a)). The presence of Zn-Al phases at the interfacial layer was noted (Figure 4.14(b)). The occurrence of Fe-Al phases also decreased. FeAl phase was detected at the interface.



(a) (b)

Figure 4.14: SEM images of IMCs at 2.0 mm/s. (a) Weld cross-section, (b) Interfacial region (A).

At the highest welding speed of 2.5 mm/s, the interfacial layer was very thin as expected (Figure 4.15(a)). Rapid heating and cooling occurred at high welding speed leading to reduced penetration depth. Therefore, the diffusion of Fe and Al elements was restricted. The only phase identified at the interface was Zn-Al phase (Figure 4.15(b)).



(a) (b)

Figure 4.15: SEM images of IMCs at 2.0 mm/s. (a) Weld cross-section, (b) Interfacial region (A).

The two mechanisms which govern the IMC layer thickness at the interface are nucleation and growth which are both controlled by the quantity of stored energy, heat input and the level of plastic deformation [136]. High heat input levels offer the activation energy required for the generation and diffusion growth of IMCs. If plastic deformation at the interface is severe, it leads to stored energy. The stored energy consequently influences IMC nucleation and growth due to atomic diffusion through high energy paths such as dislocations and grain boundaries [136].

4.3 XRD analysis of Z225 /Al 5754 dissimilar weld joints

Laser welded samples were exposed to X-ray diffraction tests. Table 4.3 and 4.4 present the quantity calculated by the FullProf! software for each phase detected by XRD analysis for constant laser welding speed and constant laser power respectively. Figure 4.15 displays the diffractogram pattern for the sample produced at 1.0 mm/s. The diffractogram patterns for other parameters are displayed in Appendix A. The XRD peaks on the diffractogram patterns represent the various intermetallic phases which were created at the laser welded dissimilar joints. The different phases had a tendency of overlapping in the same peak.

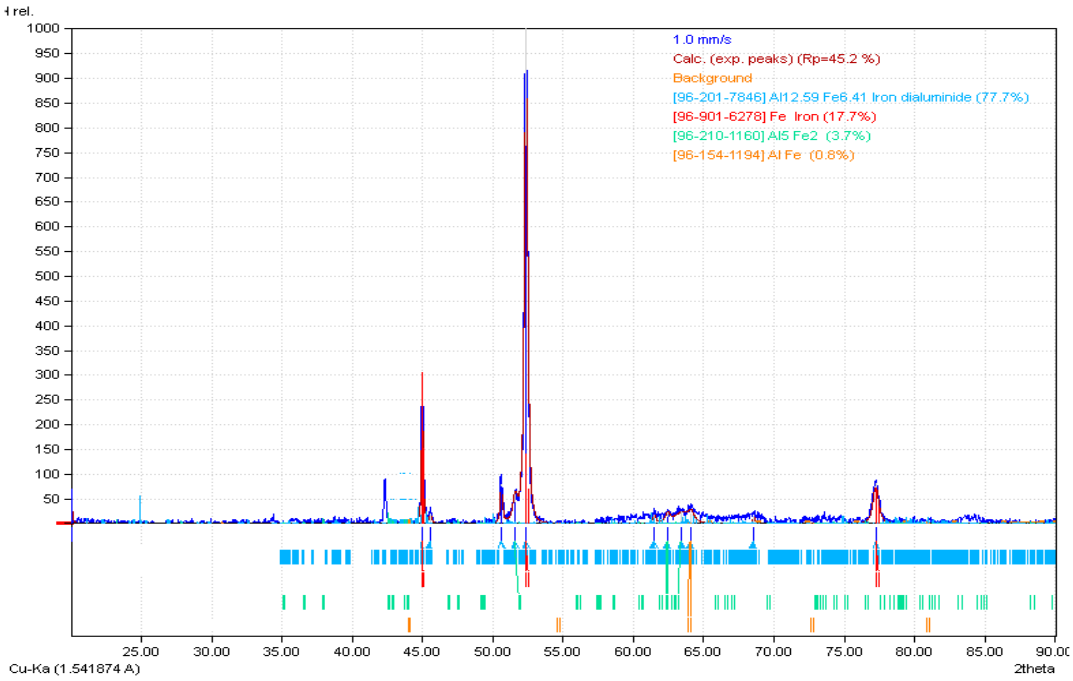


Figure 4.16: XRD pattern for 1.0 mm/s showing the detected elements and IMC phases detected.

The IMCs detected were FeAl, $FeAl_2$ and Fe_2Al_5 for most welding condition. It was also observed that the occurrence of different IMCs on a weld joint increased with an increase in heat input. It can be observed from Table 4.3 that at 1.0 mm/s all three IMC phases (FeAl, $FeAl_2$ and Fe_2Al_5) were present. However, at 2.5 mm/s only FeAl was present. This is because 1.0 mm/s resulted in the deepest weld penetration depth which according to Schimek *et al*. [63] led to high degree of mixing between Fe and Al atoms resulting in brittle IMCs. The quantity of $FeAl_2$ and Fe_2Al_5 phases decreased with an increase in laser welding speed. The sample produced at 2.5 mm/s on the other hand had a shallow penetration depth and less mixing of Fe and Al atoms. FeAl was present in all the samples, however, the quantity of the phase fluctuated as laser welding speed was increased. The results also implied that the quantity of Zn increased as the laser welding speed increased. The reason behind this may be that the Zn at high heat input evaporated or reacted with Al to create Zn-Al phases which were predicted by EDS results.

From Table 4.4, FeAl, $FeAl_2$ and Fe_2Al_5 were identified at 1700 W whereas at 1400 W only FeAl was detected. Accordingly, the quantity of Fe, Al and Zn also decreased with an increase in heat input due to the creation of IMCs. There was however no relationship established between the quantity of each IMC phase and the change in laser welding power. Some of the IMC phases such as Fe_4Al_{13} and Zn-Al phases which were predicted by EDS analysis were not confirmed by XRD tests. The reason behind this could be that the phases were only present in negligible quantities. XRD like most scientific measuring instruments has some limitations. The technique has more precision for larger crystalline structures compared to tiny sections [137]. As a result, structures which are only present in small quantities often cannot be detected by XRD measurements [137]. The FeAl and $FeAl_2$ two-phased IMC mixture was also not detected by XRD. It is possible that it was identified as either FeAl or $FeAl_2$ in XRD.

Table 4.3: Elements and phases detected from XRD analysis at constant laser power of 1500 W.

Laser welding speed	**Quantity (%)**						
(mm/s)	**Fe**	**Al**	**Zn**	**FeAl**	**$FeAl_2$**	**Fe_2Al_5**	**Total**
1.0	17.7	0	0	0.8	77.7	3.7	100
1.5	20.1	78.4	0	0.2	0.5	0.7	100
2.0	24.3	74.7	0.3	0.6	0	0.1	100
2.5	46.2	21.0	27.9	4.9	0	0	100

Table 4.4: Elements and phases detected from XRD analysis at constant laser speed of 3.0 mm/s.

Laser welding power	**Quantity (%)**						
(W)	**Fe**	**Al**	**Zn**	**FeAl**	**$FeAl_2$**	**Fe_2Al_5**	**Total**
1400	58.9	34.2	3.9	3.1	0	0	100
1500	53.6	1.5	2.0	0	0	42.9	100
1600	22.8	0.4	0	0.1	75.7	0	100
1700	13.3	26.6	0	6.4	18.0	35.7	100

4.4 Electrochemical corrosion behaviour of Z225/Al 5754 weld surfaces

Electrochemical potential tests were performed to study the corrosion properties of dissimilar weld joint surfaces between Z225 and Al 5754. Figure 4.16 and Figure 4.17 display the acquired polarization curves which were extrapolated to acquire the corrosion potential (E_{corr}) and corrosion current density (i_{corr}) recorded in Table 4.5 and 4.6. The changes in open circuit potential (OCP) are displayed in Appendix B and the values are recorded in Table 4.5 and 4.6.

4.4.1 Influence of NaCl concentration on the corrosion properties of the weld joints

The weld joints produced using 1.0 mm/s and 1500 W had the deepest weld penetration and the thickest interfacial layer. The parameters displayed the presence of most IMC phases. As a result, these parameters were used to study the impact of NaCl concentration on the corrosion response of the dissimilar weld joints. The samples were exposed to 2.5 %, 3.5 % and 4.5 % NaCl concentration. The polarization curves and electrochemical properties are given in Figure

4.17 and Table 4.5 respectively. The i_{corr} increased with an increase in concentration. The corresponding OCP values became more negative as the NaCl concentration increased from 2.5 % to 4.5 %. This means that the corrosion resistance of the weld surfaces decreased with an increase in NaCl concentration. In kinetics, the corrosion rate becomes more rapid as i_{corr} increases and as the corrosion potential becomes more positive, the corrosion dynamics become more stable [138].

The samples were further analysed under SEM to check how the microstructure varied as NaCl concentration increased. The type of corrosion which was discovered was pitting corrosion. Pitting corrosion occurs at the localized areas of the material and results in the creation of pits/pores [139]. The mechanism of pitting corrosion begins when the metal undergoes oxidation, leading to localized acidity, which is sustained by the parting of the anodic and cathodic half reactions. Electromigration of anions to the pit occurs due to the acidic environment. The localized acidity also leads to the development of a potential gradient. The side products created during the corrosion process have a tendency of filling the pits created on the metal surface [140]. The pits act as the anode while the metal surface behaves as the cathode. The metal cations produced within the pit leads to extreme positive charge then attract chlorine anions of the electrolyte. The corrosion rate is then accelerated by the reaction between the resultant metal chloride and water present in the surroundings [140].

It was observed that the severity of pitting corrosion did not change much as NaCl concentration increased (See Appendix C.)**.** The classification of the pits according to ASTM Standard G46 [141], showed that the pitting was under class two as the density and size of the pits were approximately $1\times10^4/m^2$ and 2.0 mm^2 respectively.

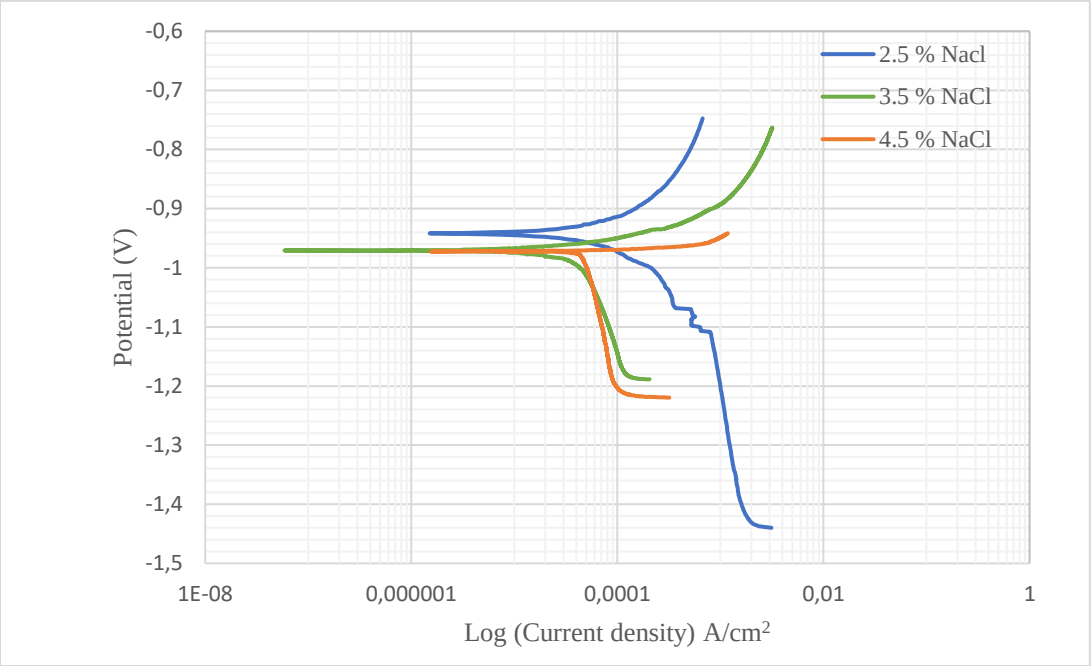


Figure 4.17: Polarization curves indicating the effect of NaCl concentration on the corrosion properties of dissimilar weld joints between Z225 and Al 5754.

Table 4.5: Effect of NaCl concentration on the electrochemical properties

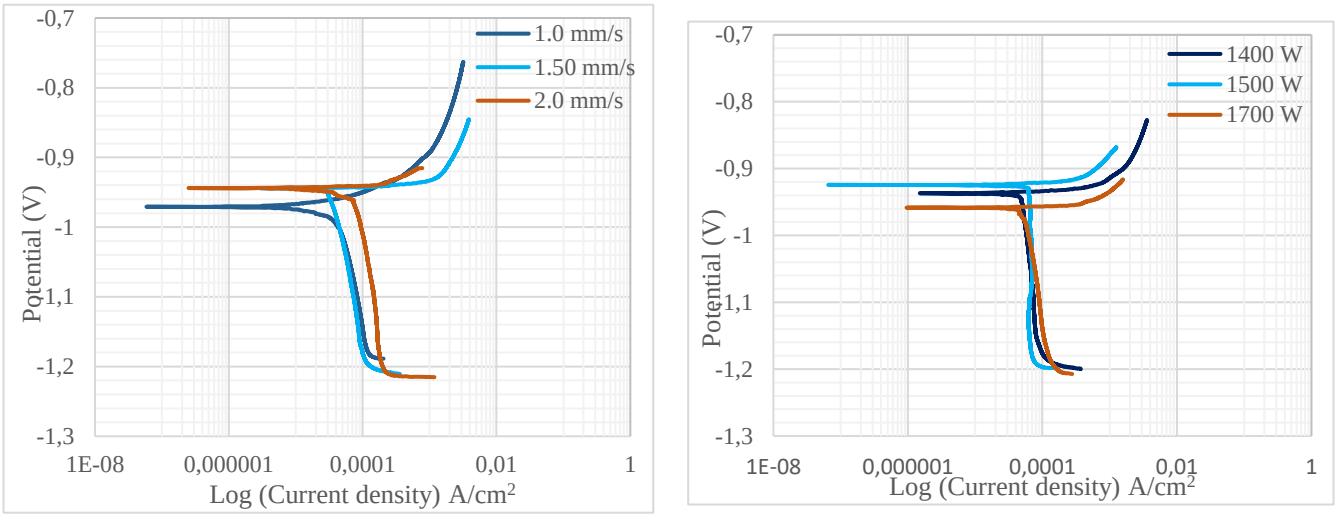
Laser welding power (W)	**Laser welding speed (mm/s)**	**NaCl concentration (%)**	**Corrosion current density (A/cm^2)**	**Corrosion potential (V)**	**OCP value (V)**
1500	1	2.5	4.56×10^{-5}	-0.950	-0.9393
		3.5	4.85×10^{-5}	-1.01	-0.9879
		4.5	6.04×10^{-5}	-1.01	-1.0184

4.4.2 Influence of welding parameters on the corrosion properties of the weld joints

The chloride ion concentration can remarkably vary between bodies of water [139]. Therefore, the effect of chloride ion concentration on the corrosion process plays a significant role because of the great presence of salt in the surroundings. The approximate salt level of the sea is 3.5 % [139]. As a result, the influence of laser welding speed and power on the corrosion properties of

the dissimilar weld joints were studied by keeping the electrolyte concentration constant at 3.5 wt.% NaCl (Figure 4.18 and Table 4.6). When speed was increased from 1.0 to 2.0 mm/s (Figure 4.18 (a)), the i_{corr} increased from 1.78×10^{-5} A/cm^2 to 6.04×10^{-5} A/cm^2. The OCP had a negative shift from -0.988 V to -1.014 V. In other words, as heat input was decreased, the corrosion resistance was compromised. This may be an indication that elevating the interfacial layer thickness had a positive influence on the corrosion properties of the Z225/Al 5754 dissimilar joints. Saleh *et al* [110] reported similar results and concluded that the corrosion resistance increased with an increase in the interfacial layer thickness. These results however contradict those obtained by Shi *et al*. [108] as they discovered that the presence of IMCs within the interfacial region led to the disbanding of the nearby weld seam, which accelerated the rate of corrosion [108]. It was further stated that as the thickness of the IMC layer increased, the corrosion resistance was reduced because increasing heat input resulted in higher i_{corr} [108].

Figure 4.18 (b) display the influence of laser welding power on the corrosion properties. An increase from1400 W to1700 W increased i_{corr} from 4.56×10^{-5} A/cm^2 to 7.03×10^{-5} A/cm^2 while the OCP value became more positive (Table 4.6). The shapes of the anodic and cathodic branches of the polarization curves were very similar meaning that the corrosion behaviour of the samples was comparable. None of the anodic branched exhibited a period of passive behaviour. Corrosion rate increased as laser power increased because as heat input increases, the volume of corrosion pits increases and then the corrosion rate becomes higher [139]. The tests were conducted 3 times for each set of parameters and the results showed the same trend.



(a) (b)

Figure 4.18: Polarization curves indicating the effect (a) Laser welding speed and (b) laser welding power on the corrosion properties of dissimilar weld joints.

Table 4.6: Effect of laser welding parameters on the electrochemical properties.

Laser welding power (mm/s)	**Laser welding speed (W)**	**NaCl concentration (%)**	**Corrosion current density (A/cm^2)**	**Corrosion potential (V)**	**OCP value (V)**
1500	1.0	3.5	1.78×10^{-5}	-0.98	-0.9879
	1.5		3.57×10^{-5}	-0.96	-0.9592
	2.0		6.04×10^{-5}	-0.96	-1.0144
1400	3.0		4.56×10^{-5}	-0.944	-1.0196
1500			6.04×10^{-5}	-0.932	-0.9972
1700			7.03×10^{-5}	-0.970	-1.0055

4.5 Mechanical properties

The influence of laser welding speed and power on the mechanical properties of the Z225/Al 5754 joints were studied by performing microhardness and tensile shear strength tests on the samples. The creation of IMC phases is a crucial subject in dissimilar metals welding as it can increase hardness while decreasing the toughness of the weld joint. Besides the presence of IMCs, the size of grains is also correlated to the hardness of materials [32].

4.5.1 Microhardness

Hardness distribution curves can be useful when interpreting the microstructure of the weld and mechanical characteristics [142]. Microhardness measurements were first taken along the path perpendicular to the welding direction, that is, from the weld surface to the weld root with an average increment of approximately 125 µm. Then microhardness values were measured along the transverse section through the BM, HAZ, WM at three different penetration levels which were at the top, middle and bottom profiles of the weld joint.

4.5.1.1 Effect of laser welding power on microhardness along the perpendicular direction of the weld joint

Microhardness distribution curves of the weld joints for constant laser welding speed of 3.0 mm/s and laser power of 1400 W, 1500 W, 1600 W and 1700 W are displayed in Figure 4.19.

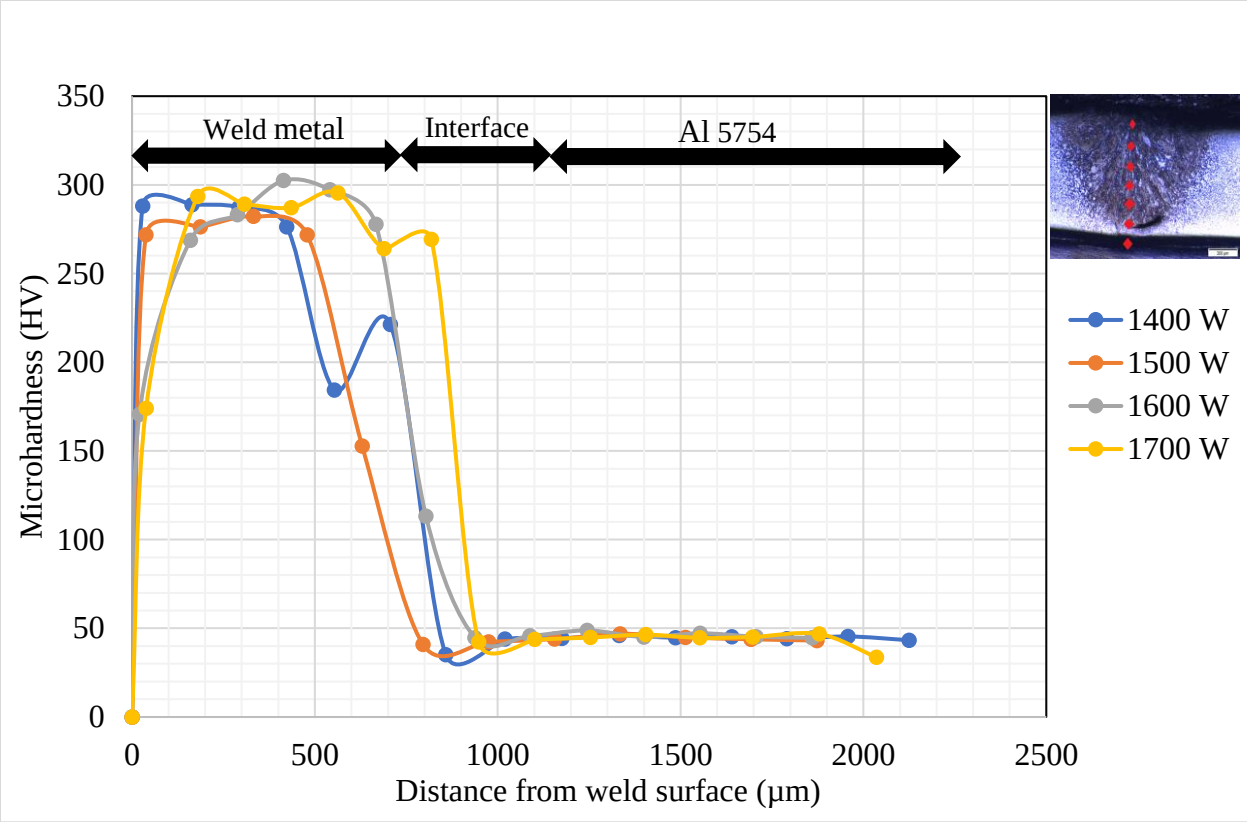


Figure 4.19: Effect of laser welding power on WM microhardness

It can be noticed that the microhardness curves show a similar trend. This observation was expected as the corresponding optical micrographs displayed similar grain structures. The microhardness of the WM and the interfacial region was much higher compared to Al 5754 base metal. The elevated hardness observed at the interfacial area is largely related to the presence of IMCs in that region. The average microhardness values of the WM ranged between 214.4 HV and 220.42 HV. The microhardness values of Al 5754 BM for all conditions were almost the same throughout and ranged between 43.43 HV and 45.91 HV. It was noted that the hardness values within the FZ had very slight variations. This may be because as welding power was increased, there were few IMC phases created [87].

4.5.1.2 Effect of laser welding speed on microhardness along the perpendicular direction of the weld joint

Figure 4.18 shows the impact of laser welding speed on the microhardness of weld joints at a constant laser power of 1500 W.

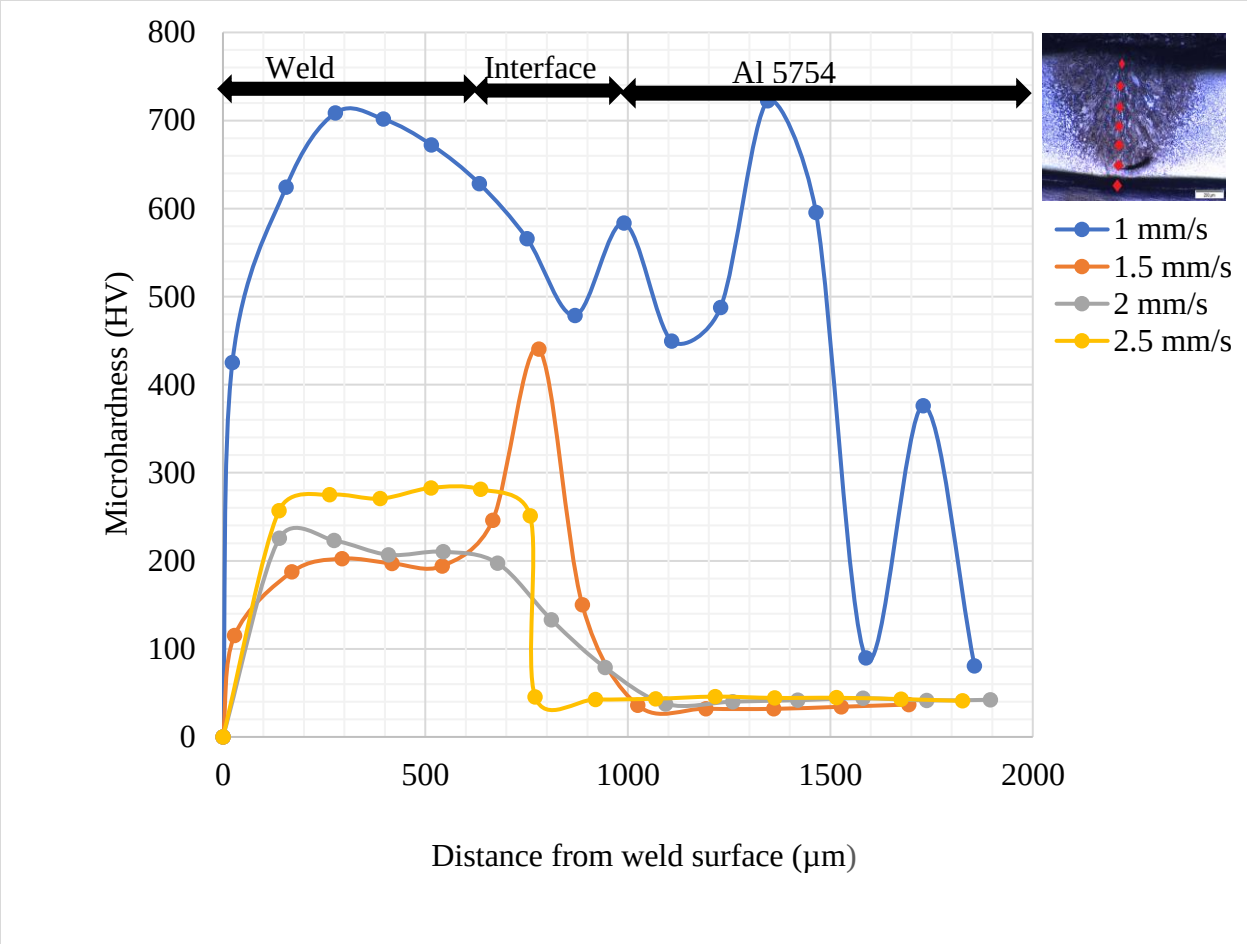


Figure 4.20: Effect of laser welding speed on weld metal microhardness

The highest microhardness values were observed at the lowest laser welding speed of 1.0 mm/s. The maximum hardness measured at the WM had a value of 708.6 HV. According to the reference values listed in Table 2.6, the value did not fall within any of the given ranges. This may be because the corresponding EDS composition predicted a two-phased mixture of FeAl and $FeAl_2$ IMC as the dominant phase. The microhardness profile exhibited fluctuations in hardness values due to the different IMCs that were detected within the weld metal. Oyyaravelu *et al.* [143] observed a similar behaviour and reported that the discrepancies in microhardness values were caused by the differences in carbon content within the weld metal. Furthermore, the fluctuations were alluded to the variances in metallurgical phase components throughout the weld metal [143]. As laser welding speed was increased from 1.0 to1.5 mm/s, the average microhardness of the weld joint drastically decreased to 184.54 HV. The curve had a peak at the interface whose value was measured as 440.4 HV. The EDS analysis composition at this point

showed the presence of FeAl. This observation supports the claim made by Wan *et al*. [143] that, the high microhardness at the interfacial area is often attributed to the presence of IMCs and plastic deformation which takes place during the laser welding process. As the speed was increased to 2.0 mm/s, the average microhardness of the WM increased to 199.32 HV. At 2.5 mm/s, the WM microhardness had an average of 269.55 HV.

Basically, as laser welding speed was increased from 1.5 mm/s to 2.5 mm/s, the average microhardness of the weld metal increased. The corresponding grain structures in Figure 4.5 showed that the grain sizes decreased as laser welding speed increased. This is because LBW is a non-equilibrium process and can thus produce weld joints with a finer microstructure and higher hardness through rapid solidification mechanism [32]. Grain refinement within a material leads to more grains which are close to each other and possess different orientation. As a result, distortions are prohibited from travelling, crossing, and accumulating between the grains which limits chances for crack initiation and eventual failure [133]. Strengthening of materials through grain size refinement is controlled by the Hall-Petch relationship which informs us that materials strength which is equivalent to the theoretical strength of the material and hardness could be achieved through grain size reduction [130]. Although the microhardness increased as speed increase from 1.5 mm/s to 2.5 mm/s, the values did not reach the levels observed at the lowest speed of 1.0 mm/s.

4.5.1.3 Effect of laser welding speed on microhardness along the transverse direction of the weld joint

Figure 4.19 illustrates the microhardness profiles in the transverse direction at varying laser welding speed (1.0 mm/s to 2.5 mm/s) and constant laser welding power (1500 W). The hardness values of both BMs were not substantially affected by the change in penetration depth at all conditions. Maximum hardness in all welding condition was recorded within the WZ. Generally, the increase started showing at the HAZ and increased further towards the centre of the weld where the maximum values were observed.

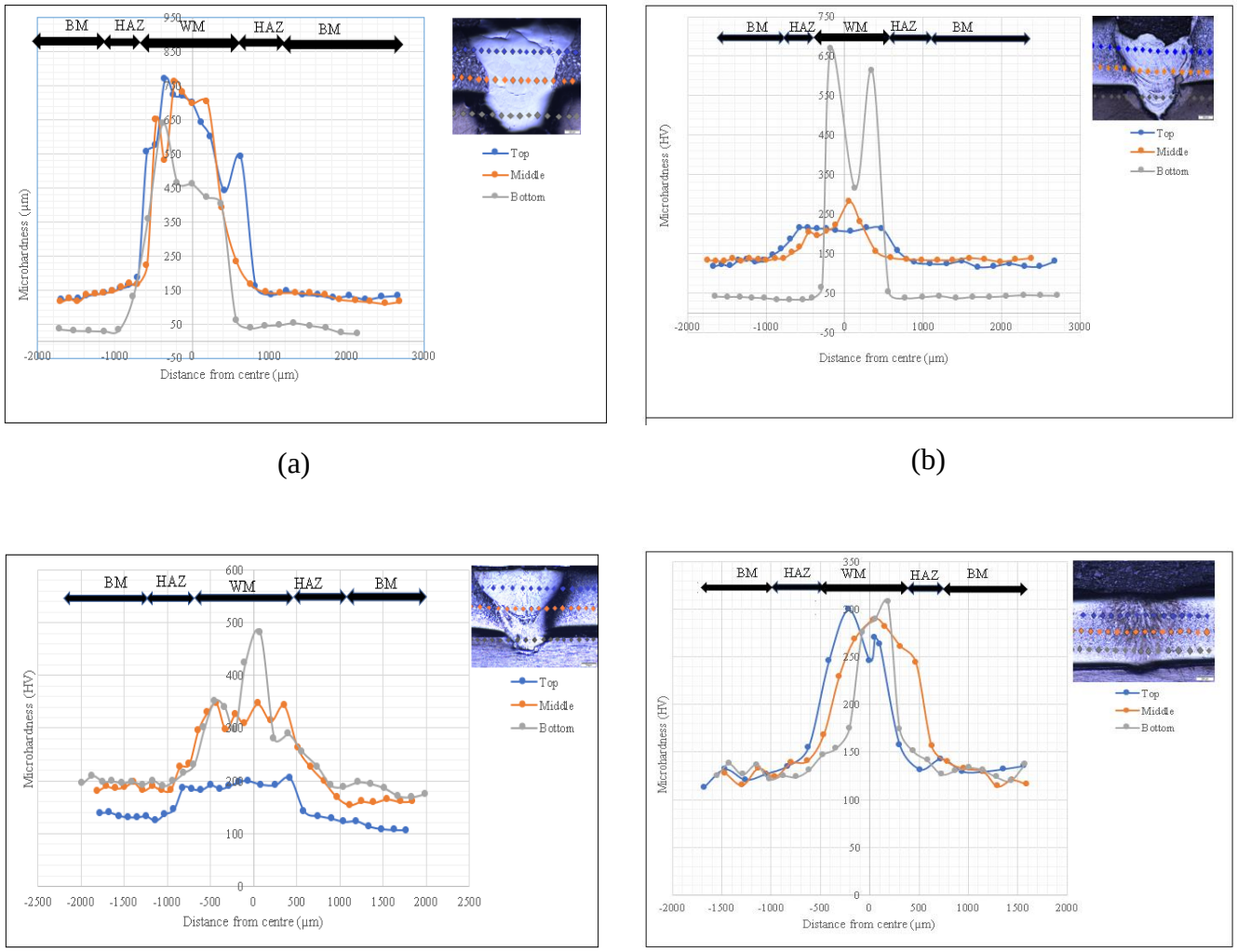


Figure 4.21: Effect of laser welding speed on the transverse microhardness measurements. (a) 1.0 mm/s, (b) 1.5 mm/s, (c) 2.0 mm/s, and (d) 2.5 mm/s.

For 1 mm/s, the hardness values within the FZ were substantially higher compared to other laser welding conditions (Figure 4.19(a)). This is due to the presence of IMC which were formed throughout the FZ. The microhardness values of the WM for the top, middle, and bottom profiles were all high. Raising the welding speed to 1.5 mm/s reduced the occurrence of IMCs and thus the average microhardness values within the FZ were also decreased (Figure 4.19 (b)). However, there were two notable peaks which most probably denoted the IMCs especially because they occurred at the bottom area near the interfacial region. The microhardness values corresponding to the peaks were 668.4 and 614.0 HV respectively. A similar behaviour was observed for 2.0

mm/s as there was also a sharp increase in hardness at the centre for the bottom profile which was measured as 481.8 HV (Figure 4.19 (c)).

It was noted that as laser speed was increased from 1 mm/s to 2.0 mm/s, since the cooling rates were accelerated, the hardness distribution for top profiles was much more uniform. This is because at this level of penetration the IMCs are almost completely absent as it has been proven by the chemical composition from EDS analysis around this region. Rapid cooling rates decrease the degree of heat flow and diffusion within the molten pool during laser welding [87]. As a result, the extents at which the atoms of BMs mix are limited and thus restrict IMC growth. This leads to a hardness distribution which is more even [87]. Kashani *et al*. [87] stated that a uniform microhardness distribution of the FZ can be achieved if the reaction between base metal elements is limited to reduce the formation of IMCs. The highest hardness values were observed for the lowest laser welding speed (1mm/s). Despite the presence of IMC, it was noted that the middle profile had slightly higher hardness values compared to the top and bottom profiles for the conditions when laser power was kept constant.

4.5.1.4 Effect of laser welding speed on microhardness along the transverse direction of the weld joint

Figure 4.20 presents the transverse microhardness profiles for constant laser welding speed of 3.0 mm/s.

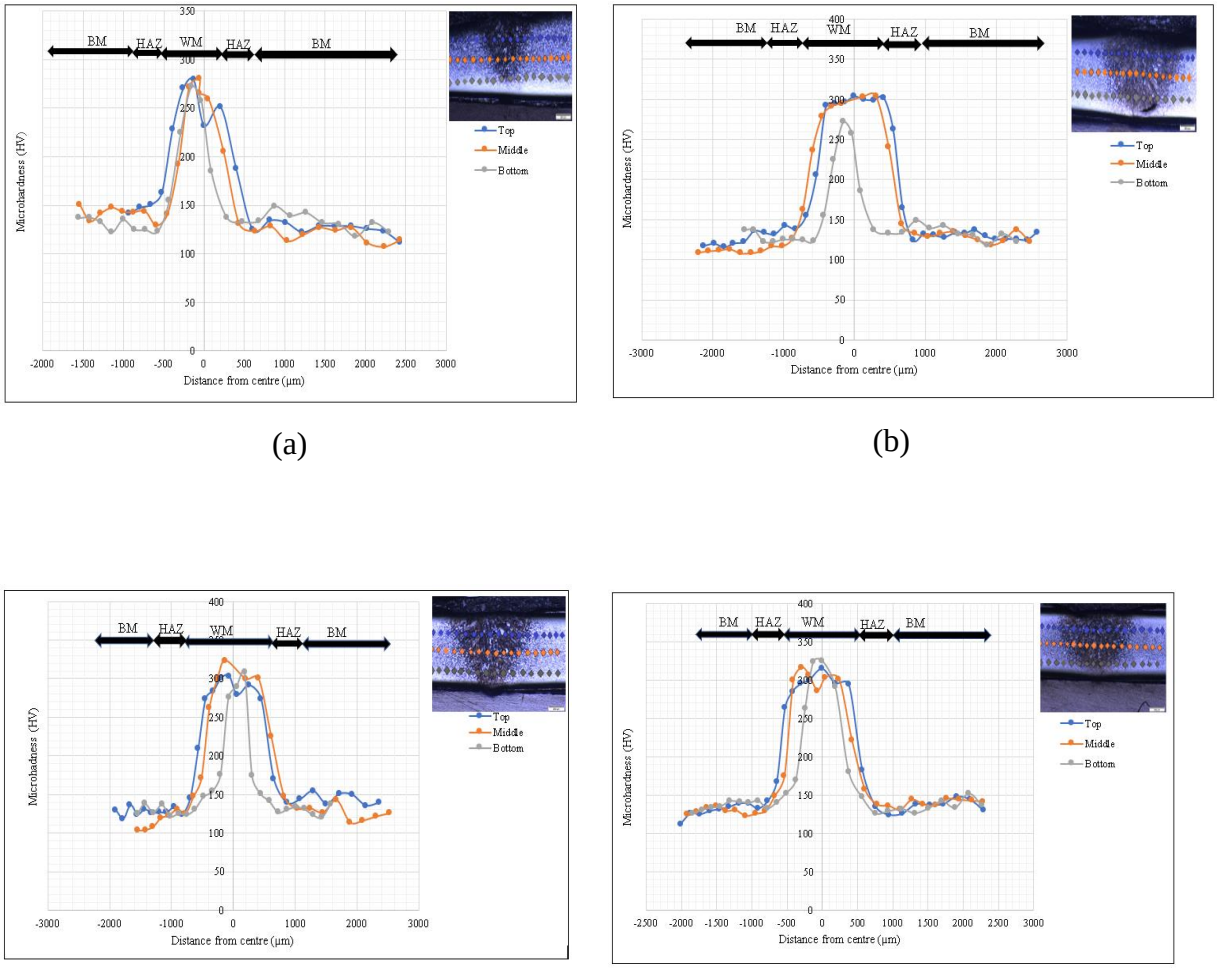


Figure 4.22 : Effect of laser welding power on the transverse microhardness measurements. (a) 1400 W, (b) 1500 W (c) 1600 W and (d) 1700 W.

The microhardness profiles for the change in laser power from 1400 to 1500 W were all similar. There were no large differences between the top, middle and bottom profiles of the weld joint microhardness values in all conditions. No peaks indicating the presence of IMCs were detected on the microhardness profiles. However, the average microhardness of the weld metal increased from 244.54 HV to 289.98 HV when power increased from 1400 W to 1700 W.

4.5.2 Tensile properties

The dissimilar weld joints were subjected to tensile shear strength tests to study the effect of laser welding speed and power on tensile properties.

4.5.2.1 Effect of laser speed welding on the tensile properties of Z225/Al 5754 weld joints.

The results revealed that most samples experienced interfacial failure. According to Wallerstein *et al*. [144], this observation may be attributed to the creation of the IMC phases at the interface. The interfacial region is naturally the most fragile zone of dissimilar joints. The only exception was the sample produced at 1.0 mm/s as it failed at the HAZ of the aluminium side. It should be noted that the mechanical attributes of the HAZ are non-uniform. This is caused by the gradual transformation from the properties of the WM to those of the BM away from the weld zone. As a result, the tensile strength of the HAZ can be expressed as the average of the WM strength and the BM strength [145], [146]. During the welding process, there is an abrupt variation in geometry from the base materials. As the geometry changes, the tensile properties are affected. Stress concentration which results at the weld root further leads to localized stresses causing failure at the weaker BM [127]. Therefore, the crack originated at the stress concentration and proceeded through the HAZ of Al 5754 base metal. This observation supports the information provided by Sadek [67] regarding materials with different coefficient of thermal expansion. It was stated that the large difference in thermal expansion induces internal stresses which cause failure at the HAZ during service [67].

The tensile response of the samples was compared from stress-strain curves in Figure 4.21. The measured quantities for UTS, YS and % elongation are recorded in Table 4.5. The results indicated that there was no huge influence on the tensile strength properties for conditions which were controlled by changing laser welding speed.

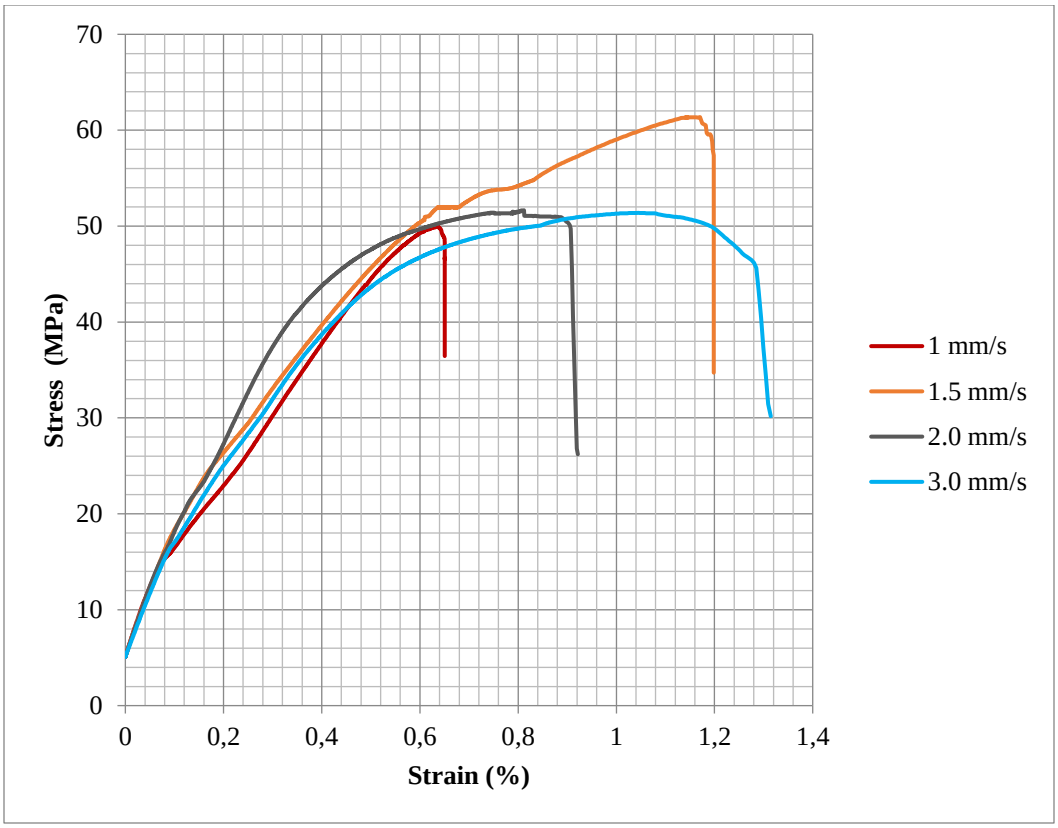


Figure 4.23 : Stress-strain curves for constant laser power of 1500 W and varying laser welding speed.

Table 4.7: Effect of laser welding speed on tensile behaviour

Laser Power, (W)	Laser welding speed, (mm/s)	Maximum force [F_m], kN	Ultimate tensile strength [UTS], MPa	Non proportional Elongation [NPE], %
1500	1	0.59	50	0.34
	1.5	0.74	61	1.08
	2	0.62	51	0.44
	3	0.62	51	0.7

The UTS values were similar. However, some degree of ductility was observed for the sample produced at 1.5 mm/s and 1500 W. The sample had the highest NPE of 1.08 %. According to Dinda [89], high % elongation results from of a regular microstructure throughout the WM. The uniform microstructure yields compositional allocations that subdue cracking caused through stress concentration by improving the trai-axiality of stress condition [89]. Ironically, the micrograph of the weld joint produced at 1.5 mm/s and 1500 W revealed both circular and columnar grain structure.

4.5.2.2 Effect of laser welding power on the tensile properties of Z225/Al 5754 weld joints.

The stress-strain curves showing the impact of laser welding power on tensile behaviour are displayed in Figure 4.24. It was noted that compared to laser welding speed, the change in laser power had a greater impact on the tensile properties of the weld joints. The opposite was however expected because according to the results obtained by Kim *et al*. [30], laser welding speed had the most impact on tensile strength followed by laser power and then the focal point [30]. However, it should be noted that Kim *et al*. [30] used a different grade of galvanized steel, that is, SGCD1. Therefore, it is possible that the Z255 and Al 5754 combination responded differently to the change in laser welding parameters.

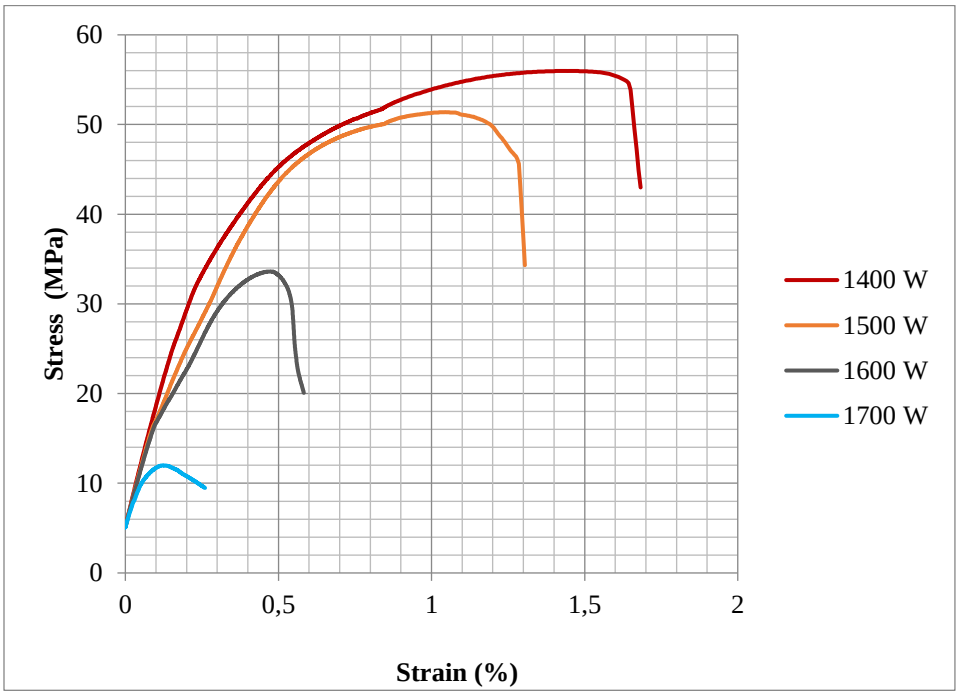


Figure 4.24 : Stress-strain curves for different laser powers and constant speed of 3.0 mm/s.

The results recorded in Table 4.6 show that there was an indirect relationship between laser power and tensile properties. As the heat input was increased by increasing power, both the UTS, NPE % decreased. The maximum achievable UTS and NPE % were 51.51 MPa and 0.81 % respectfully at 1400 W. The highest laser power of 1700 W achieved the lowest UTS and NPE % of 12 MPa and 0.068 % respectfully. This inverse relationship between laser power and tensile strength was most likely caused by the creation of IMCs as heat input was increased. The higher

the heat input, the thicker the IMC layer which increases the brittleness of the joint, reducing the joint strength [136].

Table 4.8: Effect of laser welding power on tensile properties at constant speed of 3.0 mm/s.

Laser Power, (W)	Maximum force [F_m], kN	Ultimate tensile strength [UTS], MPa	Non proportional Elongation [NPE], %
1400	0.62	51	0.81
1500	0.62	51	0.70
1600	0.4	33	0.26
1700	0,14	12	0.068

4.6. Summary

Chapter 1 of the dissertation introduced the research topic and the knowledge areas. The chapter also gave a context of the research problem and the research question the project seeks to address. The topic was further explored in Chapter 2, by means of an in-depth literature review from related topics. Key findings from similar research were presented in Chapter 2. The focus of Chapter 3 was to give a detailed description of the methodology followed to obtain the results in Chapter 4.

The findings in Chapter 4 indicated that laser welding speed and power both affect the microstructural characteristics, corrosion resistance and mechanical properties. At constant laser power, the weld pool decreased with an increase in laser welding speed. Generally, the weld penetration, weld width and HAZ measurements decreased as speed was increased from 1.0 mm/s to 2.5 mm/s. There was an undercut defect observed at 1.5 mm/s which led to smaller weld bead dimensions than anticipated. The grain size also decreased as laser welding speed was increased.

At constant laser welding speed, the weld bead dimensions increased with an increase in power. At lower powers, insufficient penetration was noticed. The grain structure was not severely affected by a change in power. A fine columnar microstructure was observed throughout.

The SEM/EDS results showed that at high heat inputs, the interfacial layer thickness increased. As a result, at high heat inputs, the EDS composition indicated high mixing between Fe and Al atoms at the interface. More IMC phases were detected at higher heat inputs. It was also

observed that the effect of speed on the IMC formation was greater than the impact of power. The XRD analysis performed on the weld joints confirmed the presence of FeAl, $FeAl_2$ and Fe_2Al_5. The quantity of the phases increased with an increase in heat input.

Electrochemical corrosion tests were conducted to analyse the impact of NaCl concentration on corrosion properties of Z225/Al 5754 weld surface. Increasing NaCl concentration decreased the corrosion resistance of the weld surface. The value of i_{corr} increased at corrosion increased and the OCP value became more negative.

The effect of laser welding speed and power on the corrosion resistance were tested using 3.5 % NaCl concentration. At constant power, as the laser speed increased, the i_{corr} increased and the OCP value became more negative. Therefore, better corrosion properties were observed at lower laser welding speeds. At constant laser welding speed, the i_{corr} increased as laser welding power increased. As a result, the best corrosion performance was observed at the lowest speed on 1.0 mm/s.

The microhardness of the weld metal at varying laser powers were comparable. The change in power did not show any major effect on the microhardness of the weld metal. On the other hand, when welding speed was changed, the lowest speed produced the highest hardness values at the weld metal due to the presence of brittle IMCs.

Tensile shear strength results revealed that as laser power increased from 1400 W to 1700 W, the UTS and % elongation drastically decreased. When laser speed was altered, the UTS values did not change much, generally. At 1.5 mm/s, the maximum UTS and maximum % elongation of 61 MPa and 1.08 % respectively were obtained. However, the parameters which passed the tensile shear strength was the combination between 1.0 mm/s and 1500 W.

Chapter 5 : CONCLUSIONS AND RECOMMENDATIONS

5.1 Conclusions

The aim of the research project was to determine laser welding process parameters which offer sound weld joints between Z225 and Al 5754 for application within the automotive industry. The following general conclusions were reached:

- Increasing heat input by increasing laser welding power and decreasing laser welding speed increased the weld bead dimensions of the Z225/ Al 5754 weld joints.
- The larger the grains of the weld metal, the higher the microhardness values and the better the tensile properties of the joints.
- The interfacial layer thickness and IMC phases decreased with a decrease in laser welding power and an increase in laser welding speed.
- Increasing the NaCl concentration increased the i_{corr} value leading to a decrease in the corrosion resistance of the weld joint surfaces.
- An increasing in both laser welding power and laser welding speed increased the $i_{corr,}$ decreasing the corrosion resistance.

The optimum parameters for welding laser welded dissimilar joints between Z225 and Al 5754 of 0.8 mm and 1.2 mm thickness respectively were found to be 1.0 mm/s and 1500 W. These parameters gave the best corrosion properties, the highest microhardness, and the best tensile strength properties.

5.2 Validation of hypotheses

The results obtained from the experiments led to the following confirmations about the hypotheses.

- Hypothesis 1: Accepted because it was discovered that the interfacial layer thickness and IMC phases increased with an increase in heat input.
- Hypothesis 2: Rejected since the corrosion resistance increased with an increase in heat input.

- Hypothesis 3: Rejected as the microhardness values and tensile strength properties improved as heat input increase.

5.3 Recommendations

Literature has limited information in terms of the conditions that lead to the creation of two-phased IMCs and their properties. Therefore, future research should be based on the creation, stability, and properties of such IMC phases.

There was a contradiction from literature in terms of whether increasing the interfacial layer thickness improve the corrosion properties of dissimilar joints. As a result, it would be advisable for prospect research to concentrate on the relationship between corrosion properties, the thickness of the interfacial region and the types of IMC phases.

To obtain the optimum laser welding parameters between Z225 and Al 5754, more experiments should be done between the laser welding speed of 1.0 and 1.5 mm/s with 1500 W, as the parameters produced desirable weld joint properties.

The current research implicates a positive contribution to research intended for the automotive industry and creates a guideline for selecting the most appropriate laser welding parameters for joining Z225 and Al 5754. It has been proven that it is possible to join Z225 and Al 5754 for manufacturing vehicle bodies. Choosing the correct parameters is significant in obtaining weld joints with the most desirable quality. The results indicated that the most suitable properties were obtained at slower laser welding speeds that would result in slower production. However, it is also imperative for car manufacturers to prioritize passenger safety.

Chapter 6 . APPENDICES

Appendix A: XRD analyses of dissimilar joints between Z225 and Al 5754

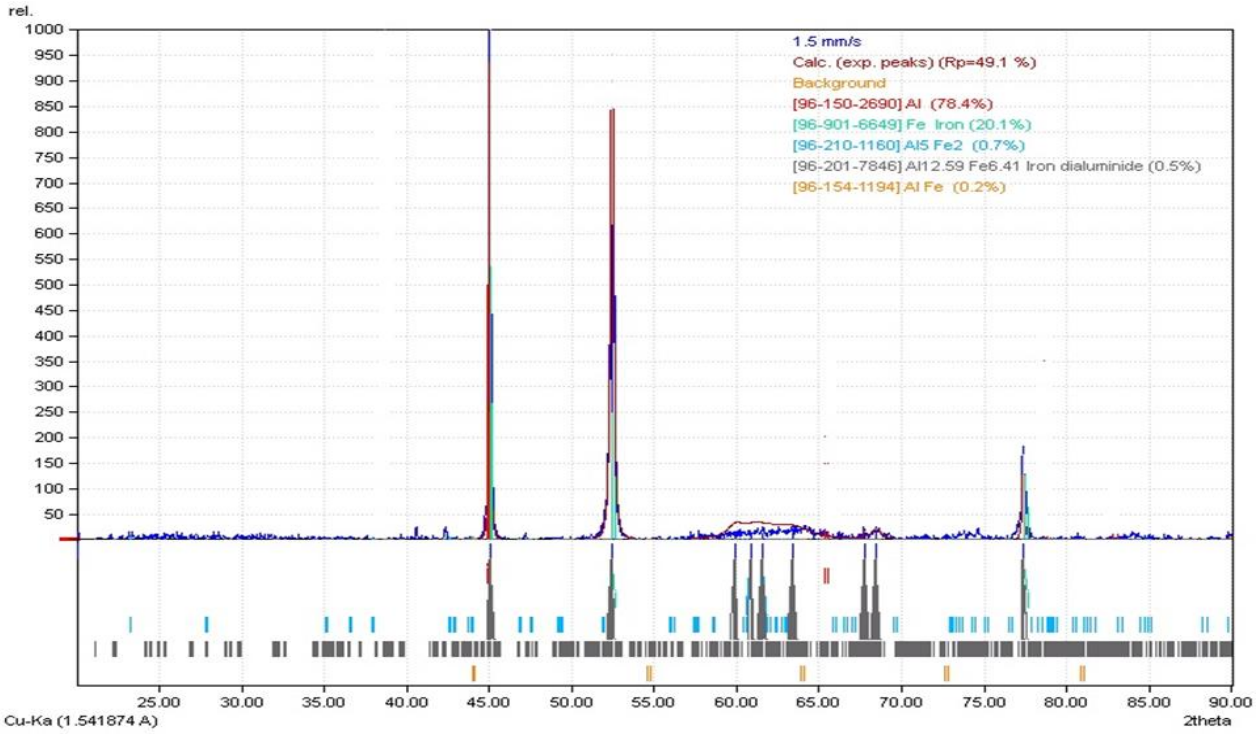


Figure 6.1: XRD pattern for 1.5 mm/s showing the quantity of elements and IMC phases

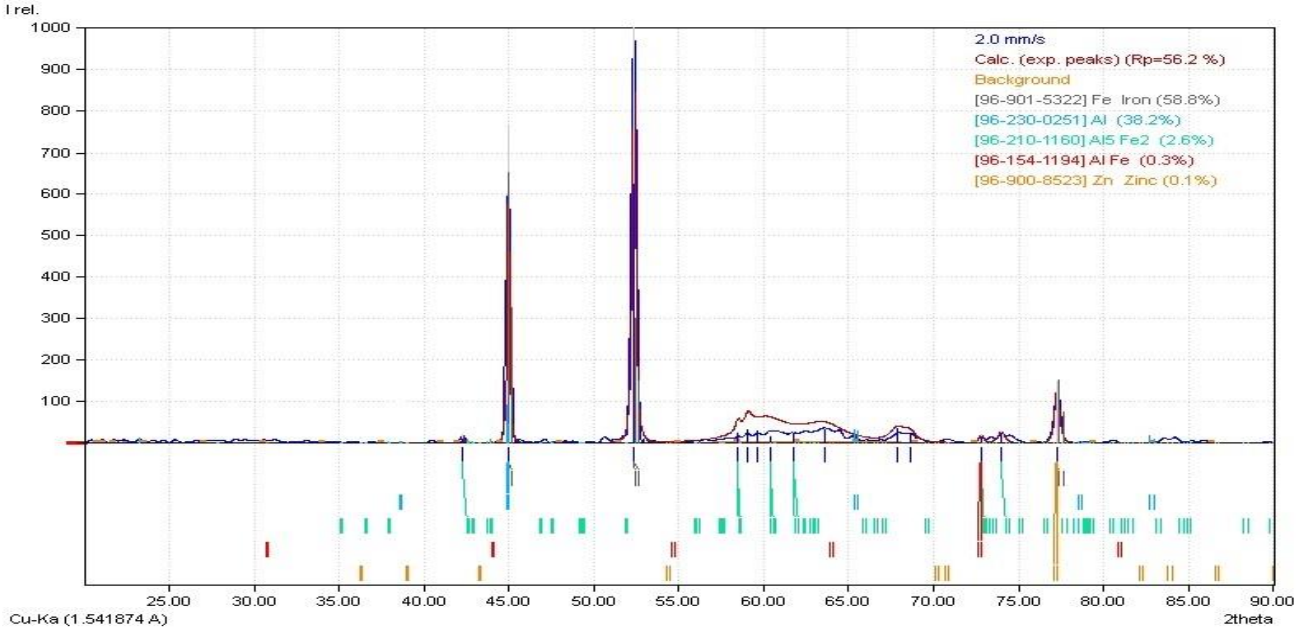


Figure 6.2: XRD pattern for 2.0 mm/s showing the quantity of elements and IMC phases

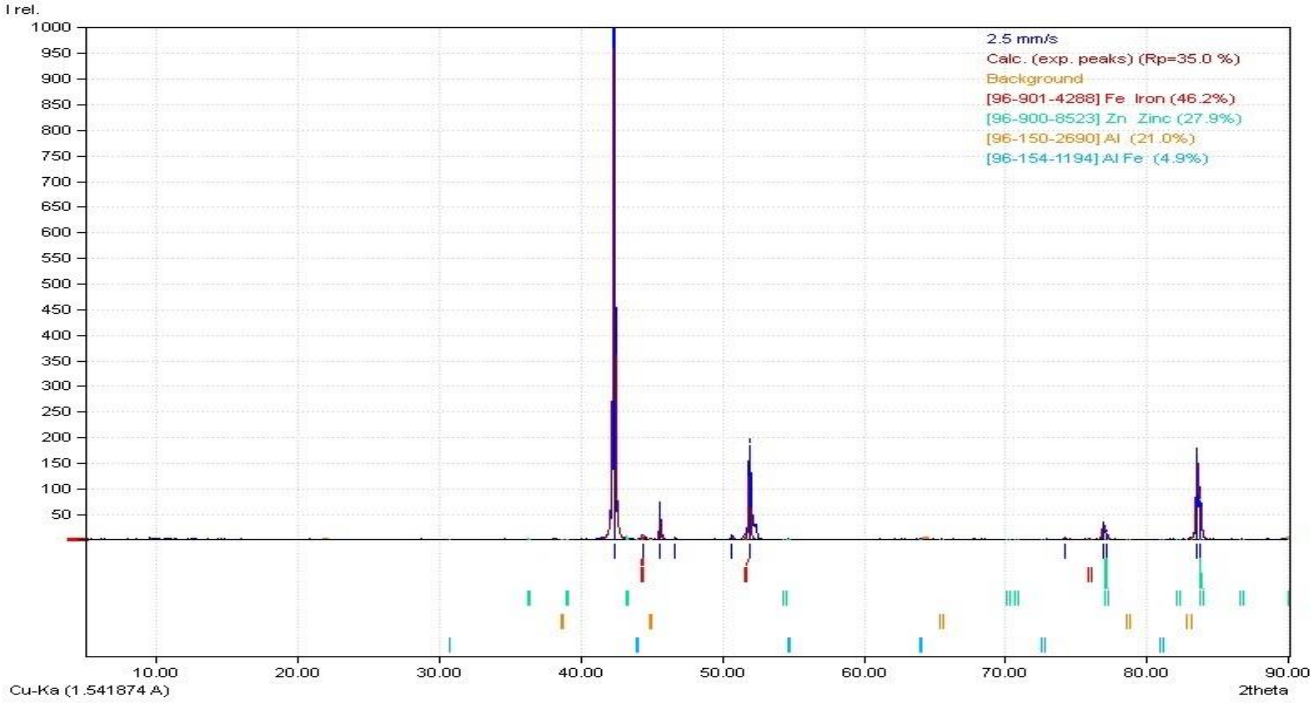


Figure 6.3: XRD pattern for 2.5 mm/s showing the quantity of elements and IMC phases

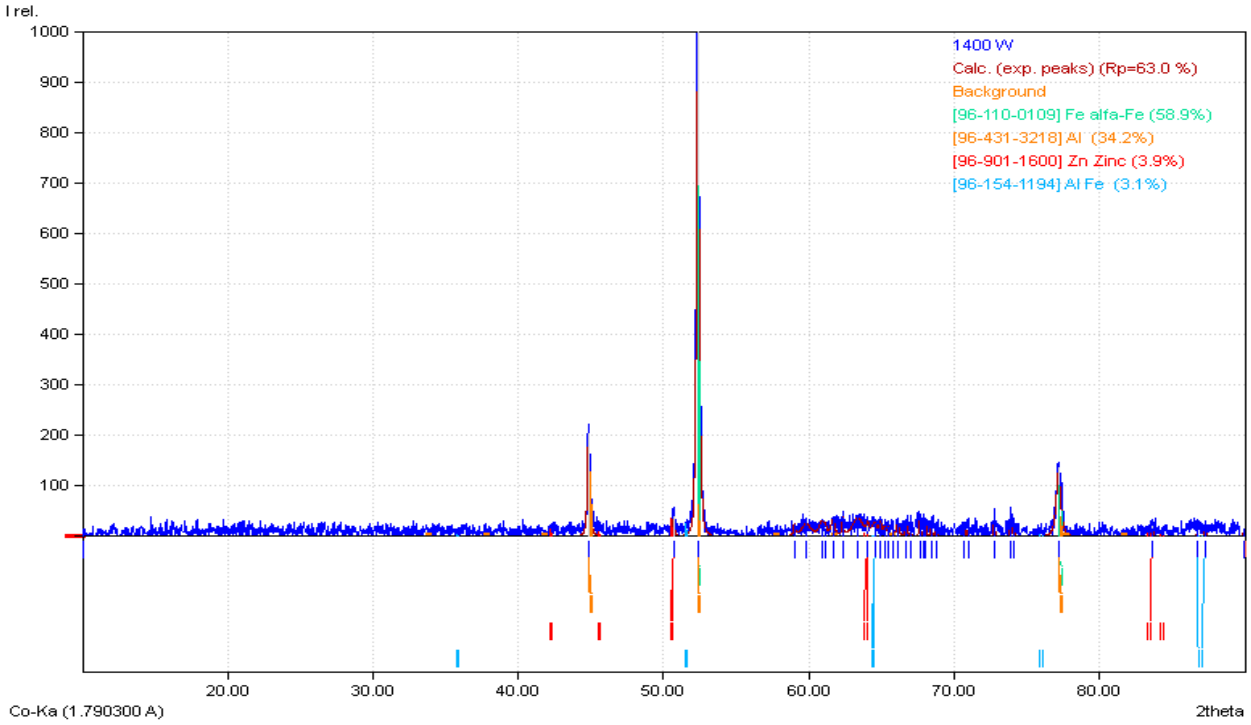


Figure 6.4: XRD pattern for 1400 W showing the quantity of elements and IMC phases

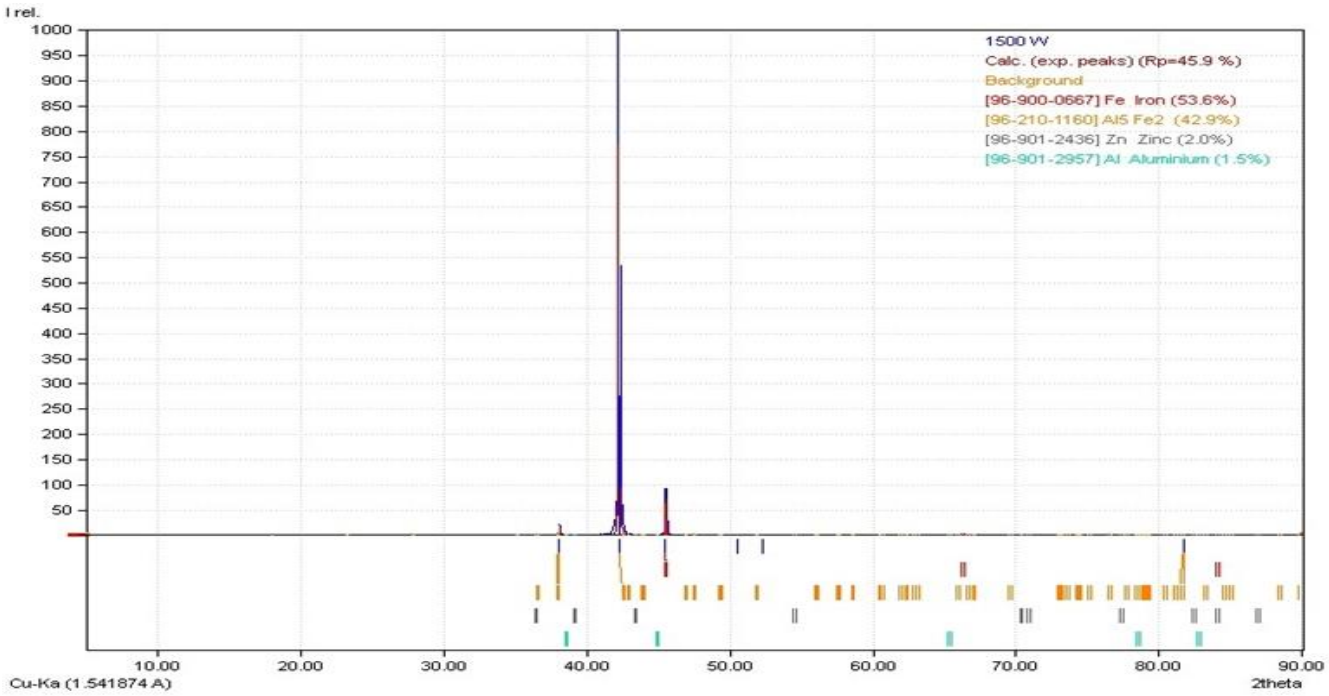


Figure 6.5: XRD pattern for 1500 W showing the quantity of elements and IMC phases

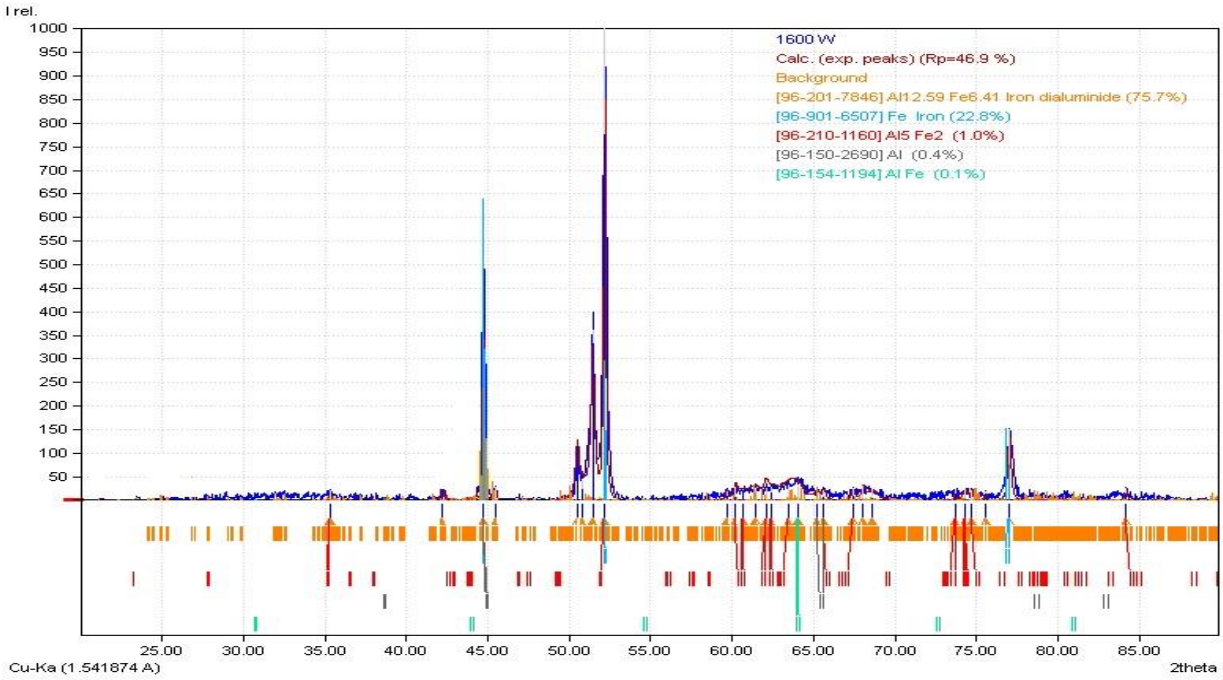


Figure 6.6: XRD pattern for 1600 W showing the quantity of elements and IMC phases

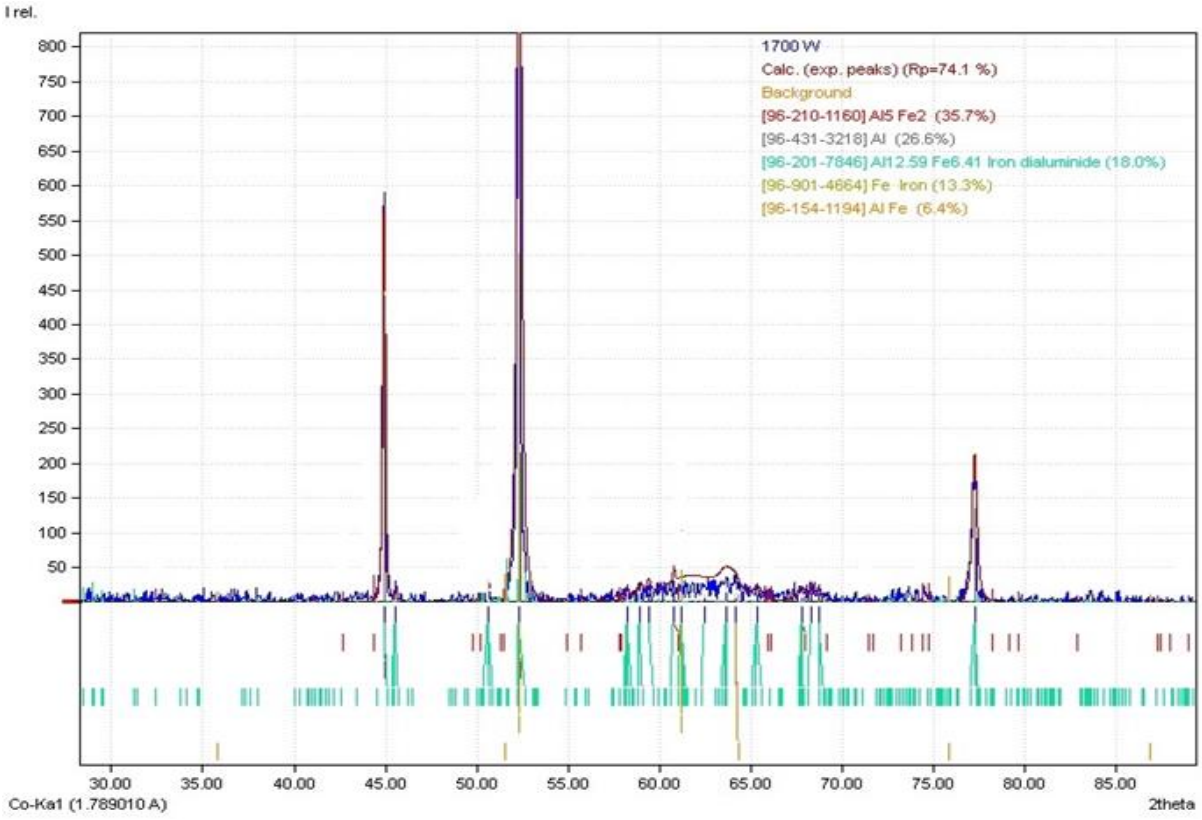


Figure 6.7: XRD pattern for 1700 W showing the quantity of elements and IMC phases

Appendix B: Effect of NaCl concentration and welding parameters on OCP values of dissimilar weld joints

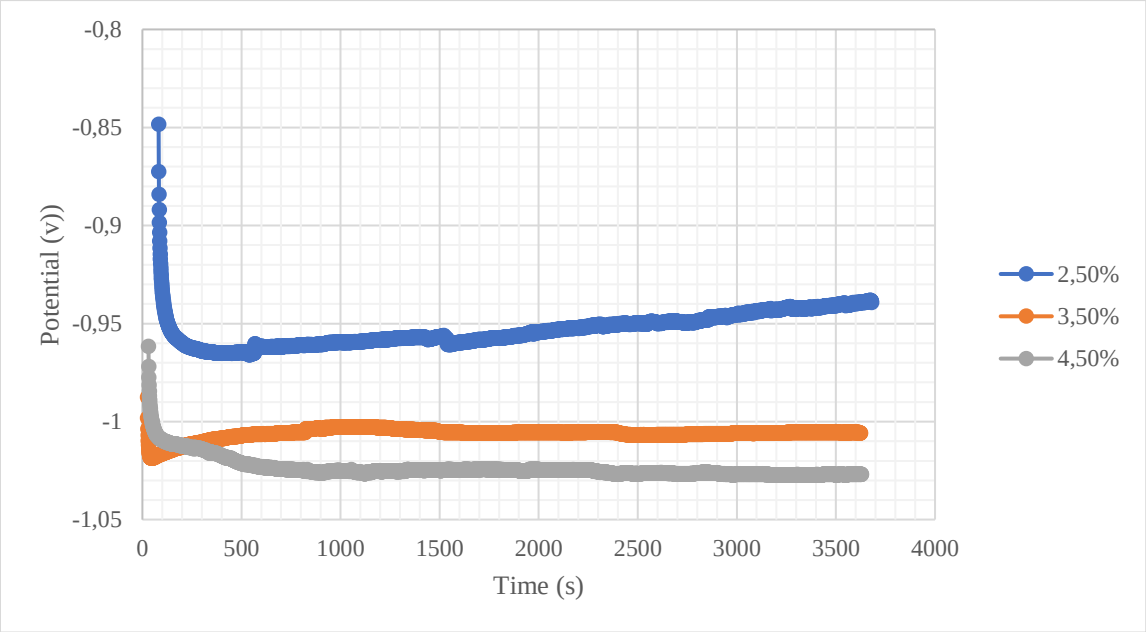


Figure 6.8: Impact of NaCl concentration on the OCP values

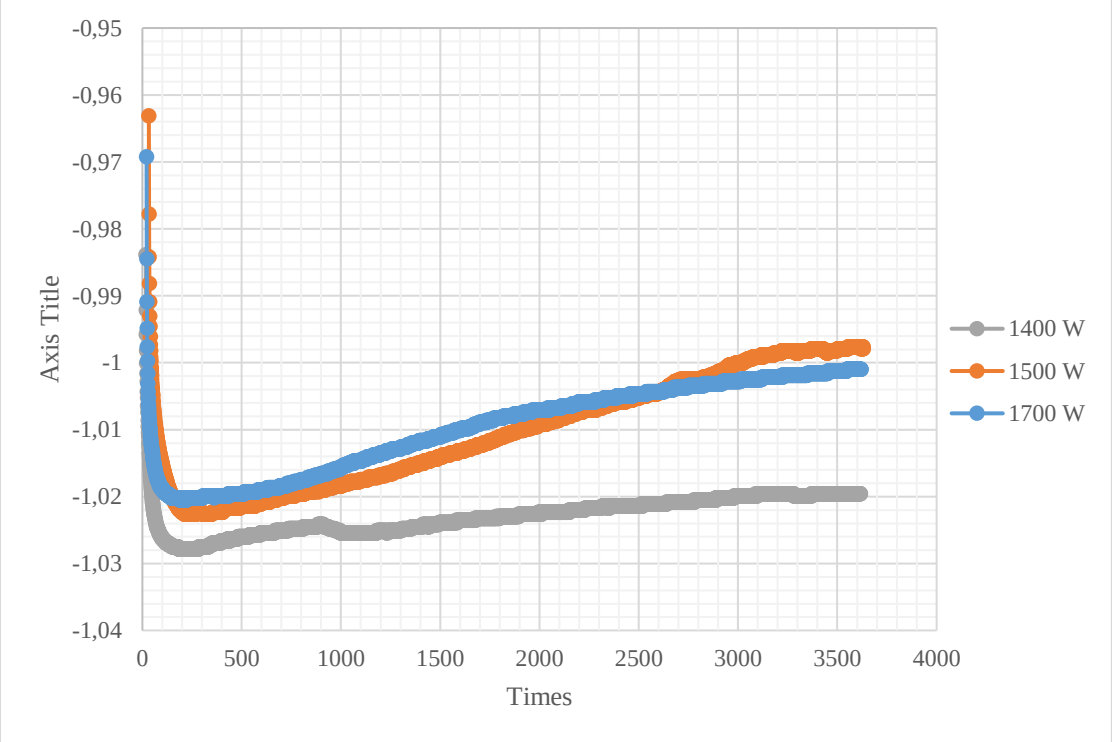


Figure 6.9: Impact of laser welding power on OCP values

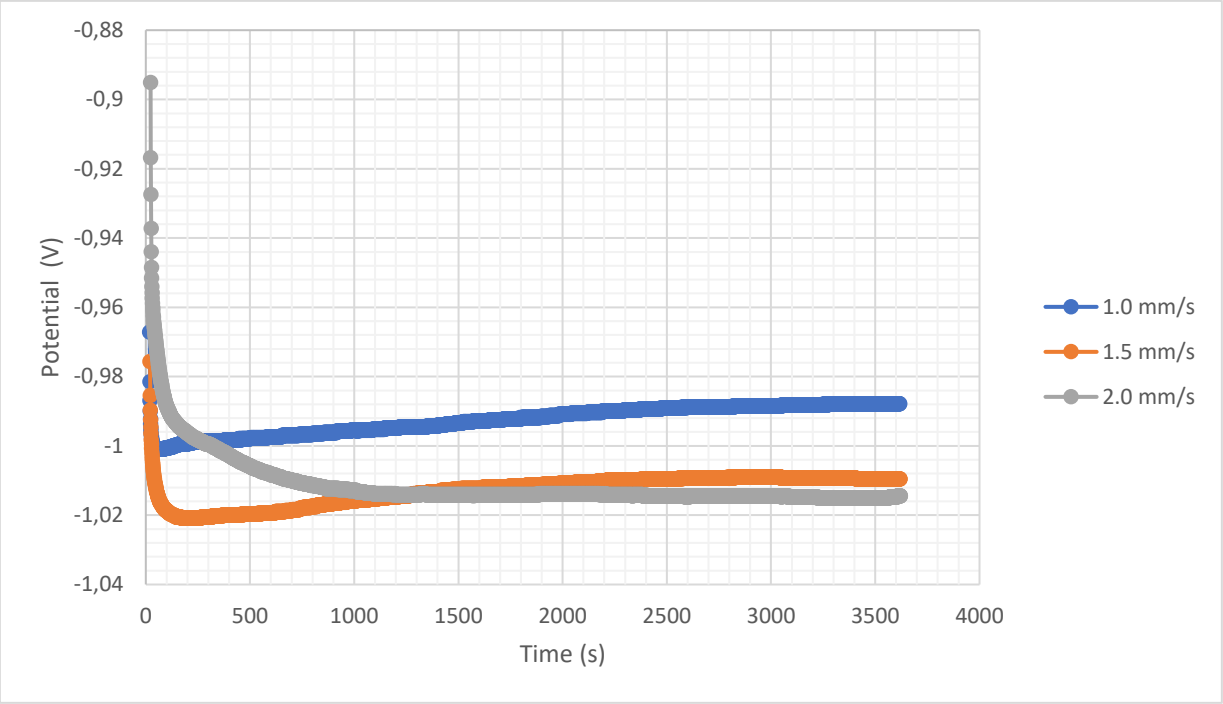


Figure 6.9: Impact of laser welding speed on OCP values

Appendix C: Pitting corrosion on weld joint surfaces

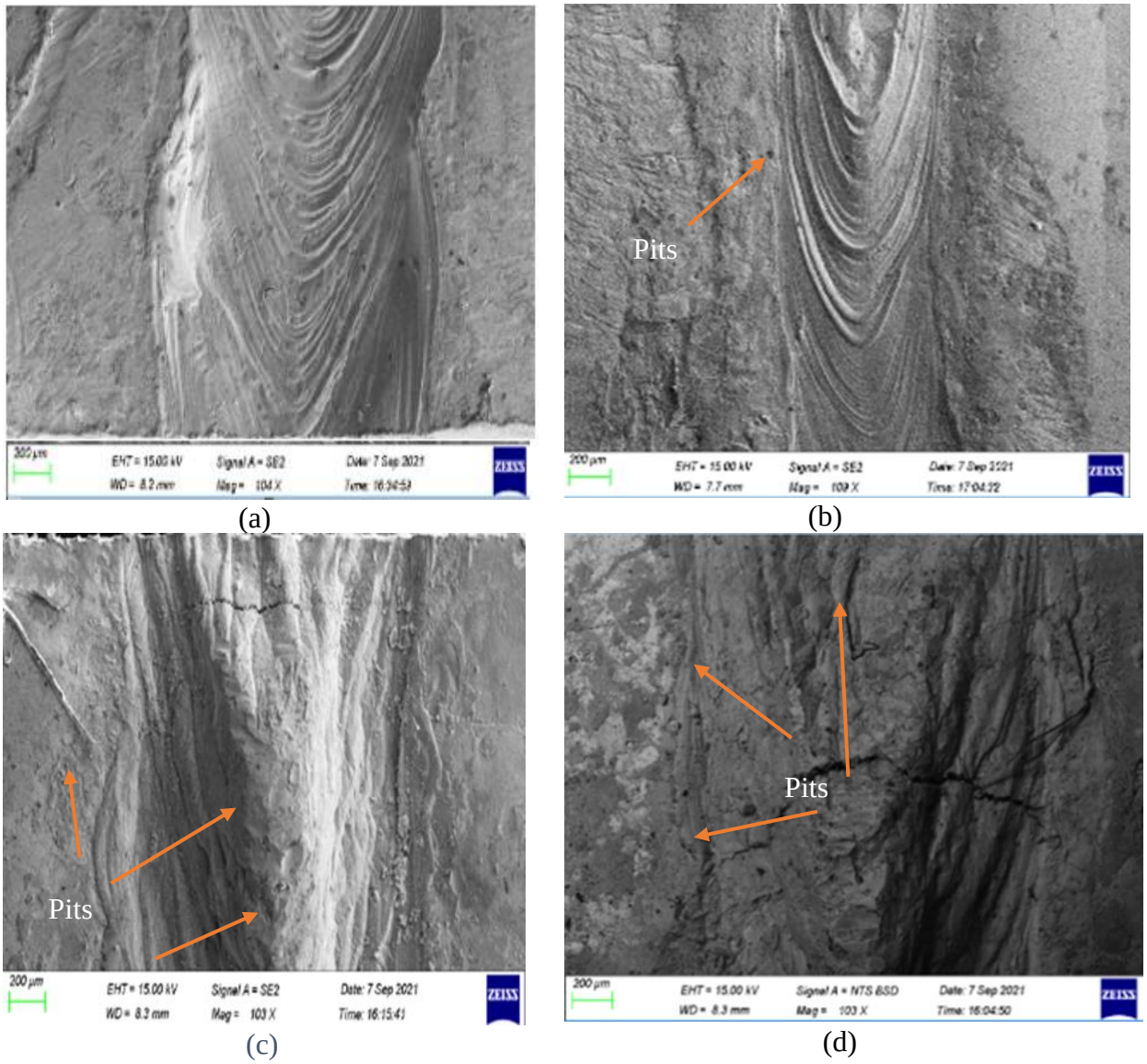


Figure 6.10: Z225/Al 5754 surface before and after being exposed to different NaCl concentrations. (a) before exposure, (b) after being exposed to 2.5 % NaCl, (c) 3.5 % NaCl, (d) 4.5 % NaCl

REFERENCES

[1] C. Yuce, F. Karpat, N. Yavuz, Investigations on the microstructure and mechanical properties of laser welded dissimilar galvanized steel–aluminium joints, Int. J. Adv. Manuf. Technol., 104 (2019), pp. 2693-2704.

[2] J. Hirsch, Recent development in aluminium for automotive applications. Trans. Nonferrous Met. Soc. China, 24 (2014), pp. 1995-2002.

[3] A. Gullino, P. Matteis, F. D'Aiuto, Review of aluminum-to-steel welding technologies for car-body applications, Metals (Basel) 9 (2019), p.315.

[4] G. Qianqian, J. Long, P. Yu, S Jiang, W. Huang, J. Zhou, Effect of steel to aluminium laser welding parameters on mechanical properties of weld beads, Opt. Lasers Technol., 111 (2019), pp. 387-394.

[5] R. Yuan, S. Deng, H. Cui, Y. Chen, F. Lu, Interface characterization and mechanical properties of dual beam laser welding-brazing Al/steel dissimilar metals, J. Manuf. Process., 40 (2019), pp. 37-45.

[6] H. Ozaki, M. Kutsuna, S. Nakagawa, K. Miyamoto, Laser roll welding of dissimilar metal joint of zinc coated steel to aluminium alloy, J. Laser Appl., 22 (1) (2010), pp. 1-6.

[7] M. M. Atabaki, M. Nikodinovski, P. Chenier, J. Ma, M. Harooni, R. Kovacevic, Welding of aluminum alloys to steels: an overview, J. Manuf. Sci. Prod., 14 (2) (2014), pp. 59-78.

[8] H. Ozaki, M. Kutsuna, Dissimilar metal joining of zinc coated steel and aluminum alloy by laser roll welding, Weld. Process., Ch 2 (2012), p. 33-54.

[9] J. Yang, Y.L. Li, H. Zhang, Microstructure and mechanical properties of pulsed laser welded Al/steel dissimilar joint, Trans. Nonferrous Met. Soc. China, 26 (2016), pp. 994-1002.

[10] S. Meco, G. Pardal, S. Ganguly, R.M. Miranda, L. Quintino, S. Williams, Overlap conduction laser welding of aluminium to steel, Int. J. Adv. Manuf. Technol., 67 (2013), pp. 647-654.

[11] P. Wang, X. Chen, Q. Pan, B. Madigan, J. Long, Laser welding dissimilar materials of aluminum to steel: an overview, Int. J. Adv. Manuf. Technol., 87 (2016), pp. 3081-3090.

[12] R. Cao, J.H. Sun, J.H. Chen, P.C. Wang, Cold metal transfer joining of aluminium AA6061-T6-to-galvanized boron steel, J. Manuf. Sci. Eng.,136 (5) (2014), pp. 351-373.

[13] M.R. Arghavani, M. Movahedi, A.H. Kokabi, Role of zinc layer in resistance spot welding of aluminium to steel, Mater. Des., 102 (2016), pp.106-114.

[14] C. Wang, L. Cui, G. Mi, P. Jiang, X. Shao, Y. Rong, The influence of heat input on microstructure and mechanical properties for dissimilar welding of galvanized steel to 6061 aluminium alloy in a zero-gap lap joint configuration, J. Alloy. Compd., 726 (2017), pp. 556-566.

[15] Z. Cheng, J. Huang, Z. Ye, J. Yang, S. Chen, Butt brazing of titanium alloys/stainless steel plates by MIG-TIG double-sided arc welding process with copper filler metal, J. Mater. Res. Technol., 8 (2019), pp. 1566-1570.

[16] M. Roulin, J. W. Luster, G. Karadeniz, A. Mortensen, Strength and structure of furnace brazed joints between aluminium and stainless steel, Weld. J., (1999), pp. 151-155.

[17] A. O'Brien, C. Guzman, Welding Handbook, 9th ed.: American Welding Society Miami, (2007).

[18] N. Aratho, EAA Aluminium Automotive, Manual Joining, (2018) [Online], Available: **Error! Hyperlink reference not valid.** [Accessed: 12 Jun. 2020].

[19] A.T. Clare, O. Oyelola, T.E. Abioye, P.K. Farayibi, Laser cladding of rail steel with CoCr, J. of Surf. Eng., 29 (10) (2013), pp. 731-736.

[20] M. Ge, J. Friedrich, L. Vigna, 4 Charts explaining greenhouse gas emissions by countries and sectors, World Institute Resources, (2020) [Online], Available: https://www.wri.org/blog/2020/02/greenhouse-gas-emissions-by-country-sector [Accessed: 01 Feb. 2021].

[21] F. Posada, A. Isenstadt, Meeting South Africa's new passenger vehicle CO2 emission standards: The technology deployment costs, fuel savings, and consumer benefits, Int. Council. Clean. Trans., 9 (2019).

[22] F. Posada, South Africa's new passenger vehicle CO_2 emission standards, Baseline determination and benefits assessment, White paper, (2018) [Online], Available: https://www.theicct.org/sites/default/files/publications/South-Africa-PV-emission-stds_ICCT-White-Paper_17012018_vF.pdf. [Accessed: 07 Jul. 2020].

[23] G. Fontaras, N.G. Zacharof, B. Ciuffo, Fuel consumption and CO_2 emissions from passenger cars in Europe, Laboratory versus real world emissions, Prog. Energy Combust. Sci., 60 (2017), pp. 97-131.

[24] J. Lipshaw, What is lightweighting and how does it improve fuel economy in vehicles, Union of concerned scientists, (2020) [Online], Available https://blog.ucsusa.org/science-blogger/lightweighting-and-fuel-economy-in-vehicles [Accessed: 01 Feb. 2021].

[25] K.R Balasubramanian, S.N. Siva, G. Buvanashekaran, K. Sankaranarayanasamy, Numerical and experimental investigation of laser beam welding of AISI 304 stainless steel sheet, Adv. Prod. Eng. Manag., 3(2) (2008), pp. 93-105.

[26] M. Gao, C. Chen, S.W. Mei, L. Wang, X.Y. Zeng, Parameter optimization and mechanism of laser–arc hybrid welding of dissimilar Al alloy and stainless steel, Int. J. Adv. Manuf. Technol., 74 (2014), pp. 199-208.

[27] W. Chung, J. Huang, L. Tsay, C. Chen, Microstructure and stress corrosion cracking behaviour of the weld metal in alloy 52-A508 dissimilar welds, Mater. Trans., 52 (2011), pp. 12-19.

[28] G. Sierra, P. Peyre, F. Deschaux-Beaume, D. Stuart, G. Fras, Galvanised steel to aluminium joining by laser and GTAW processes, Mater. Charact., 20 (59) (2008), pp. 1705-1715.

[29] K.Y. Benyounisa, A.G. Olabi, Optimization of different welding processes using statistical and numerical approaches - A reference guide, Adv. Eng. Software, 39 (2008), pp. 483-496.

[30] C. Kim, W. Choi, J. Kim, S. Rhee, The Relationship between the weldability and the Process Parameters for Laser-TIG Hybrid Welding of Galvanized Steel Sheets, The Japan Institute of Metals, Mater. Trans., 49 (1) (2008), pp. 179-186.

[31] A. Karim, Y. Park, A Review on Welding of Dissimilar Metals in Car Body Manufacturing, J. Weld. Join., (2020).

[32] H-C Chen, Fibre laser welding of dissimilar materials, Ph.D. dissertation, Dept. Eng. Phys. Sci., The University of Manchester, Manchester, England (2010).

[33] C.Y. Lee, D.H. Choi, Y.M. Yeon, S.B. Jung., Dissimilar friction stir spot welding of low carbon steel and Al-Mg alloy by formation of IMCs, Sci. Technol. Weld. Join., 14 (2009), pp. 216-220.

[34] P.B. Srinivasan, W. Dietzel, R. Zettler, Effects of inhibitors on corrosion behaviour of dissimilar aluminium alloy friction stir weldment, Corros. Eng. Sci. Technol., 42 (2007), pp. 161-167.

[35] Y.C. Chen, T. Komazaki, T. Tsumura, K. Nakata, Role of zinc coat in friction stir lap welding Al and zinc coated steel, Mater. Sci. Technol., 24 (2008), pp. 33-39.

[36] W. W. Duley, Laser Welding, 1st ed.: Wiley- Interscience, New York, (1999).

[37] W. M. Steen, Laser Material Processing, 3rd ed.: Springer Verlag, London, (2003).

[38] T.E. Abioye, J.A. Folkes, T. Clare, D.G. McCartney, Concurrent Inconel 625 wire and WC powder laser cladding: process stability and microstructural characterisation, J. Surf. Eng., 29 (9) (2013), pp. 647-653.

[39] J. Rodelas, Laser welding for high reliability, high consequence applications, (2019) [Online] Available: https://www.osti.gov/servlets/purl/1511985 [Accessed: 20 Oct. 2021].

[40] R. Singh, S. S. Sangwan, A review of laser welding for bead width and weld hardness, Int. J. Sci. Res. Eng. Dev.,3 (8) (2015), pp. 787-789.

[41] S. Popov, Fiber laser overview and medical applications, in Tunable laser applications, New York USA, CRC Press, 2 (2009), pp. 197-226.

[42] P.K. Farayibi, T.E. Abioye, J.W. Murray, P.K. Kinnel, A.T. Clare, Surface improvement of laser clad Ti-6Al-4V using plain waterjet and pulsed electron beam irradiation, J. Mater. Process. Technol., 218 (2015), pp. 1-11.

[43] N. Michalis, A. Christophe, High power fiber lasers: A review, IEEE J. Sel. Top. Quantum Electron, 20 (5) (2014), pp. 1-23.

[44] D. Kim, S. Rhee**,** Optimization of GMA welding process using the dual response approach, Int. J. Prod. Res., (2004), pp. 4505-4515.

[45] N. Muhammad, Y.H.P. Manurung, M. Hafidzi, S.K. Abas, G. Tham, E. Haruman, Optimization and modelling of spot-welding parameters with simultaneous multiple response consideration using multi-objective Taguchi method and RSM, J. Mech. Sci. Technol., 26 (2012), pp. 2365-2370.

[46] A. Kouadri, L. Barrallier, Texture characterisation of hexagonal metals: Magnesium AZ91 alloy welded by laser processing, Mater. Sci. Eng., 429 (2006), pp. 11-17.

[47] R. P. Martukanitz, A critical review of laser beam welding, Proc. SPIE-Int. Soc. Opt. Eng., 5706 (2005), pp. 11-24.

[48] N. B. Dahotre, S. P. Harimkar, Laser Fabrication and Machining of Materials: 1st ed.:,Springer, USA, (2008).

[49] L. Quintino, A. Costa, R. Miranda, D. Yapp, V. Kumar, C.J. Kong, Welding with high power fiber lasers - A preliminary study, Mater. Des., 28 (2007), pp. 1231-1237.

[50] S. K. Cho, Y.S. Yang, K.J. Son, J.Y. Kim, Fatigue strength in laser welding of the lap joint, Finite Elem. Anal. Des., 40 (9-10) (2004), pp. 1059-1070.

[51] I. Miyamoto, T. Kosumi, S.Park, T. Ooie, Applications of single-mode fiber lasers to novel microwelding, Proc. SPIE-Int. Soc. Opt. Eng., 5662 (2004), pp. 507-514.

[52] S. A. David, T. DebRoy, Current issues and problems in welding science, Science, 257 (5069) (1992), pp. 497-502.

[53] J. Zhou, H.L. Tsai, Porosity formation and prevention in pulsed laser welding, J. Heat Trans., 129 (2007), pp. 1014-1024.

[54] S. Katayama, M. Mizutani, A. Matsunawa, Development of porosity prevention procedures during laser welding, Proc. SPIE - Int. Soc. Opt. Eng., 4831 (2003), pp. 281-288.

[55] T.Y. Kuo, Y.D. Lin, Effects of different shielding gases and power waveforms on penetration characteristics and porosity formation in laser welding of Inconel 690 alloy, Mater. Trans., 48 (2007), pp. 219-226.

[56] K. Klages, A. Gillner, A. Olowinsky, F. Wagner, Laser beam micro welding of dissimilar metals, 4th Int. symposium on L.P.M June 21-24, 2003, Munich Germany.

[57] T. Kataoka, R. Ikeda, K. Yasuda, Y. Hirata, Development of a low-spatter CO2 arc welding process with a high-frequency, Weld. Int., 23 (2009), pp. 353-359.

[58] J.R Berretta, W. de Rossi, Laser Welding. In: Q.J. Wang, Y.W. Chung, (eds) Encyclopedia of Tribology. Springer, (2013), Boston, MA.

[59] Z. Sun, R. Karppi, Application of electron beam welding for the joining of dissimilar metals: an overview, J. Mater. Process. Technol., 59 (1996), pp. 257-267.

[60] Z. Sun, J. C. Ion, Laser-welding of dissimilar metal combinations, J. Mater. Sci., 30 (1995), pp. 4205-4214.

[61] Y. Shurong, F. Ding, D. Bizhe, Laser beam welding of dissimilar metals of aluminum alloy and galvanized steel sheet, 2nd Int. Conf. Mech. Autom. Control Eng., 15-17 July 2011, Inner Mongolia China, pp. 5030-5032.

[62] B. Jose'Roberto, W, de Rossib, The Pulsed Nd: YAG laser welding of AISI 304 to AISI 420 stainless steels. J. Opt. Lasers Eng., 45 (2007), pp. 960-966.

[63] M. Schimek, A. Springer, S. Kaierle, D. Kracht, V. Wesling, Laser-welded dissimilar steel-aluminium seams for automotive light weight construction, Phys. Procedia., 39 (2012), pp. 43-50.

[64] N. Farabi, D.L. Chen, J. Li, Y. Zhou, S.J. Dong, Microstructure and mechanical properties of laser welded DP600 steel joints, Mater. Sci. Eng. A-527 (2010), pp.1215-1222.

[65] I.N. Fridlyander, Current-technology aluminium alloys for aerospace applications, Met. Sci. Heat Treat., 43 (7) (2001), p.297.

[66] H. Babel, J. Gibson, M. Tarkanian, C. Parrish, M. Prietto, A. Ordonez-Chu, H. Haberl, J. Kabisch, J. Clark, R.J. Ogren, O.S. Said, 2099 aluminium-lithium with key-locked inserts for aerospace applications, J. Mater. Eng. Perform., 16 (5) (2007), pp. 584-591.

[67] A. Sadek, Dissimilar materials weldability concepts, (2015) [Online] Available: https://ewi.org/wp-content/uploads/2016/01/Dissimilar-Metal-Weldability-Concepts_Alber-Sadek.pdf [Accessed: 16 Aug. 2020].

[68] F.A. Ovat, The effect of electrodes on the mechanical Properties of welded steels, department of mechanical engineering, MEng. Dissertation, University of Agriculture Makurdi, Makurdi, Nigeria (2004).

[69] J. P. Dudeja, Analysis and advantages of welding dissimilar metals by fiber lasers, IJASTEMS, 4 (8) (2018), pp. 1-5.

[70] R. R. Boyer, An overview on the use of titanium in the aerospace industry, Mater. Sci. Eng., 213 (1996), pp. 103-114.

[71] H. Laukant, C. Wallmann, M. Müller, M. Korte, B. Stirn, H.G. Haldenwanger, U. Glatzel, Fluxless laser beam joining of aluminium with zinc coated steel, Sci. Technol. Weld. Join., 10 (2005), pp. 219-226.

[72] M.J. Torkamany, S. Tahamtan, J. Sabbaghzadeh, Dissimilar welding of carbon steel to 5754 aluminium alloy by Nd: YAG pulsed laser, Mat. Des., 31 (2010), pp.458-465.

[73] A. Mathieu, S. Mattei, J. Viala, D. Grevey, Laser brazing welding using hot (88%-Aluminum, 12%-Silicon) filler material to join steel with aluminum. In: Laser materials processing conference, Proceeding of ICA-LEO'05, Miami, FL USA, (2005), pp. 985-991.

[74] C. Dharmendra, K.P. Rao, J. Wilden, S. Reich, Study on laser welding–brazing of zinc coated steel to aluminium alloy with a zinc-based filler, Mater. Sci. Eng. A, 528 (2011), pp. 1497-1503.

[75] G.L. Qin, Z. Lei, Y.H. Su, B.L. Fu, X.M. Meng, S.Y. Lin, Large spot laser assisted GMA brazing-fusion welding of aluminum alloy to galvanized steel, J. Mater. Process. Technol., 214 (2014), pp. 2684-2692.

[76] W. Liu, J.J. Ma, M.M. Atabaki, R. Kovacevic, Joining of advanced high-strength steel to AA 6061 alloy by using Fe/Al structural transition joint, Mater. Des., 168 (2015), pp. 146-157.

[77] J. Ma, M. Harooni, B. Carlson, R. Kovacevic, Dissimilar joining of galvanized high-strength steel to aluminum alloy in a zero-gap lap joint configuration by two-pass laser welding, Mater. Des., 58 (2014), pp. 390-401.

[78] J.J. Ma, F. Kong, B. Carlson, R. Kovacevic, Two-pass laser welding of galvanized high-strength dual-phase steel for a zero-gap lap joint configuration, J. Mater. Process. Technol., 213 (3) (2012), pp.495-507.

[79] S. Yan, Z. Hong, T. Watanabe, T. Jingguo, CW/PW dual-beam YAG laser welding of steel/aluminum alloy sheets, Opt. Lasers Eng., 48 (2010), pp. 732-736.

[80] K. Saida, H. Ohnishi, K. Nishimoto, Fluxless laser brazing of aluminium alloy to galvanized steel using a tandem beam-dissimilar laser brazing of aluminium alloy and steels, Weld. Int., 24(3) (2010), pp.161-168.

[81] L. Agudo, D. Eyidi, C.H. Schmaranzer, E. Arenholz, N. Jank, J. Bruckner, A.R. Pyzalla, Intermetallic Fe_xAl_y-phases in a steel/Al-alloy fusion weld, J. Mater. Sci., 42 (2007), pp. 4205-4214.

[82] L. H. Shah, M. Ishak, Review of research progress on aluminium-steel dissimilar welding, Mater. Manuf. Proc., 29 (8) (2014), pp. 928-933.

[83] L. Shao, Y. Shi, J.K. Huang, S.J. Wu, Effect of joining parameters on microstructure of dissimilar metal joints between aluminum and galvanized steel, Mater. Des., 2015, 66 (2015), pp. 453-458.

[84] M.J. Rathod, M. Kutsuna, Joining of aluminum alloy 5052 and low-carbon steel by laser roll welding, Weld. Res., 83 (2004), pp. 16-26.

[85] D. Yang, T. Lixiaoyan, Optimization of weld bead geometry in laser welding with filler wire process using Taguchi's approach, J. Opt. Laser Technol., 44 (2012), pp. 2020-2025.

[86] K. Bouché, F. Barbier, A. Coulet, Intermetallic compound layer growth between solid iron and molten aluminium, Mater. Sci. Eng., 249 (1998), pp. 167-175.

[87] H. T. Kashani, P. Kah, J. Martikainen, Laser overlap welding of zinc-coated steel on aluminum alloy, Phys. Procedia 78 (2015), pp. 265-271.

[88] X. Cao, X. Zhou, H. Wang, Z. Luo, J. Duan, Microstructures and mechanical properties of laser offset welded 5052 aluminum to press-hardened steel, J. Mater. Res. Technol., (9) (3) (2020), pp. 5378-5390.

[89] S.K. Dinda, S.K. Basiruddin, G.G. Roy, P Srirangam, Microstructure and mechanical properties of electron beam welded dissimilar steel to Fe-Al alloy joints, Mater. Sci. Eng. A., 677 (2016), pp. 182-192.

[90] D. Krishnaja, M. Cheepu, D. Venkateswarlu, A review of research progress on dissimilar laser weld-brazing of automotive applications, IOP Conference Series: Mater. Sci. Eng., 330 (2018).

[91] G. Padmanaban, V. Balasubramanian, An Optimization of laser beam welding process parameters to attain maximum tensile strength in AZ31B magnesium alloy, J. Opt. Laser Technol., 42 (2010), pp. 1253-1260.

[92] A.B. Pereira, A. Cabrinha, F. Rocha, P. Marques, P.M Fábio, A.O. Fernandes, R.J. Alves de Sousa, Dissimilar metals laser welding between DP1000 steel and aluminium alloy 1050, Metals, 9 (2019), p. 102.

[93] P. Peyre, G. Sierra, F. Deschaux-Beaume, D. Stuart, G. Fras, Generation of aluminium–steel joints with laser-induced reactive wetting. Mater. Sci. Eng. A, 444 (2007), pp.327-338.

[94] L. Arthur, Introductory welding metallurgy: instructor's manual: American Welding Society, New York, 1968.

[95] C. T. Kwok, S.L. Fong, F.T Cheng, H.C. Man, Pitting and galvanic corrosion behavior of laser-welded stainless steels, J. Mater. Process. Technol., 176 (2006), pp. 168-178.

[96] D.S. Nagesh, G.L. Datta, Prediction of weld bead geometry and penetration in shielded metal-arc welding using artificial neural networks, J. Mater. Process. Technol., 123 (2) (2002), pp. 303-312.

[97] A. Ruggiero, L. Tricarico, A.G. Olabi, K.Y. Benyounis, Weld-bead profile and costs optimization of the CO2 dissimilar laser welding process of low carbon steel and austenitic steel AISI 316, J. Opt. Laser Technol., 43 (2010), pp. 82-90.

[98] A. Evdokimov, A. Obrosov, R. Ossenbrink, S. Weiß, V. Michailov, Mechanical properties of dissimilar steel-aluminium welds, Mater. Sci. Eng. A, 722 (2018), pp. 242-254.

[99] A. Kouadri-David, Study of metallurgic and mechanical properties of laser welded heterogeneous joints between DP600 galvanized steel and aluminium 6082, Mater. Des., 54 (2014), pp.184-195.

[100] O. Seffer, R. Pfeifer, A. Springer, S. Kaierle, Investigations on laser beam welding of different dissimilar joints of steel and aluminium alloys for automotive lightweight construction, Phys. Procedia., 83 (2016), pp. 383–395.

[101] D. Narsimhachary, K. Dutta, S.M. Shariff, G. Padmanabham, A. Basu, Mechanical and microstructural characterization of laser weld-brazed AA6082-galvanized steel joint, Journal of Materials Processing Technol. 263 (2019), pp. 21-32.

[102] R. Shabadi, M. Suery, A. Deschamps, Characterization of joints between aluminium and galvanized steel sheets, Metallurgical and Materials Characterization A, 44A (2013), pp. 2672-2682.

[103] J. Vrenken, C. Goos, T.V.D Veldt, W. Braunschweig, Fluxless laser brazing of aluminium to steel, Join. Automotive Eng., (2009), pp. 1-9.

[104] C. Yuce, F. Karpat, N. Yavuz, Effects of Heat Input in Laser Welding of Dissimilar Galvanized Steel to Aluminium Alloy, Proceedings of the 4th World Congress on Mechanical, Chemical, and Material Engineering (MCM'18) Madrid, Spain, August 16-18, 2018).

[105] K.J. Lee, S. Kumai, T. Arai, Interfacial microstructure and strength of steel to aluminium alloy lap joints welded by a defocused laser beam, Mater. Trans., 46 (8) (2005), pp. 1847-1856.

[106] S. Meco, S. Ganguly, S. Williams, N. McPherson,2014. Effect of laser processing parameters on the formation of intermetallic compounds in Fe-Al dissimilar welding, J. Mater. Eng. Perform., 23 (2014), pp. 3361-3370.

[107] K. J. Lee, S. Kumai, Characterization of intermetallic compound layer formed at the weld interface of the defocused laser welded low carbon steel/6111 aluminium lap joint, Mater. Trans., 47 (4) (2006), pp.1178-1185.

[108] Y. Shi, J. Li, G. Zhang, J. Huang and Y. Gu, Corrosion Behavior of Aluminum-Steel Weld-Brazing Joint, J.Mater. Eng. Perform, 25 (5) (2016), pp. 1916-1923.

[109] J. Wloka, H. Laukant, U.Glatzel, S.Virtanen, Corrosion properties of laser beam joints of aluminum with zinc-coated steel, Corr. Sci., 49 (2007) pp.4243-4258.

[110] M.I. Saleh, T.I. Khan, H.J. Roven, Transient liquid phase bonding of AA-6063 to UNS S32304 using Cu interlayer, Procedia Chem., 19 (2016), pp.517-524.

[111] M. Pouranvari, S. P. H. Marashi, Critical review of automotive steels spot welding, process, structure and properties, Sci. Technol. Weld. Join., 18(5) (2013), pp. 361-403.

[112] G. Sierra, P. Peyre, F. Deschaux-Beaume, D. Stuart, G. Fras, Steel to aluminium keyhole laser welding, Mater. Sci. Eng. A, 447 (2007), pp. 197-208.

[113] S. Hirose, T. Itoh, M. Makita, S. Fujii, S. Arai, K. Sasaki, H. Saka, Defect structure of deformed Fe2Al5 intermetallic compound, Intermetallics, 11 (2003), p. 633-643.

[114] M. N. Eff, A Fundamental Investigation into intermetallic formation and growth in the aluminum-iron system using resistance-based diffusion couples, Ph.D, dissertation, Dept. Mater. Sci. Eng., The Ohio State University, Ohio, USA, (2019).

[115] H. Kang, S. Lee, C. Hu, The role of pre-formed Fe2Al5 in P/M processing of Fe_3Al, Mater. Sci. Eng. A, 398 (2005), pp. 360-366.

[116] Y. Su, X. Hua, Y. Wu, Influence of alloy elements on microstructure and mechanical property of aluminium–steel lap joint made by gas metal arc welding, J. Mater. Process. Technol., 214 (2014), pp.750-755.

[117] H-C. Chen, A.J. Pinkerton, L. Li, Z. Liu, A.T. Mistry, Gap-free fibre laser welding of Zn-coated steel on Al alloy for light-weight automotive applications, Mater. Des., 32 (2011), pp. 495-504.

[118] W. F. Gale, T. C. Totemeier, Smithells Metals Reference Book, 8th ed.: Elsevier, USA (2004).

[119] B. Cevik, B. Gülenç, The effect of welding speed on mechanical and microstructural properties of 5754 Al (AlMg3) alloy joined by laser welding, Mater. Res., 5 (8) (2018), p. 11.

[120] Anon, Matweb, Material Property data, (2020) [Online] Available: http://www.matweb.com/search/datasheet.aspx?matguid=af58cf14010141b1a1cd94def4826389&ckck=1.

[Accessed: 19 Jun. 2020]

[121] Anon, Protection against rust with zinc coating, Online [Available] https://www.ssab.co.za/products/steel-categories/metal-coated-steels/coatings/zinc-coating [Accessed: 28 Jun. 2020].

[122] S. Bannour, K. Abderrazak, S. Mattei, J. E. Masse, M. Autric, H. Mhiri, The influence of position in overlap joints of Mg and Al alloys on microstructure and hardness of laser welds, J. Laser Appl. 25 (3) (2013), pp.2001-2008.

[123] S. Sattari, H. Bisadi, M. Sajed, Mechanical Properties and Temperature Distributions of Thin Friction Stir Welded Sheets of AA5083, Int. J. Appl. Mech., 2(1) (2012), pp.1-6.

[124] A. K. Tilekar, N. K. Kamble, Optimization of laser welding parameters: A review, Int. Res. J. Eng. Technol., 4 (6) (2017), pp. 1631-1633.

[125] W.Chen, Laser welding of thin sheets of galvanized steel and aluminum alloy, Retrospective Theses and Dissertations (2006), p. 19379.

[126] J. Sundqvist, Heat conduction effects during laser welding, Licentiate thesis, Lulea University of Technology, Dept. of Sci. and Maths., Sweden (2015).

[127] E.J. Ashcroft, Mechanical and Metallurgical properties of dissimilar metal joints using novel joining techniques, PhD thesis, Sheffield Hallom University, Sheffield, England (2008).

[128] M.S. Abdel Rahman, N.A. Abdel Raheem, M.R. El Koussy, Effect of heat input on the microstructure and properties of dissimilar weld joint between Incoloy 28 and super- austenitic stainless steel, Acta. Metall. Sin., 27 **(**2014), pp**.** 259-266.

[129] K.Y Benyounis, A.G. Olabi, M.S.J Hashmi, Effect of laser-welding parameters on the heat input and weld-bead profile, J. Mater. Process. Technol., 164-165 (2005), pp. 978-985.

[130] W. Xu, Z. Li, X. Sun, Effect of welding speed on mechanical properties and the strain-hardening behavior of friction stir welded 7075 aluminum alloy joints, J. Mater. Eng. Perform., 26(4) (2017), pp.1938-1946.

[131] G. Phanikumar, K. Chattopadhyay, P. Dutta, Modelling of transport phenomena in laser welding of dissimilar metals, Int. J. Numer. Methods Heat Fluid Flow, 11(2001), pp.156-171.

[132] A. Haboudou, P. Peyre, A.B. Vannes, G. Peix, Reduction of porosity content generated during Nd: YAG laser welding of A356 and AA5083 aluminium alloys. Mater. Sci. Eng**.** A, 363 (1-2) (2003), pp. 40-52.

[133] Anon, Heat input and its effects on material properties, [Online] Available:https://www.esabna.com/us/en/education/blog/heat-input-and-its-effects-on-material-properties.cfm [Accessed : 05 Jul.2021]

[134] M. Kreimeyer, F. Wagner, G. Sepold, Development of a combined joining-forming process for aluminum-steel joints, 23rd ICALEO, 4-7 October 2004, p. 519.

[135] A. R. Marder, The metallurgy of zinc-coated steel, Prog. Mater. Sci., 45 (2000), pp. 191-271.

[136] L. Wan, Y. Huang, Microstructure and Mechanical Properties of Al/Steel Friction Stir Lap Weld, Metals, *7* (12) (2017), p.542.

[137] S. Johnson, Advantage and disadvantages of XRD and XRF, (2018) [Online] Available: https://sciencing.com/advantages-disadvantages-xrd-xrf-6054766.html [Accessed: 31 Aug. 2021]

[138] Z. Zhang, Y. Yu, J. Zhang, X. Wang, Corrosion Behavior of Keyhole-Free Friction Stir Spot Welded Joints of Dissimilar 6082 Aluminum Alloy and DP600 Galvanized Steel in 3.5% NaCl Solution, Metals, 7 (338) (2017).

[139] M. F. B. Ibrahim, Effect of different sodium chloride (NaCl) concentration on corrosion of coated steel, BSc (Eng) report, Dept. Mech.Eng. Universiti Malaysia Pahang, Malaysia (2013).

[140] Anon, Pitting corrosion, [Online] Available: https://byjus.com/chemistry/pitting-corrosion/ [Accessed: 25. Nov 2020].

[141] D.W. Hoeffner, Chapter 5-Pitting Corrosions: Morphology and characterization, (2015) pp.1-16.

[142] H. Eisazadeh, A. Achuthan, J.A Goldak, D.K Aidun, Effect of material properties and mechanical tensioning load on residual stress formation in GTA 304-A36 dissimilar weld, J. Mater. Process. Technol, 222 (2015), pp.344-355.

[143] R. Oyyaravelu, P. Kuppan, N. Arivazhagan, Metallurgical and mechanical properties of laser welded high strength low alloy steel, J. Adv. Res., 7 (3) (2016), pp. 463-472.

[144] D. Wallerstein, A. Salminen, F. Lusquinos, R. Comesana, J. del Val Garcia, A.R Rodriguez, A. Badaoui, J. Pou, Recent developments in laser welding of aluminum alloys to steel, Metals, 11 (4) (2012), p. 622.

[145] D. Bernasciutti, A. Lanzutti, G. Rupil, E. Fraenkel Haeberle, Microstructural and mechanical characterisation of laser-welded lap joints with linear and circular beads in thin low carbon steel sheets, Mater. Des., 62 (2014), pp. 205-216.

[146] Miyazaki Y, Furusako S. Tensile shear strength of laser welded lap joints, Nippon Steel Tech. Rep, 95 (2007), pp. 2

materials

MDPI

Article

Microstructural Characterization and Mechanical Properties of Laser Beam-Welded Dissimilar Joints between A6000 Aluminum Alloy and Galvanized Steel

Nkopane Angelina Ramaphoko [1,*], Samuel Skhosane [2] and Nthabiseng Maledi [1]

[1] School of Chemical and Metallurgical Engineering, University of the Witwatersrand, Private Bag 3, Johannesburg 2050, South Africa; Nthabiseng.Maledi@wits.ac.za

[2] Laser Enabled Manufacturing National Laser Centre CSIR, Pretoria 0001, South Africa; SSkhosane@csir.co.za * Correspondence: 481333@students.wits.ac.za

Abstract: This paper presents the laser beam welding process of a lap joint between galvanized steel (Z225) and an aluminum alloy (A6000) from an IPG fiber laser. Welding of steel to aluminum has become popular in the automotive industry as a means of reducing the total vehicle body mass. This approach reduces fuel consumption and, ultimately, carbon emissions. Laser welding parameters used to control heat input for the study were laser power ranging between 800 and 1200 W, as well as laser welding speeds between 2 and 4 m/min. Distinct features of the dissimilar joints were microscopically examined. The SEM-EDS technique was employed to study the intermetallic phases along the Fe-Al interface. The outcome revealed the presence of "needle-like phases" and"island-shaped phases" at high heat inputs. Traces of both Fe_2Al_5 and $FeAl_3$ phases were detected. For low heat input, there was evidence of insufficient fusion. Weld width was influenced by welding parameters and increased with an increase in heat input. Mechanical properties of the joints indicated that the microhardness values of the weld joints were higher than those of both base metals. The maximum tensile shear strength obtained was 1.79 kN for a sample produced at 1200 W and 3 m/min.

Keywords: laser welding; heat input; IMCs; microstructure; mechanical properties

1. Introduction

In the past, car manufacturers produced heavy vehicles in order to meet passenger safety and aesthetic requirements [1]. The cars were heavy due to the predominant usage of steel for most car body parts. There has been an introduction of more stringent rules to protect the environment by lessening the amount of car exhaust emissions such as CO_2 and NO_x. Therefore, the automobile industry strives to decrease the total mass of vehicles as there is strong evidence that this measure is one of the most effective methods for reducing fuel consumption and consequently decreasing the release of harmful greenhouse gases. The New European Driving Cycle (NEDC) reported that there is a proportional relationship between vehicle weight and fuel consumption. It was stated that decreasing vehicle weight by 100 kg could save fuel by 0.3–0.5 L/100 km [2].Initially, the approach used to address the matter was to reduce the thickness of the steel sheets used for car panels. However, the method was unsuccessful as it decreased the strength of the cars and thus compromised passenger safety. In recent times, it has been discovered that the most effective means of decreasing the car mass is by replacing some steel parts with lighter materials such as aluminum alloys [2]. As a result, the application of the method within the car manufacturing sector requires the joining of dissimilar materials. Aluminum alloys that are mostly used for this purpose are the 5000 and 6000 series alloys because they possess exceptional corrosion properties, suitable strength, and excellent surface characteristics [3]. Welding of dissimilar materials is a process of joining materials with different physical properties by means of a heat source [4]. The technique allows for the manufacturing of weld joints with required traits for certain applications. Nevertheless,

welding of dissimilar materials presents difficulties due to the formation of inevitable hard and brittle intermetallic compounds (IMCs) at the weld interface, which adversely impacts the soundness of the weld joint [5].
Research has verified the success of laser welding of dissimilar materials over conventional welding processes because it is characterized by thin heat-affected zone (HAZ), high energy density, less deformation, high welding speed, and great control of heat input [6]. Furthermore, the quality of dissimilar metals weld joints may be enhanced by a suitable selection of laser welding parameters. Sierra et al. [7] emphasized the significance of laser welding parameters from the conclusions of their research. It was discovered that various arrangements of welding parameters influence the IMC layer thickness. It was concluded that increasing laser welding speed reduced the IMC layer thickness. Tilekar et al. [8] also conducted similar research; however, the focus was on the analysis of the weld bead dimensions (weld penetration depth and weld width). It was found that the welding speed and laser power are the parameters that have a significant impact on the weld width and weld penetration [8]. In research by Torkamany et al. [9], a pulsed Nd: YAG laser was applied to combine a 0.8 mm-thick steel to a 2.0 mm-thick aluminum alloy [9]. The impact of laser power and pulse duration on the soundness of the weld joint was examined. The results revealed the presence of IMCs within the weld zone. It was stated that the mechanical properties of dissimilar weld joints are substantially influenced by the composition of parent metals, welding parameters, and shape contacts of the weld bead, which are impacted by input welding parameters [10].

Several efforts have been made to optimize the welding parameters in order to attain weldments of high quality, acceptable geometry, and low surface roughness. Cheohlee et al. [11] noticed that the tensile strength is mostly influenced by welding speed, followed by laser power and the focal point. It was also concluded that the parameters that produced appropriate microstructure and mechanical properties were laser power ranging between

0.6 and 2.4 kW, welding speed ranging between 0.82 and 3 m/min, focal position between −0.8 and −0.2 mm, and shielding gas of flowrate between 5 and 15 L/min [11].

The aim of the experiment by Zhang et al. [12] was to achieve deep penetration from a high-intensity fiber laser of 10 kW intensity. The process parameters under the spotlight were welding speed, focus lens, focus size, shielding gas, and laser power. Shielding gases helium, nitrogen, and argon (He, N_2, and Ar) were considered as output parameters [12]. SEM analysis and a transverse tensile strength test were also conducted. The findings revealed that it was difficult to achieve full weld penetration by proper focal position when thick samples are used. Helium gas resulted in the greatest penetration, followed by N_2 and Ar. This is because helium has the lowest density and has better ionization energy compared to the other two gases [12].

One of the major challenges encountered during laser fusion welding between galvanized steel and aluminum alloys is the creation of pores within the weld seam, especially when using the keyhole technique [13]. This is caused by the fact that the

melting and boiling points of Zn are lower than those of Al and Fe. Since high temperatures are applied during fusion welding, the zinc layer covering the steel tends to vaporize and become trapped during solidification creating pores [13,14]. In order to control the escape of Zn vapor, a special clamping system that has a tiny opening at the aluminum-steel interface may be used to allow the Zn vapor to escape and thus reduce pore formation [15]. However, the advantage of using galvanized steel in reactive welding methods is that the zinc layer improves the wettability of molten aluminum on the solid steel [13]. It has also been shown that the shear strength of the weld joint can be enhanced to values as high as 200 MPa by regulating the laser welding parameters such as the heat source location to control the exclusive melting of base metals.

Numerous articles on different combinations of dissimilar materials for application within the automotive industry have been reported. However, little work has been reported on the combination of Z225 and A6000 specifically. As a result, the purpose of the current work was to determine the optimum laser welding parameters for producing Z225 and A6000 joints with microstructural and mechanical properties suitable for manufacturing vehicle body parts.

2. Materials and Methods

2.1. Materials and Laser Welding Method

Galvanized steel (Z225) and an aluminum alloy (A6000) were used as parent/base materials. The zinc coating on the steel plate was 60 g/cm^2. The samples were cut using a

CO_2 laser cutter into plates of 50 mm length and 30 mm width. The thicknesses of Z225 and

A6000 plates were 0.8 and 1.2 mm, respectively. The elemental composition and mechanical characteristics of the parent metals are given in Tables 1 and 2, respectively.

Table 1. Chemical composition of parent metals [15].

Elements (wt.%)			
	Si	**Mg**	**Cu**
A6000	1.0	0.5	<0.1
Material	C	Si	P
Z225	<0.15	<0.60	<0.05

Table 2. Mechanical properties of ɔarent metals.

Parent Metal	**Yield Strength (MPa)**	**Ultimate Tensile Strength (MPa)**	**Elongation (%)**
A6000	225	303	15
Z225	350	375	35

Acetone was used to remove the impurities from the surfaces of the plates, as they tend to melt during welding and create defects. The plates were then arranged into a lap joint with a 3 mm-wide overlap. A toggle system on a fixed gantry table was used in order to maintain constant pressure during welding and to prevent a microscopic gap

between the metal plates for maximum heat conduction. A Precitec YW 50 welding head (made by Precitec Engineering in Lahore, Pakistan) was mounted to a KUKA KR60L30HA automated arm robot manufactured by KUKA located in Gersthofen, Germany to perform the laser welding process. The weld seam was created from an IPG fiber laser with a 1.06 µm wavelength and 3000 W maximum power at a −5 mm defocused laser beam and 171 mm focusing lens. An inert helium gas discharged at a 15 L/min flowrate was used as a shielding gas to avoid oxidation on the heated surfaces. A 12 mm gap between the laser head and workpiece was maintained throughout the joining process.

The laser-welded dissimilar lap joints were exposed to destructive testing methods for characterization. A Struers Secotom-10 abrasive cutting machine (manufactured by Struers in Ballerup, Denmark) was used to cut the cross-section of the weld joints for microscopic and macroscopic evaluation. The machine was set at a feed speed of 120 mm/s and 3500 r/min wheel speed. Black phenolic resin was used to mount the samples in a hot mounting press for 5 min at 200 °C. The samples were ground and polished with 220, 800, and 1200 SiC, respectively using a Saphir 520 single wheel grinder/polisher with Rubin 500 head (by Unitron Instrumentation Technology Pvt. Ltd in Bengaluru, India) in order to achieve a mirror finish surface. The surfaces were then etched with 3% Nital solution (3% HNO_3, 97% ethyl alcohol) to expose the microstructure and break down the grain boundaries.

2.2. Microstructure

The weld microstructural analysis was performed using an Olympus SC 50 optical microscope by Olympus Life Science in Waltham, MA, USA at magnifications between 10× and 50× to examine the grain sizes. The weld bead dimensions were measured from the installed AxioVision imaging software. Three measurements were taken on the same area, and the average value was used. The samples were then cut to less than 5 mm sections. Scanning electron microscope (SEM) with electron dispersive spectrum (EDS) (Carl Zeiss MGA Sigma FESEM) produced by Carl Zeiss Microscopy in White Plains, NY, USA was then employed. The machine was set at 20 kV electron high tension (EHT). The SEM was used to examine the morphology and composition of the dilution zone. The EDS was then used to detect the present elements at different sections. A Bruker D8 advanced X-ray diffractometer (Manufactured by Bruker in Bremen, Germany) with a monochromator was used to perform an X-ray Diffractor (XRD) analysis. The IMC phases were identified from the spotted elemental peak using the Diffract Eva software (Version 5.2.0.3). The equipment used a monochromator with a solid detector as well as a Cu Kα radiation source with a wavelength of 1.5406, step size of 0.02° and theta ranging between 2.5° and 45°. The voltage and current applied were 40 kV and 40 mA, respectively.

2.3. Mechanical Properties

Mechanical tests were performed on the samples to determine the impact of welding parameters.

2.3.1. Microhardness Testing

A microhardness tester FM-700 (by Vickers in Shanghai, China at 300 gf load and

10 s dwell time was used to establish hardness profile along a horizontal line crossing from the Z225 base metal through the weld joint toward the A6000 base metal. A total of 16 indentations were performed on the Z225 base metal, weld metal, and the A6000 base metal for each sample.

2.3.2. Tensile Strength Testing

Samples were cut into specimens of 0.9 mm width and 75 mm length to conduct a tensile shear strength test, which was conducted in accordance with ASTM E8 geometry. A Zwick/Roell universal testing machine (manufactured by Zwick/Roell Group in Ulm, Germany) was used to determine the strength of weld joints. The experiment was carried out at 25 °C temperature, 1 mm/s crosshead speed, and a nominal force of 20 kN load. The direction of the applied stress was perpendicular to the weld seam, as shown in Figure 1.

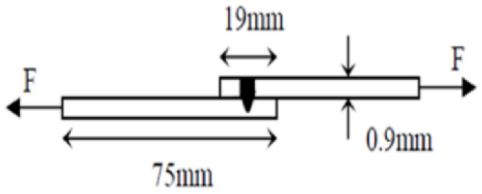


Figure 1. Specimen used for tensile shear strength test indicating direction of applied stress [16].

2.4. Experimental Principle

Laser welding was performed during the experiments. A lap joint was arranged by positioning steel on top of aluminum. The flow of heat infiltrates through the steel plate toward the aluminum by means of a positive gradient of thermal conductivity [17]. The melting point of aluminum is significantly lower than that of steel, and this makes it possible to liquefy aluminum, whereas steel is heated but retains its solid form. The power density of the laser spot subjected to the work piece determines the mode in which the laser beam gets into contact with the material [18]. The schematic representation of the experimental hypothesis in Figure 2 demonstrates a typical lap joint produced by conduction mode. In order to regard a weld in conduction mode, the power density should not be greater than 10^6 W/cm^{2,} and the aspect ratio should be smaller than 0.5 [18]. No filler material was added in all the experiments.

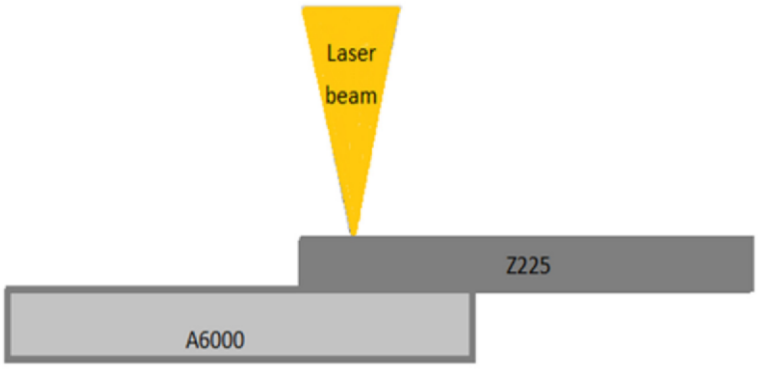


Figure 2. Schematic representation of laser welding process of a lap joint [4].

2.5. System Parameters

The aim of the investigation was to determine the effect of laser welding parameters on the quality of a dissimilar joint between Z225 and A6000. Heat input was controlled by altering laser welding speed and laser power. Equation (1) was used to calculate the heat input values. Increasing laser power and decreasing laser welding speed increases heat input. The combinations of parameters used are recorded in Table 3. A constant beam diameter of 13 mm was used for producing all the samples [19].

$$\text{Heat input (J/mm)} = \text{Laser power (W)}/\text{Welding speed (m/min)} \quad (1)$$

Table 3. Welding system parameters.

System Parameters		
Power (W)	**Welding Speed (m/min)**	**Heat Input (10^5 J/mm)**
800	3	16
950	2	28.5
950	3	19
950	4	14.25
1000	3	20
1200	3	24

3. Results and Discussion

3.1. Microstructure

The optical micrographs showing the cross-sections of the weld joints produced under different conditions are depicted in Figures 3 and 4. Figure 3b revealed evidence of undercutting. The defect most likely resulted from the weld metal failing to sufficiently wet the base metals due to either incorrect cleaning of the base metals or beam asymmetry [20]. In some cases, undercut defect is caused by evaporation of the zinc coating as heat input increases. The Zn vapor tends to accumulate pressure, which induces disturbances on the flow of the melt, causing the undercut [8]. In Figure 4b,c, it can be noticed that there was insufficient fusion due to a reduction in heat input. Pores were also detected for weld joint in Figure 4b. This may have been due to evaporation of the Zn-coating and entrapment of the vapor during solidification. It can be observed that the grains for the weld metal produced at higher heat inputs (Figures 3c and 4a) have a coarse columnar structure. This was caused by grain growth due to high heat input, which typically results in a deficit of ductility [21].

Furthermore, irregular and complex phases were detected for weld joint produced at 1200 W and 3 m/min. These phases were analyzed at higher magnification (see Figure 5b). Island-shaped structures were observed at the A6000/weld interface. These resulted from the occurrence of conduction at the weld pool because of higher heat input [22]. The increased mobility of the molten pool increased the contact of steel and aluminum atoms and increased the entrapment of Al and Zn. In addition, between the “islands” and the weld metal, needle-like phases were detected within the Al substrate. Similar results were observed by Cui et al. [18]. They detected complex and irregular structures with several needle-like shapes within the microstructure near the steel/Al interface. The creation of the structures was attributed to high welding heat input [18]. The frequency of formation of such irregular phases generally increases with an increase in weld penetration [23].

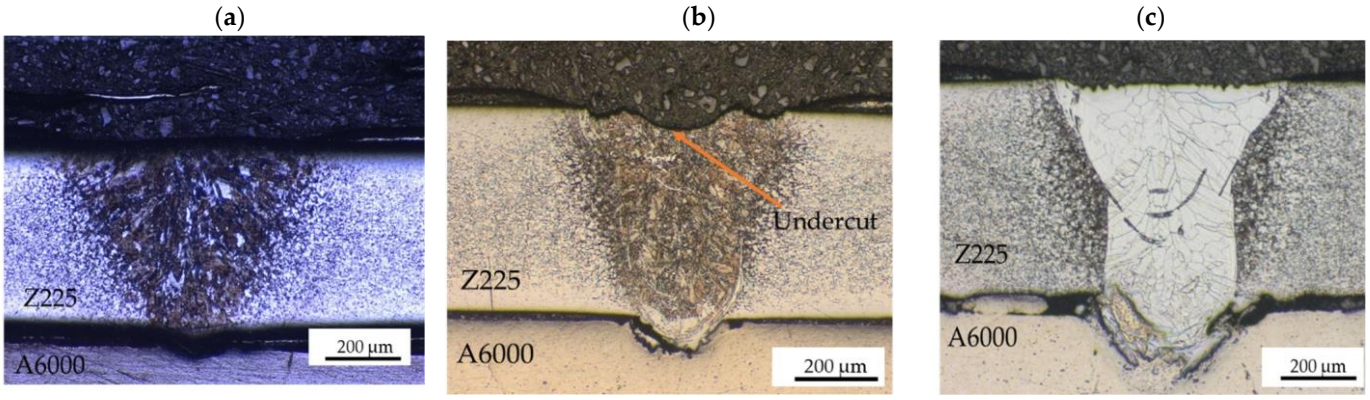


Figure 3. Optical micrographs for 3 m/min and different laser powers at 20× showing: (**a**) insufficient fusion at 800 W; (**b**) undercutting at 1000 W; (**c**) columnar grain structure at 1200 W.

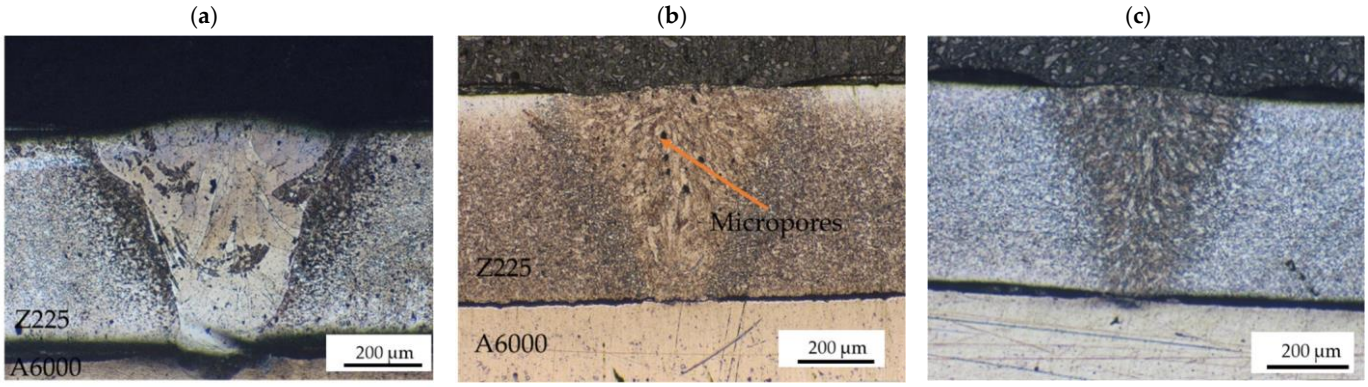


Figure 4. Optical micrographs for 950 W and different laser welding speeds at 20× magnification showing (**a**) columnar grain structure at 2 m/min; (**b**) micropores at 3 m/min; (**c**) insufficient fusion at 4 m/min.

The influence of laser power on the microstructure of the weld metal was further analyzed and observed at higher magnification, as displayed in Figure 6. It can be observed that the grain structure for both 800 and 1000 W was similar. Both samples are characterized by a fine microstructure. As power was increased to 1200 W, the grain size increased, and the structure changed from a fine to a coarser equiaxed microstructure in the middle of the weld metal. Columnar grains were observed at the weld and base metal interface. Epitaxial grain growth was evident within the weld metal, and the grain orientation was random. The observed differences in microstructure of the weld metal in the middle and the edges are often caused by the fact that in laser beam welding, the melt undergoes a rapid transition from liquid to solid in a short period. This causes different regions of the weld to undergo different solidification rates, which create variations in microstructure [24].

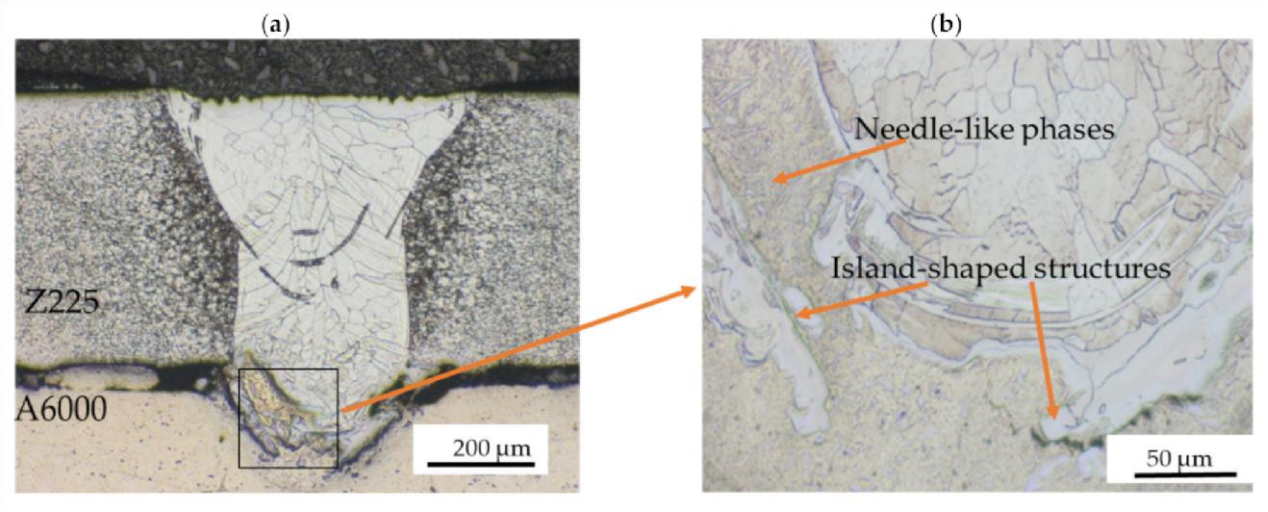


Figure 5. Optical micrographs for 1200 W and 3 m/min showing (**a**) columnar grain structure at 20×; (**b**) weld interface with irregular phases at 50×.

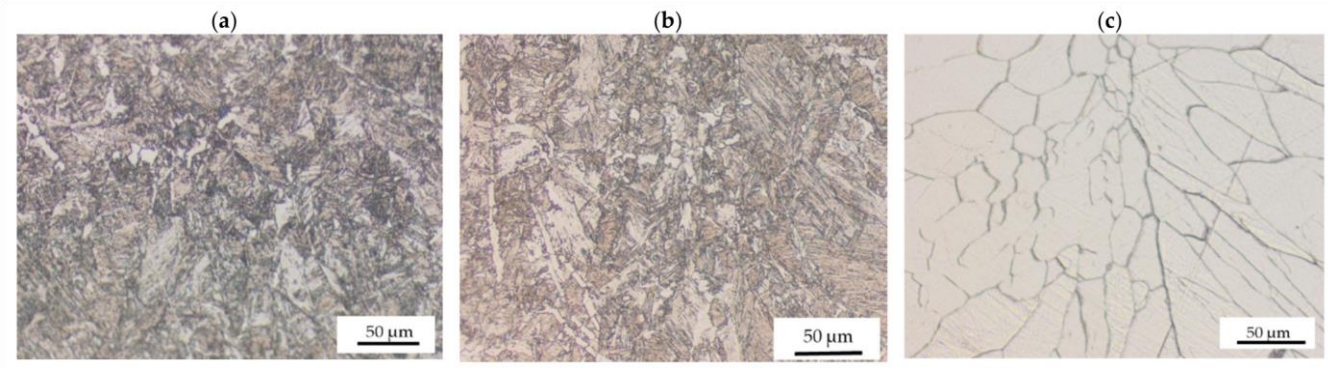


Figure 6. Optical micrographs for 3 m/min and different laser powers at 50× showing: (**a**) fine grain structure 800 W; (**b**) fine grain structure at 1000 W; (**c**) large columnar grain structure at 1200 W.

Figure 7 displays the effect of laser welding speed on the grain structure of the fusion zone.

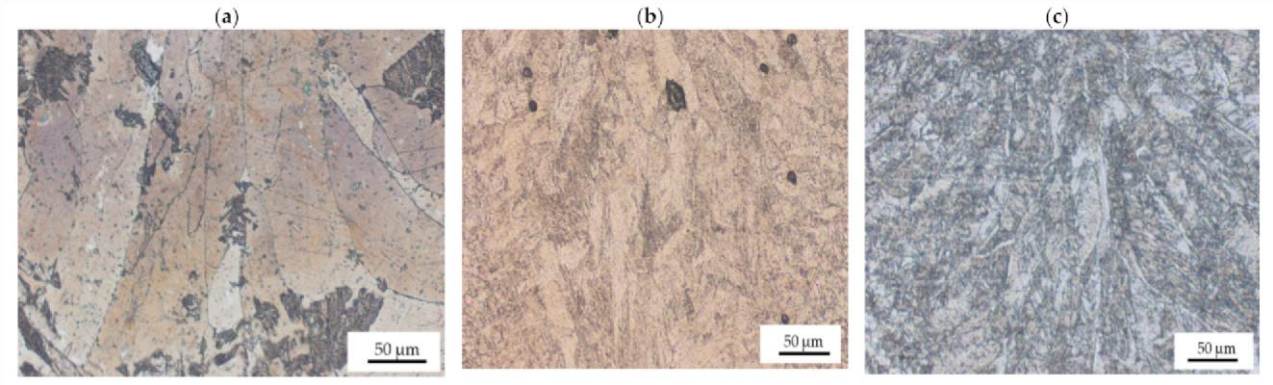


Figure 7. Optical micrographs for 950 W and different laser welding speeds at 50× magnification showing (**a**) large columnar grain structure at 2 m/min; (**b**) micropores at 3 m/min; (**c**) fine equiaxed grain structure at 4 m/min.

The size of the grains at 2 m/min was large and decreased as the laser welding speed increased to 4 m/min. When laser welding speed was 3 and 4 m/min, a fine columnar microstructure was observed. The microstructure of the weld was determined by welding speed as it influences the weld pool size and shape [25]. As the weld pool becomes larger, the grain structure becomes coarser. In general, the grain size of the weld metal decreases with an increase in laser welding speed [25]. This is because low laser welding speed leads to high heat input, which results in slow cooling rates. Therefore, grain growth occurs because of slower solidification rates in the weld pool [25].

The measurements of the weld bead express the soundness of a weld joint. The average values obtained from a digital analysis for weld width and weld penetration depth measurements for the samples were used and are presented in Figure 8. It was observed that when laser power was increased from 800 to 1000 W, the penetration depth was reduced from 881 to 764 µm; however, it then increased to 946 µm when the laser power was 1200 W. The drop in weld penetration was due to the undercut that was observed in Figure 3b. The weld width, on the other hand, increased linearly with laser power (Figure 8a). Weld bead dimensions for three varying laser welding speeds at a constant power of 950 W are displayed in Figure 8b. The weld width decreased as heat input decreased. At high welding speeds, the molten pool becomes smaller and thus results in a reduced weld width.

The weld penetration was initially reduced from 770 to 747 µm when the welding speed was changed from 2 to 3 m/min. When weld speed was further increased to 4 m/min, the weld penetration increased to 789 µm. The reduction in weld width as welding speed increased was caused by a reduction in absorption of laser-induced plasma by the top surface of the samples at higher laser speeds [26]. The fluctuations in weld penetration depths experienced may have resulted from variances in gaps between Z225 and A6000 plates caused by inconsistencies of the clamping device [6]. One other important observation made was that in both cases (Figure 8a,b), the weld width was increased by increasing heat input. However, the increase was more pronounced when laser speed was altered. This further proves that laser welding speed is the parameter that significantly influences the weld width [4].

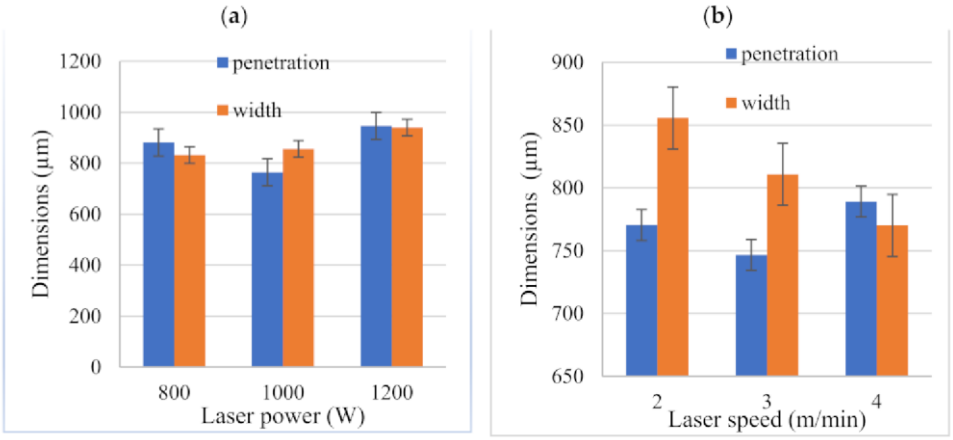


Figure 8. Effect of system parameters on the weld bead dimensions, (**a**) effect of laser power; (**b**) effect of laser welding speed.

From the optical micrographs, it was noted that the thickness of the interfacial layer was mostly affected by a change in laser welding power compared to a change in speed. As a result, the effect of laser welding power was further studied using the SEM/EDS technique. Figure 9. Displays the microstructures of the weld metal as laser welding power was changed.

The weld microstructures for 800 and 1000 W were comparable. They revealed a fine microstructure. Laser welding is characterized by rapid cooling rates. Therefore, the atoms within steel often do not have sufficient time to diffuse into new positions. The rear-arrangement of atoms occurs quickly and creates numerous needle-shaped features displayed in Figure 9a,b [27]. As power increased to 1200 W, the grain size increased.

Figure 10 displays the SEM images showing the EDS points and the position of the EDS line scan. The IMC layer thickness increased with an increase in laser power from 800 to 1200 W (Figure 10a–c). This observation resulted from high heat input, which elevated the molten metal temperature and thus increased interaction between Fe and Al atoms, increasing the thickness of the IMC layer.

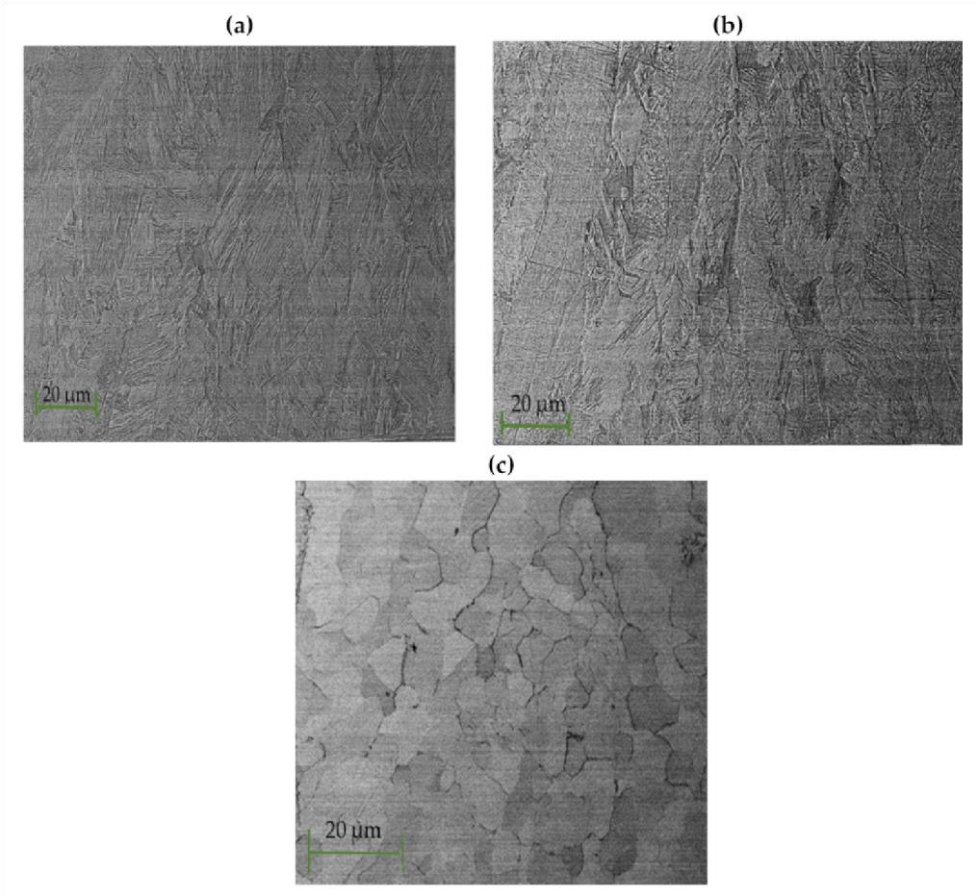


Figure 9. SEM images showing the effect of laser welding power on the microstructure of the weld metal, (**a**) 800 W; (**b**) 1000 W; (**c**) 1200 W.

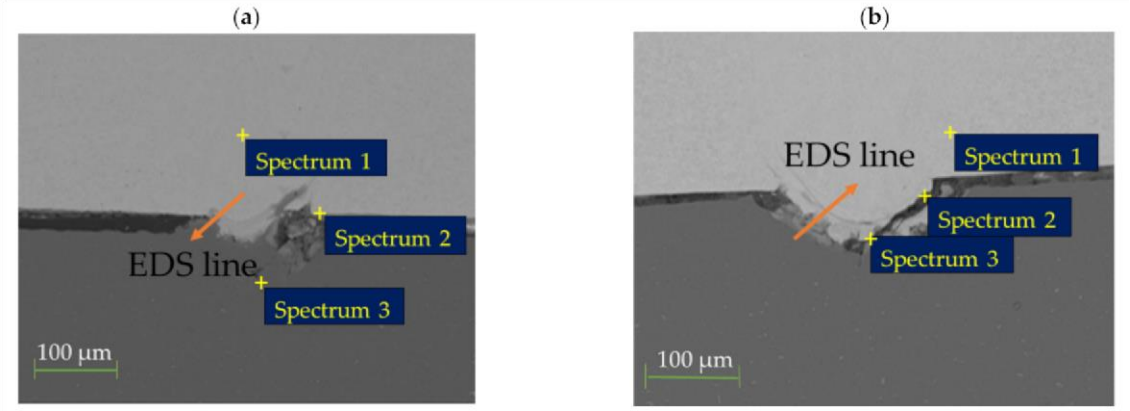


Figure 10. *Cont*.

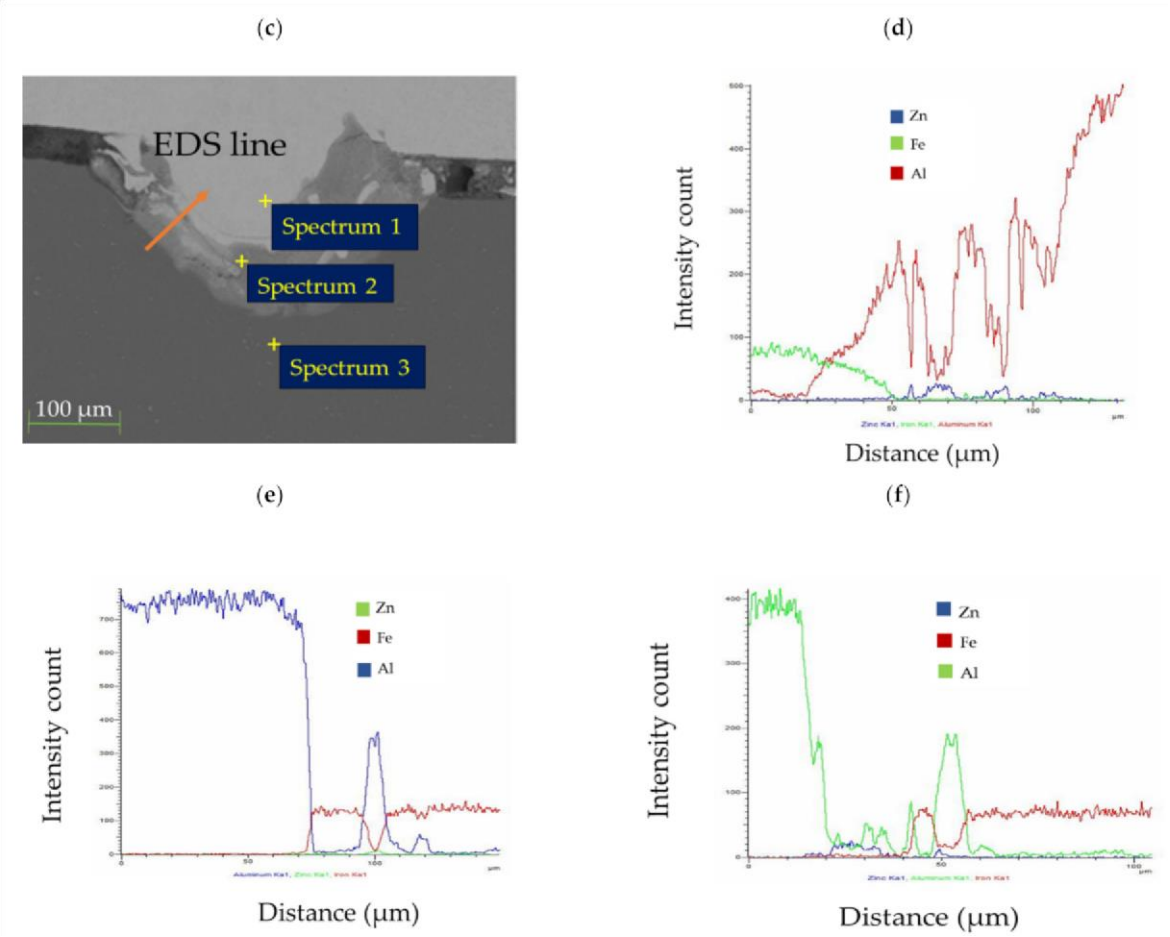


Figure 10. SEM images showing direction of EDS line scan and EDS points; (**a**,**d**) 800 W; (**b**,**e**) 1000 W; (**c**,**f**) 1200 W.

The distribution of individual elements through the weld interface was detected by EDS analysis for varying power at three different points for each sample (Figure 10a–c). The changes of the Al and Fe content are shown in Table 4. It can be observed that the composition of the phases is associated with the distance from the Z225/A6000 interface to the point of measurement. For laser powers of 800 and 1000 W, there was very little interdiffusion between Fe and Al atoms. As a result, fewer IMC phases were

detected. At laser power of 1200 W, there was more interdiffusion due to increased heat input. Near Z225, the predicted phase was Fe_2Al_5, and then the A6000 side contained $FeAl_3$. Initially, the Al atoms spread toward steel and created a Fe_2Al_5 IMC layer that then nucleated within the steel/Al interface [28]. This phase is often characterized by plate-like patterns [27].

Over time, the thickness of Fe_2Al_5 increased and halted the fusion of solid steel and molten

Al. Since the Fe atoms are larger than Al atoms, the diffusion of Fe atoms is reduced through the Fe_2Al_5 layer. It then created a needle-like $FeAl_3$ IMC layer at the interface between the Fe_2Al_5 layer and Al [28]. This explains the island-shaped and needle-like structures that were detected from the optical micrographs in Figure 5b. The EDS line scan across the interfaces (Figure 10d–f) further revealed the uneven distribution of elements at the interface. At the areas where the mixing of elements occurred, the intensity of Al was much higher compared to that of Fe. This observation further explains the existence of the $FeAl_3$ and Fe_2Al_5 phases, which are both Al-rich IMCs. The line scans also showed that the mixing of Fe and Al atoms increased as laser power increased. The XRD analyses were not able to confirm the exact IMC phases because, in most cases, the concentration of the IMC phases was below the detection limit.

4

Table 4. EDS elemental distribution and probable IMC phases.

Power	**800 W**			**1000 W**			**1200 W**		
Weight (%)	**Fe**	**Al**	**Phase**	**Fe**	**Al**	**Phase**	**Fe**	**Al**	**Phase**
Spectrum 1	100.0	0	Fe-rich	100	0	Fe-rich	77.60	22.40	Fe-rich
Spectrum 2	94.05	5.95	Fe-rich	24.04	75.96	$FeAl_3$	34.13	65.87	Fe_2Al_5
Spectrum 3	0.24	99.76	Al-rich	1.08	98.92	Al-rich	20.21	79.79	Al-rich

3.2. Mechanical Properties

A microhardness test was performed to analyse the weld mechanical properties, and the results are demonstrated in Figure 11. It was detected that the hardness values of the weld metal were higher than those of Z225 and A6000. The higher hardness within the weld metal was caused by the transition of phases that occurred within the heated material, followed by rapid cooling [29]. This behavior was observed for all different combinations of laser welding parameters. The susceptibility of the weld metal to cracking was thus increased by high hardness in comparison to the base metals as reported in the work of [30]. The high hardness within the weld metal compared to the hardness of both base metals may be due to rapid cooling rates, which results in the creation of a mixture of martensite and bainite [31]. The average hardness of the weld metal was decreased with an increase in laser power (Figure 11a). When the welding speed was increased from 2 to 4 m/min, the average weld metal hardness increased from ~239.5 to ~315 HV (Figure 11b). In general, as laser welding speed increases, the grain refinement phenomenon occurs because of rapid heating and cooling rates, which lead to structural changes and consequently increased hardness levels [32]. It was observed in Figure 4 that as laser welding speed was increased, the grain size decreased. The Hall-Petch relationship tells us that through grain size refinement, the theoretical strength of the material and hardness can be achieved [32]. These results support findings observed by Sahin et al. [33] as they also noted an increase in weld metal hardness as welding speed increased. Since the IMC layer formed was too narrow, its microhardness value was not acquired. However, there were fluctuations of the weld metal hardness, which may represent different zones of the weld metal, such as the HAZ. Oyyaravelu et al. [31] obtained similar fluctuations in hardness of steel laser-welded joints. They attributed the fluctuations to the alterations in metallurgical phase components. It was further reported that the HAZ may have experienced softening, which is often caused by decarburization, which results in a carbon-denuded zone whereby relatively low thermal conductivity is observed [31]. The variations in carbon content within the weld metal were also given as a possible reason for the fluctuations [31].

The effect of laser power on the mechanical strength is displayed in Figure 12a. It was noted that tensile strength increased with an increase in laser power. This could have resulted from the higher wetting length experienced at higher laser powers, which enhanced the strength of the weld joints even though the microstructures revealed that these weld joints somewhat had greater IMCs at the interface. Reduced strength at lower laser powers was caused by a reduction in wetting length. Similar results were reported by Narsimhacharya et al. [34]. Their tensile test results showed a reduction in tensile strength as laser power was reduced. They concluded that high joint efficiency can be achieved by increasing laser power [34]. Expand on the similarities observed in your study and literature. Figure 12b presents tensile shear test results of the dissimilar weld joints at varying welding speeds. Greater failure loads were attained at lower laser welding speeds. As welding speed increased, the tensile strength was decreased. A possible reason behind this is that there was insufficient infiltration of heat across the weld joint to create a solid bond as heat input was decreased. In addition, an increase in welding speed from 2 to 4 m/min might have been significantly high for a power of 950 W and a −0.5 mm defocused beam combination as observed by Zhengwei et al. [35]. Even though the maximum strength was acquired for weld joints produced under the lowest welding speed, this procedure would not be acceptable in the automobile industry as it would result in low productivity.

From the analysis of the weld grains in Figures 3b and 4a, it was expected that the strength would decrease as heat input increases since the grain sizes were larger and are often characterized by a reduction in ductility [22]. As a result, there was no direct correlation between grain sizes and the strength of the weld joints. The reason for this behavior may be that the samples that were exposed to high heat input experienced grain growth, but a stronger bond was formed compared to the samples produced at lower heat inputs, whereby insufficient fusion resulted in a weak bond.

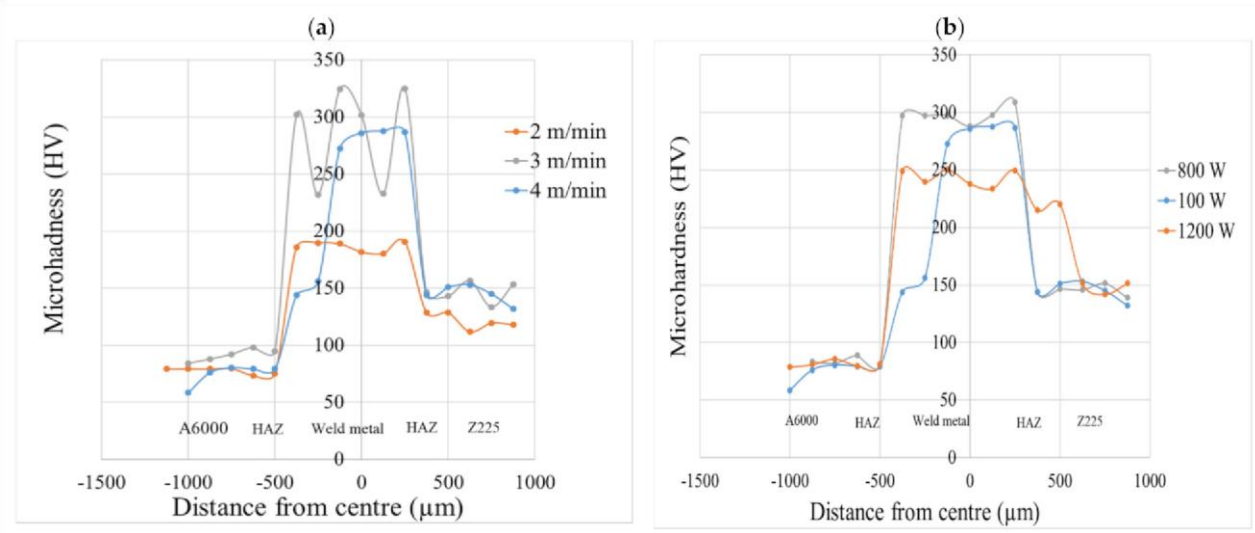


Figure 11. Effect of laser parameters on microhardness; (**a**) effect of laser power; (**b**) effect of laser welding speed.

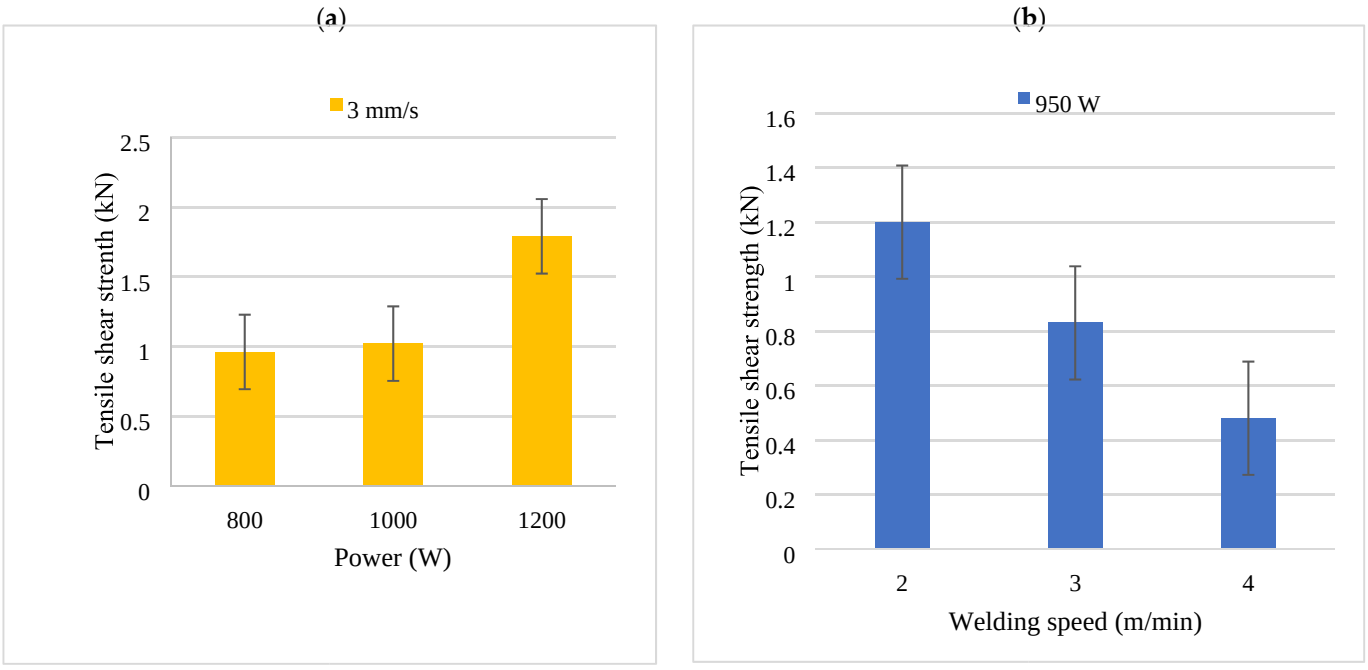


Figure 12. Effect of laser parameters on tensile shear strength; (**a**) effect of laser power; (**b**) effect of laser welding speed.

4. Conclusions

The findings obtained from the experiments performed on the dissimilar weld joint between Z225 and A6000 led to the following deductions: Weld bead measurements

revealed that the weld width increased with an increase in heat input, whereas weld penetration fluctuated. Laser welding speed was the parameter that affected the weld width the most. Increasing heat input increased the presence of island-shaped structures and needle-like structures, which were identified as Fe_2Al_5 and $FeAl_3$, respectively. The IMC layer was increased with an increase in laser power. An increase in heat input improved the tensile strength of the joints. The microhardness of the weld bead was higher than the hardness of both base metals. Laser power of 1200 W and 3 m/min laser speed were identified as ideal parameters and produced a weld joint of the highest strength (1.79 kN).

Author Contributions: Conceptualization, N.A.R. and N.M.; methodology, N.A.R., N.M. and S.S.; software, S.S.; validation N.A.R. and N.M.; formal analysis, N.M.; investigation, N.A.R. and S.S.; resources, N.M. and S.S.; data curation, N.A.R., S.S. and N.M.; writing—original draft preparation, N.A.R.; writing—review and editing, N.A.R. and N.M.; visualization, N.A.R., S.S. and N.M.; supervision, N.M.; project administration, N.A.R. and N.M.; funding acquisition, N.M. All authors have read and agreed to the published version of the manuscript.

Funding: This research received no external funding.

Institutional Review Board Statement: Not applicable.

Informed Consent Statement: Not applicable.

Data Availability Statement: Not applicable.

Acknowledgments: The author acknowledges the academic supervisor Nthabiseng Maledi, Sam Skhosane from Council for Scientific and Industrial Research (CSIR), lab technicians Donald Mahole and Shadrack Moqabolane, as well as the University of the Witwatersrand School of Chemical and Metallurgical Engineering.

Conflicts of Interest: The authors declare no conflict of interest.

References

1. Berger, L.; Lesemann, M.; Sahr, C.; Hart, S.; Taylor, R. SuperLIGHT-CAR—The multi-material car body. In Proceedings of the 7th European LS-DYNA Conference, Salzburg, Austria, 14–15 May 2009; pp. 1–10.
2. Fontaras, G.; Zacharof, N.G.; Ciuffo, B. Fuel consumption and CO2emissions from passenger cars in EuropeLaboratory versus real-world emissions, Prog. Energy Combust. *Prog. Energy Combust. Sci.* **2017**, *60*, 97–131. [CrossRef]
3. Smallman, R.E.; Bishop, R.J. *Modern Physical Metallurgy and Materials Engineering*, 6th ed.; Butterworth-Heinemann: New Dehli, India, 1999.
4. Guan, Q. Effect of steel to aluminium laser welding parameters on mechanical properties of weld beads. Opt. *Opt. Laser Technol.* **2019**, *111*, 387–394. [CrossRef]
5. Chen, H.-C. Fibre Laser Welding of Dissimilar Materials. Ph.D. Thesis, Faculty of Engineering and Physical Sciences, The University of Manchester, Manchester, UK, 2010.
6. Gao, M.; Chen, C.; Mei, S.W.; Wang, L.; Zeng, X.Y. Parameter optimization and mechanism of laser–arc hybrid welding of dissimilar Al alloy and stainless steel. *Int. J. Adv. Manuf. Technol.* **2014**, *74*, 199–208. [CrossRef]
7. Sierra, G.; Peyre, P.; Beaume, F.D.; Stuart, D.; Fras, G. Steel to aluminium braze welding by laser process with Al–12Si filler wire. *Sci. Technol. Weld. Join.* **2008**, *13*, 430–437. [CrossRef]
8. Tilekar, A.; Kamble, N.K. Optimization of laser welding parameters. *Int. Res. J. Eng. Technol.* **2017**, *4*, 1631–1633.
9. Torkamany, M.J.; Tahamtan, S.; Sabbaghzadeh, J. Dissimilar welding of carbon steel to 5754 aluminum alloy by Nd: YAG pulsed laser. *Mater. Des.* **2010**, *31*, 458–465. [CrossRef]
10. Yilbas, B.S.N.; Arif, A.F.M.; Aleem, B.J.A. Laser welding of mild steel sheets under nitrogen assisting gas ambient. *Opt. Laser Technol.* **2010**, *42*, 760–768. [CrossRef]
11. Cheolhee, K.; Woongyong, C.; Jeonghan, K.; Sehun, R. The relationship between the weldability and the process parameters for Laser-TIG hybrid welding of galvanized steel sheets. *Mater. Trans.* **2008**, *49*, 179–186.
12. Zhang, Y.; Hu, W.; Lai, X. Optimization of laser welding thin-gage galvanized steel via response surface methodology. *Opt. Lasers Eng.* **2012**, *50*, 1267–1273.
13. Dasgupta, A.K.; Mazumder, J. Laser welding of zinc coated steel: An alternative to resistance spot welding. *Sci. Technol. Weld. Join.* **2008**, *13*, 289–293. [CrossRef]

14. Kouadri-David, A.; P.S.M. (Process and Mechanical System) Team. Study of metallurgic and mechanical properties of laser welded heterogeneous joints between DP600 galvanised steel and aluminium 6082. *Mater. Des.* **2014**, *54*, 184–195. [CrossRef]
15. Ozaki, H.; Kutsuna, M.; Nakagawa, S.; Miyamoto, K. Laser roll welding of dissimilar metal joint of zinc coated steel and aluminum alloy. *J. Laser Appl.* **2010**, *22*, 1–6. [CrossRef]
16. Theron, M.; van Rooyen, C.; Ivanchev, L.H. CW Nd:YAG laser welding of dissimilar sheet metals. In Proceedings of the 26th International Congress on Applications of Lasers & Electro-Optics, Orlando, FL, USA, 29 October–1 November 2007; pp. 391–398.
17. Michalis, N.; Christophe, A. High power fiber lasers: A review. *IEEE J. Sel. Top. Quantum Electron.* **2014**, *20*, 1–23.
18. Cui, L. Dual beam laser keyhole welding of steel/aluminium lapped joints. *J. Mater. Process. Technol.* **2018**, *256*, 87–97. [CrossRef]
19. Yuce, C.; Karpat, F.; Yavuz, N. Investigations on the microstructure and mechanical properties of laser welded dissimilar galvanized steel–aluminium joints. *Int. J. Adv. Manuf. Technol.* **2019**, *104*, 2693–2704. [CrossRef]
20. O'Brien, A.; Guzman, C. *Welding Handbook*, 9th ed.; American Welding Society: Miami, MA, USA, 2007.
21. Chen, W. Laser Welding of Thin Sheets of Galvanized Steel and Aluminum Alloy. Master's Thesis, Iowa State University, Ames, IA, USA, 2006.
22. Fabbro, R. Melt pool and keyhole behaviour analysis for deep penetration laser welding. *J. Phys. D Appl. Phys.* **2012**, *43*, 445–501. [CrossRef]
23. Sierra, G.; Peyreb, P.; Deschaux-Beaume, F.; Stuart, D.; Fras, G. Steel to aluminium key-hole laser welding. *Mater. Sci. Eng.* **2006**, *447*, 197–208. [CrossRef]
24. Phanikumar, G.; Chattopadhyay, K.; Dutta, P. Modelling of transport phenomena in laser welding of dissimilar metals. *Int. J. Numer. Methods Heat Fluid Flow* **2001**, *11*, 156–171. [CrossRef]
25. Ovat, F.A. The Effect of Electrodes on the Mechanical Properties of Welded Steels, department of Mechanical Engineering. Master's Thesis, University of Agriculture Makurdi, Makurdi, Nigeria, 2004.
26. Meng, W. The influence of various factors on the geometric profile of laser lap welded T-joints. *J. Laser Appl.* **2015**, *74*, 1625–1636. [CrossRef]
27. Martensite: Definition, Transformation & Microstructure. Available online: https://study.com/academy/lesson/martensitedefinition-transformation-microstructure.html (accessed on 17 November 2021).
28. Karim, A.; Park, Y. A Review on welding of dissimilar metals in car body manufacturing. *J. Weld. Join.* **2020**, *38*, 369–384.
29. Radek, N.; Pietraszek, J.; Goroshko, A. The impact of laser welding parameters on the mechanical properties of the weld. In Proceedings of the 13th International Conference Electromachining, Bydgoszcz, Poland, 9–11 May 2018; pp. 1–7.
30. Talabi, S.I. Effect of welding variable on mechanical properties of low carbon steel joint. *Adv. Eng. Manuf.* **2014**, *9*, 181–186. [CrossRef]
31. Oyyaravelu, R.; Kuppan, P.; Arivazhagan, N. Metallurgical and mechanical properties of laserwelded high strength low alloy steel. *J. Adv. Res.* **2016**, *7*, 463–472. [CrossRef] [PubMed]
32. Xu, W.; Li, Z.; Sun, X. Effect of welding speed on mechanical properties and the strain-hardening behavior of friction stir welded 7075 aluminum alloy joints. *J. Mater. Eng. Perform.* **2017**, *26*, 1938–1946. [CrossRef]
33. Sahin, S.; Michael, K.; Markus, K.; Michael, F.Z. Influence of process temperature on hardness of friction stir welded high strength aluminium alloys for aerospace applications. *Procedia CIRP* **2014**, *24*, 120–124.
34. Narsimhacharya, D.; Duttaa, K.; Shariffb, S.M.; Padmanabhamb, G.; Basua, A. Mechanical and microstructural characterization of laser weld-brazed AA6082-galvanized steel joint. *J. Mater. Process. Technol.* **2019**, *263*, 21–32. [CrossRef]
35. Zhengwei, G.U. Influence of welding speed on microstructure and properties of ultra-high strength steel sheets in laser welding. *ISIJ Int.* **2018**, *52*, 483–487.